ELECTRON AND PHONON DYNAMICS WITHIN ELECTRON-PHONON INTERACTION

by

SUN KANGTAI
(B.S., Sichuan University)

A THESIS SUBMITTED FOR THE DEGREE OF

DOCTOR OF PHILOSOPHY

in

PHYSICS

in the

GRADUATE DIVISION

of the

NATIONAL UNIVERSITY OF SINGAPORE

2021

Supervisor:
Professor Wang Jian-Sheng

Examiners:
Professor Feng Yuan Ping
Professor Gong Jiangbin
Professor Shi Junren, International Center for Quantum Materials, Peking University, China

Declaration

I hereby declare that this thesis is my original work and it has been written by me in its entirety. I have duly acknowledged all the sources of information which have been used in the thesis.

This thesis has also not been submitted for any degree in any university previously.

Sun Kangtai

1 July 2021

To my dear family

Acknowledgments

First and foremost, I would like to express my special appreciation to my supervisor, Prof. Wang Jian-Sheng, for his invaluable guidance, constant support, and kind words of encouragement. His immense knowledge, rigorous attitudes, and insightful suggestions have made this thesis possible.

I would also like to express my gratitude towards my seniors and collaborators, Zhang Zu-Quan, Gao Zhibin, Deng Tianqi, and Zhu Tao for their helpful discussions and happy collaborations.

I thank my friends for their encouragement when I am low in the spirit. Last but not least, I wish to thank and dedicate this thesis to my parents and family. Without their understanding and supports, I could not have been able to go through this challenging experience.

Contents

Abstract

Semiconductors, superconductors, conductive polymers and many other advanced materials have deeply affected modern society. Every special property of these materials is a macroscopic reflection of the microscopic interactions in them. Among such interactions, electron-phonon interaction (EPI) is ubiquitous in solids, indicating the interaction between the electrons and the lattice vibrations, *i.e.* the phonons. This thesis studies the electron and phonon dynamics within EPI, respectively.

For electron dynamics, we explore the electron charge transport in one-dimensional organic polymer treated as an open system with a two-terminal phonon bath. The approach is based on nonequilibrium Green's function (NEGF), generalized quantum Langevin equation and molecular dynamic (MD) simulation. We employ a semi-classical one-dimensional model to let one single electron evolve and calculate its mean squared displacement as well as the diffusion constant. The simulation results demonstrate that the charge transport behavior is bandlike when temperature is increasing. By combining deformation potential approximation with Boltzmann transport theory, we implement an analytical calculation to predict the diffusion constant and find that it drastically disagrees with our MD simulation. As an extension, we implement the same approach to simulate a quasi one-dimensional organic polymer and also compare the results with previous work which uses Boltzmann transport theory. For this more complicated polymer, we do not succeed to draw a convincing conclusion about the validity of Boltzmann transport theory due to the size limit.

For phonon dynamics, we focus on the phonon Hall effect (PHE). Since the first experimental observation of the PHE in 2005, its physical origin and theoretical explanation have been extensively investigated. While spin-orbit interactions are believed to play important roles under external magnetic fields, nonmagnetic effects are also possible. Here, we propose a mechanism of PHE which is induced by electric current in a nonequilibrium system through EPI. The influence of the drift electrons to the phonon degrees of freedom, as a correction to the Born-Oppenheimer approximation, is represented by an antisymmetric matrix which has the same form as in a typical phonon Hall model. We demonstrate the idea with a graphene-like hexagonal lattice having a finite phonon Hall conductivity under a driven electric current.

Although PHE has attracted a lot of attention in recent years with many experimental explorations published, theoretical studies are still hovering around phenomenon-based models. Moreover, previous microscopic theory was found unable to explain large thermal Hall conductivity obtained by experiments in strontium titanate (STO). Therefore, in an attempt to bridge this gap, we implement first-principles calculations to explore the PHE in real materials. Our work provides a benchmark of the PHE in sodium chloride (NaCl) under a large external magnetic field. Moreover, we demonstrate our results in Barium titanate (BTO), and discuss the results of STO in detail about their deviation from experiments. As a possible future direction, we propose that the inner electronic Berry curvature and cubic nonlinear potential play important roles in PHE in STO.

List of Figures

List of Publications

[1] K. Sun, Z. Gao, and J.-S. Wang, "Current-induced phonon hall effect", *Phys. Rev. B*, vol. 102, p. 134 311, 13 Oct. 2020. [Online]. Available: https://link.aps.org/doi/10.1103/PhysRevB.102.134311.

[2] Z. Gao, T. Zhu, K. Sun, and J.-S. Wang, "Highly anisotropic thermoelectric properties of two-dimensional as2te3", *ACS Applied Electronic Materials*, vol. 3, no. 4, pp. 1610–1620, 2021. eprint: https://doi.org/10.1021/acsaelm.0c01100. [Online]. Available: https://doi.org/10.1021/acsaelm.0c01100.

[3] K. Sun, Z. Gao, and J.-S. Wang, "Phonon hall effect with first-principles calculations", *Phys. Rev. B*, vol. 103, p. 214 301, 21 Jun. 2021. [Online]. Available: https://link.aps.org/doi/10.1103/PhysRevB.103.214301.

Chapter 1

Introduction

1.1 Electron-Phonon Interaction

The electron-phonon interaction determines the temperature dependence of the transport behaviors such as electron mobility in semiconductors, induces the conventional low-temperature superconductivity, and can play a role in topological materials [1]. Moreover, the electron-phonon interaction can also affect phonons' dynamics by a Berry phase term coming from electrons, which finally could result in the so-called phonon Hall effect [2]. Straightforwardly, the electron-phonon interaction can be understood that when there are phonons excited in a crystal, local charge imbalance caused by this lattice distortion will drag the moving electrons. In contrast, from phonons' perspective, the moving electrons are also dragging phonons at the same time, they are competing with each other to arrive at a dynamic balance. Therefore, electrons and phonons are coupled to each other all the time posing difficulty to solve their equations of motions rigorously. Translating this naive description into contemporary language, a standard form of the Hamiltonian

including the electron-phonon interaction up to lowest order is [2]

$$\begin{aligned}\hat{H} =& \sum_{n\boldsymbol{k}} \varepsilon_{n\boldsymbol{k}} c^{\dagger}_{n\boldsymbol{k}} c_{n\boldsymbol{k}} + \sum_{\boldsymbol{q}\nu} \hbar\omega_{\boldsymbol{q}\nu}(a^{\dagger}_{\boldsymbol{q}\nu} a_{\boldsymbol{q}\nu} + \frac{1}{2}) \\ &+ \frac{1}{\sqrt{N}} \sum_{\boldsymbol{k},\boldsymbol{q},mn\nu} g_{mn\nu}(\boldsymbol{k},\boldsymbol{q}) c^{\dagger}_{m\boldsymbol{k}+\boldsymbol{q}} c_{n\boldsymbol{k}} (a_{\boldsymbol{q}\nu} + a^{\dagger}_{-\boldsymbol{q}\nu}).\end{aligned} \tag{1.1}$$

In this Hamiltonian, $\varepsilon_{n\boldsymbol{k}}$ is the eigenvalue of an electron with crystal momentum $\boldsymbol{k}$ and band number n, $\omega_{\boldsymbol{q}\nu}$ is the eigenfrequency of a lattice vibration with crystal momentum $\boldsymbol{q}$ in the ν-th branch. $c^{\dagger}_{n\boldsymbol{k}}$ and $c_{n\boldsymbol{k}}$ ($a^{\dagger}_{\boldsymbol{q}\nu}$ and $a_{\boldsymbol{q}\nu}$) are the creation and annihilation operators of electron (phonon), respectively. $g_{mn\nu}(\boldsymbol{k},\boldsymbol{q})$ represents the coupling matrix element of the electron-phonon interaction.

To analyze the electron-phonon interaction, a generally accepted way is to make appropriate approximations. The best-known approximation is Born-Oppenheimer approximation handling electrons and phonons separately based on the fact that electrons are much lighter than nuclei. Equipped with this approximation, equations of motion for electrons and phonons can be solved formally by eliminating each other. With the elimination, the effect of phonons (electrons) in the equations of motion for electrons (phonons) is replaced with a phonon (electron) self-energy term using the Green's functions formalism. In this way, we can explore the electron and phonon dynamics within the electron-phonon interaction, respectively.

1.2 Trans-polyacetylene and SSH Model

Trans-polyacetylene has a dimerized structure illustrated in Fig. 1.1. It consists of conjugate (CH) groups with alternating single and double chemical bonds. In 1977, Shirakawa, Heeger, and MacDiarmid discovered high electrical conductivity

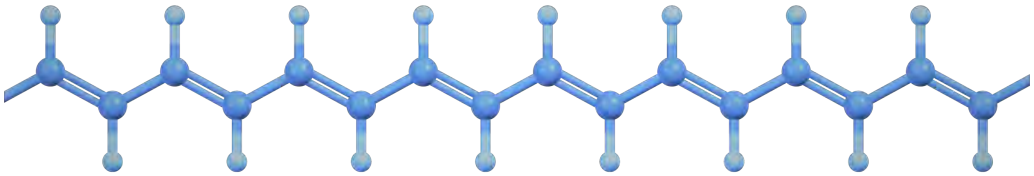

Figure 1.1: Ball-and-stick model of trans-polyacetylene.

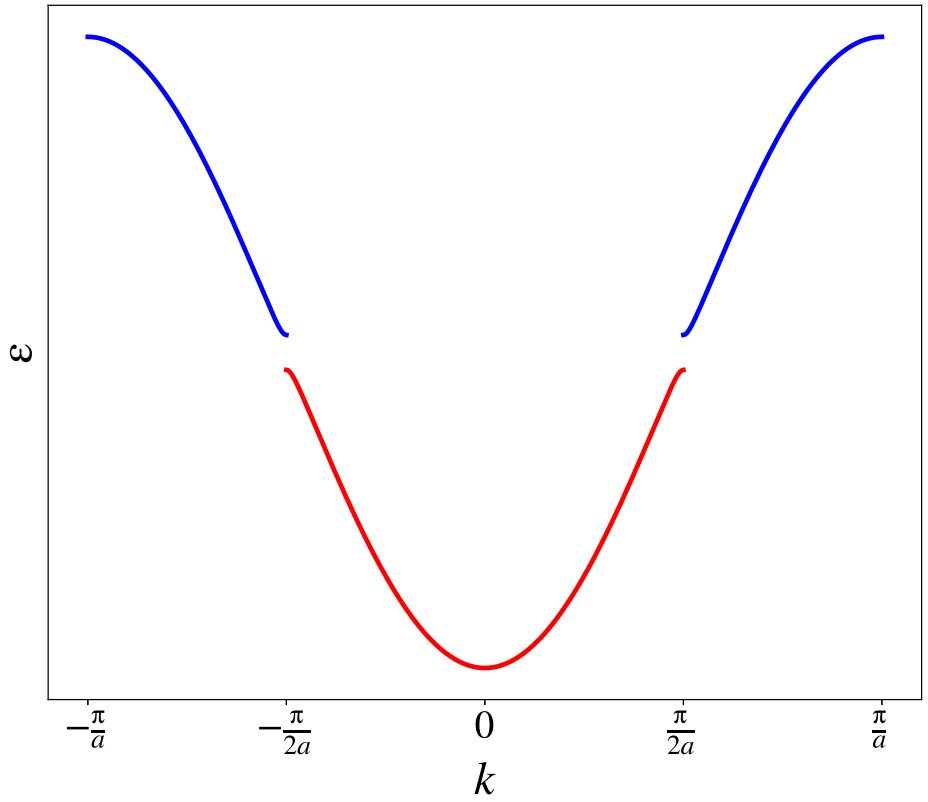

Figure 1.2: Electronic band structure of the SSH model with perfect dimerization. a is the length between two nearest (CH) group.

upon doping in the polyacetylene [3]. Inspired by their work, a new field of organic conductive polymers was launched in physics. Therefore, to explore the charge transport behavior in trans-polyacetylene, SSH model, the abbreviation of the authors Su, Schrieffer, and Heeger, was firstly proposed in 1979 [4]. There are

some assumptions made in this model to simplify the description. Firstly, the interchain electron hybridization was ignored, therefore, SSH model is a quasi one-dimensional (1-D) model. Secondly, the σ electrons are treated adiabatically due to the large gap between the σ bonding and antibonding states compared to the phonon energies, while the π electrons are approximately described by a tight-binding model. Moreover, each (CH) group is forced moving only along the bond (carbon-carbon bond) direction, which again indicates it lies in 1-D space. The original Hamiltonian [4] is given as follows:

$$\begin{aligned}\hat{H} = &-\sum_{ns}[t_0 - \alpha(u_{n+1} - u_n)](c^{\dagger}_{n+1,s}c_{ns} + c^{\dagger}_{ns}c_{n+1,s}) \\ &+ \frac{1}{2}\sum_n K(u_{n+1} - u_n)^2 + \frac{1}{2}\sum_n M\dot{u}_n^2,\end{aligned} \tag{1.2}$$

where $c^{\dagger}_{ns}$ and c_{ns} are the creation and annihilation operator of π electrons with spin s on the n-th group, respectively, u_n is the displacement of n-th group, K and M are the effective spring constant matrix and mass matrix, respectively, t_0 is the hopping integral for the undimerized 1-D chain, and α is the electron-phonon coupling constant. For the perfectly dimerized system, the displacements can be described by a general formula: $u_n = \pm(-1)^n u_0$. In this case, the effective hopping integral only has two different values, $t_0 - t_1$ and $t_0 + t_1$ with $t_1 = 2\alpha u_0$, which represent the single bond and double bond, respectively. As Fig. 1.2 shows, the dimerization will induce a band gap in the electronic band structure indicating the system becomes lower in energy due to the distortion. Therefore, previous equally spaced one-dimensional system with one electron per site is unstable, which is the so-called Peierls instability. Moreover, the dimerization introduces non-trivial

topological properties into the system so that SSH model becomes the simplest 1-D model with non-trivial topology.

1.3 Berry Phase Effect

Geometric phase did not appear in physical research until Aharonov and Bohm proposed their famous A-B effect in 1959 [5]. Subsequently, in 1984, Michael Berry systematically described the adiabatic evolution of an eigenstate around a loop in the parameter space with parameters varying slowly [6]. During the evolution, if no degeneracies in the parameter space, besides the usual dynamic factor, the eigenstate will accumulate an extra phase factor which will not be cancelled even when it reaches its starting point. This extra phase factor, therefore, will play a role in determining and relating observables. Berry's work has greatly influenced different fields of physics including the quantum chemistry so that people named this geometric phase as the Berry phase [7].

The derivation of the Berry phase and its associated quantities has already been written in many textbooks, therefore, we just briefly introduce the general formalism. Consider a time-varying Hamiltonian $H(\boldsymbol{R})$ in the parameter space spanning by a set of parameters $\boldsymbol{R} = (R_1, R_2, ...)$, where $R_i = R_i(t)$ varies in time very slowly. The parameters set moves along a closed path $\mathcal{C}$ so that $\boldsymbol{R}(T) = \boldsymbol{R}(0)$. Since the motion is adiabatic, for each $\boldsymbol{R}(t)$ point, we have following equation:

$$H(\boldsymbol{R})|n(\boldsymbol{R})\rangle = E_n(\boldsymbol{R})|n(\boldsymbol{R})\rangle, \tag{1.3}$$

where $|n(\boldsymbol{R})\rangle$ is an orthonormal basis of the corresponding eigenstates at that point.

This equation is still valid if we multiply a phase factor, also called a gauge, on both sides whether it is dependent on $\boldsymbol{R}$. Constant factor is trivial, therefore, it is natural to choose a smooth and single valued time-dependent function along the path $\mathcal{C}$. Assume the gauged eigen basis is $|\psi(t)\rangle = e^{-i\theta(t)}|n(\boldsymbol{R}(t))\rangle$, then according to quantum theory, the time evolution of the system is

$$\begin{aligned} E_n(\boldsymbol{R}(t))|n(\boldsymbol{R}(t))\rangle &= \hbar\Big(\frac{d\theta(t)}{dt}\Big)|n(\boldsymbol{R}(t))\rangle + i\hbar\frac{d|n(\boldsymbol{R}(t))\rangle}{dt} \\ \rightarrow \theta(t) &= \frac{1}{\hbar}\int_0^t E_n(\boldsymbol{R}(t'))dt' - i\int_0^t \langle n(\boldsymbol{R}(t))|\frac{d}{dt'}|n(\boldsymbol{R}(t'))\rangle dt'. \end{aligned} \tag{1.4}$$

The first term is the conventional dynamical phase. The extra second term is the Berry phase. We can rewrite the second term as follows:

$$\begin{aligned} \gamma_n &= i\int_0^t \langle n(\boldsymbol{R}(t'))|\frac{d}{dt'}|n(\boldsymbol{R}(t'))\rangle dt' \\ &\equiv \int_{\mathcal{C}} d\boldsymbol{R}\cdot\boldsymbol{A}_n(\boldsymbol{R}), \end{aligned} \tag{1.5}$$

where $\boldsymbol{A}_n(\boldsymbol{R}) \equiv i\langle n(\boldsymbol{R})|\boldsymbol{\nabla}_{\boldsymbol{R}}|n(\boldsymbol{R})\rangle$ is named as Berry connection, or Berry vector potential due to its similarity to the vector potential of magnetic filed. Obviously, the Berry connection is gauge-dependent. If we apply a gauge transformation $|n(\boldsymbol{R})\rangle \rightarrow e^{i\xi(\boldsymbol{R})}|n(\boldsymbol{R})\rangle$, the Berry connection becomes $\boldsymbol{A}_n(\boldsymbol{R}) \rightarrow \boldsymbol{A}_n(\boldsymbol{R}) - \frac{\partial\xi(\boldsymbol{R})}{\partial\boldsymbol{R}}$. After evolving along the path $\mathcal{C}$, the difference is just $\xi(\boldsymbol{R}(0)) - \xi(\boldsymbol{R}(T))$. Since we have assumed the phase factor is single-valued, $\xi(\boldsymbol{R}(0)) - \xi(\boldsymbol{R}(T))$ must be an integer multiple of 2π. Therefore, the Berry phase cannot be removed and is a gauge-invariant quantity. Although there is an imaginary sign in Eq. (1.5), the Berry phase is real because $\langle n(\boldsymbol{R})|n(\boldsymbol{R})\rangle = 1 \rightarrow \langle n(\boldsymbol{R})|\boldsymbol{\nabla}_{\boldsymbol{R}}|n(\boldsymbol{R})\rangle = -\langle n(\boldsymbol{R})|\boldsymbol{\nabla}_{\boldsymbol{R}}|n(\boldsymbol{R})\rangle^*$. Therefore, $\gamma_n = -\mathrm{Im}\int_{\mathrm{C}} d\boldsymbol{R}\cdot\langle n(\boldsymbol{R})|\boldsymbol{\nabla}_{\boldsymbol{R}}|n(\boldsymbol{R})\rangle$. With the application of Stokes

theorem, the Berry phase can be further rewritten as

$$\begin{aligned}\gamma_n &= -\mathrm{Im}\int d\boldsymbol{S}\cdot\Big(\boldsymbol{\nabla}\times\langle n(\boldsymbol{R})|\boldsymbol{\nabla}_{\boldsymbol{R}}|n(\boldsymbol{R})\rangle\Big)\\ &= -\mathrm{Im}\int d\boldsymbol{S}\cdot\Big(\langle\boldsymbol{\nabla}_{\boldsymbol{R}}n(\boldsymbol{R})|\times|\boldsymbol{\nabla}_{\boldsymbol{R}}n(\boldsymbol{R})\rangle\Big)\\ &\equiv\int d\boldsymbol{S}\cdot\Omega(\boldsymbol{R}),\end{aligned}\tag{1.6}$$

where the integral is over the area enclosed by the path $\mathcal{C}$, and

$$\Omega_{\mu\nu}(\boldsymbol{R})\equiv-\mathrm{Im}\Big[\langle\nabla_\mu n(\boldsymbol{R})|\nabla_\nu n(\boldsymbol{R})\rangle-(\mu\leftrightarrow\nu)\Big]\tag{1.7}$$

is the Berry curvature.

Going through the derivation, we can conclude that the Berry phase has three key properties. First, Berry phase cannot be cancelled by gauge transformation. This gauge invariance makes it physical and possible to be measured directly through interference phenomena [7]. Second, it is geometrical. It is not only a line-integral of the Berry connection over a closed path, but also a surface integral of the Berry curvature over an area suspending the path. Third, the Berry phase is closely related to gauge field theories and differential geometry [8]. The integral of its associated Berry curvature over an enclosed surface is quantized as integers which is known as the Chern numbers. Due to these properties, the Berry phase effects have been successfully applied to explain electrical transport behaviours such as quantum Hall effect [9, 10], anomalous Hall effect [11, 12], anomalous thermoelectric transport [13], quantum spin Hall effect [14, 15], and electron polarization [16]. These applications elegantly connect mathematics and physics, which greatly boost our understanding of condensed matter.

Berry phase not only can attend the electrical transport, but also the phonon transport. In recent years, many physicists have started to relate the phonon transport with the Berry phase, such as the Berry-phase-induced heat pumping [17], the Berry phase effect in molecular vibration [18], and the phonon Hall effect [19, 2]. However, since phonons and electrons obey different statistics, the respective Berry phase effects are not the same. Moreover, in phonon system, there may be non-Hermitian effective Hamiltonian, therefore, the corresponding Berry terms should be slightly modified. Berry phase effect in non-Hermitian system is also another intriguing field in physics.

1.4 Phonon Hall Effect

In general belief, Hall effect under magnetic field always appear in electrical transport. However, in 2005, Strohm, Rikken, and Wyder observed the counterpart in phonon transport, the phonon Hall effect. In their observation, the applied magnetic field bends part of the heat current to the direction perpendicular to both the temperature gradient and the magnetic field, which finally results in a temperature difference. The experiment was performed on samples of paramagnetic terbium gallium garnet (TGG), and the measured transverse temperature difference has 10^{-4} order of magnitude in kelvin with the magnetic field being about 4 T at an average temperature 5.45 K. The PHE was found linearly dependent on the magnetic field in the range 0 to 4 T. Subsequently, more experiments have confirmed the PHE [20, 21]. To understand this effect, in the past decade, several theoretical explanations have been proposed [22, 23, 24, 25, 2]. Currently, the most

successful microscopic theory was developed by Qin *et al.* in which the PHE is related to the Berry phase of the phononic structure [2]. Their theory introduces a correction to the traditional linear response theory, called the energy magnetization [26]. This correction successfully cancels the divergence in previous theory [25] at zero temperature which is inconsistent with thermodynamics. Inspired by these studies, the PHE can be generalized that parallel to the Hall effect in electrical transport, as long as there is a gauge potential playing a similar role as the vector potential in a magnetic field, there will be PHE. This net vector potential could come from the inner electron structure of an atomic system itself combined with an external magnetic field [27], or other more complicated interactions like magnon-phonon interaction [28]. All of the present PHEs, either experimental or theoretical, need external [29] or internal magnetic field to induce the observable phonon Hall conductivity. However, in principle, the magnetic field is not really necessary, therefore, there may be some mechanisms of the PHE without the significant magnetic field.

Furthermore, with more experiments published, it is evident that we have not reached the end of the story yet. In 2020, an experimental group found a large PHE in a perovskite, STO [21]. Their setup for the experiment is illustrated in Fig. 1.3(a) and (b) extracted from their publication. By their measurement, the transverse temperature difference is about several mK with the magnetic field in the range 0-12 T at an average temperature 24 K, and the corresponding Hall conductivity has 10^{-2} order of magnitude in the unit of W/(K-m). Linearity between the conductivity and the magnetic field is also showed in Fig. 1.3(c) and (d). The authors thought their observations can be explained by Qin's theory. However,

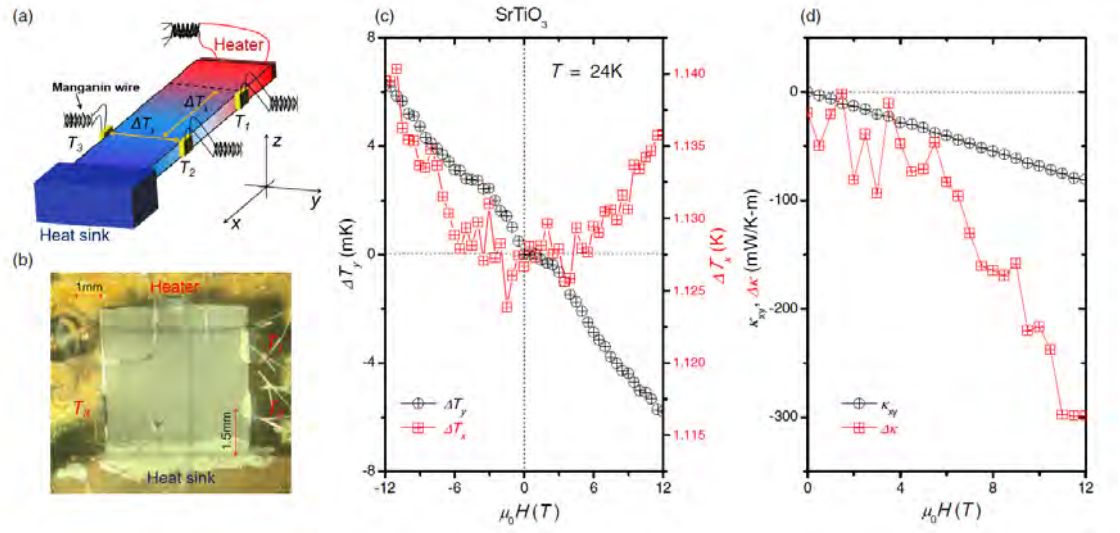

Figure 1.3: (a) Setup for measuring longitudinal and transverse temperature difference. (b) Sample. (c) Longitudinal and transverse temperature difference against the magnetic field. (d) Extracted phonon Hall conductivity κ_{xy} and field-induced change in conventional conductivity $\delta\kappa = \kappa(\mu_0 H) - \kappa(0)$ against the magnetic field. Reprinted figure with permission from [21]. Copyright 2021 by the American Physical Society.

subsequently, a theoretical group pointed out that Qin's theory cannot explain the large values in experiments and they used Boltzmann transport theory to successfully predict the ratio between the longitudinal thermal conductivity and the phonon Hall conductivity [30]. Moreover, another experimental work found that if ^{16}O in STO is replaced with its isotope ^{18}O, the phonon Hall conductivity will become two orders of magnitude smaller [31]. This is a very bizarre behavior challenging all current theories. The authors concluded that the PHE in STO with ^{16}O is more like an enhancement compared with SrTi^{18}O$_3$, and therefore they attributed the reason most likely to the behavior of the transverse optical phonon modes in STO at low temperature. All these recent experiments are performed on complex materials, therefore, it is difficult to understand them with simplified models, and

more accurate and persuasive first-principles calculations are needed.

1.5 Spin-Phonon Interaction

For a particle with spin, when it moves inside a potential, its spin will interact with its orbital quantities. A famous example resulted from the spin-orbit interaction is the shift of atoms' energy level. With the help of the electromagnetic interaction between the spin of the electrons and the magnetic field of nuclei from electrons' perspective, the spin-orbit interaction can be detected through the energy split. Similarly, for phonon transport, the vibrating ions could also interact with their spins or the local magnetization, which is called spin-phonon interaction (SPI). In the past century, the SPI has been widely studied [32, 33, 34, 35, 36, 37]. In its phenomenological description, the coupling raises between the pseudo-spin representing the Kramers doublet of ions and the lattice vibrations. It can be assumed that only the lowest Kramers doublet keeps degenerate within the crystal fields, and as a result, the energy required to jump to excited states is greater than the Debye energy [36, 37]. Therefore, as an approximation, we use a pseudospin-1/2 operator $\boldsymbol{s}_n$ to represent the doublet for n-th ion. The Raman-type SPI without external magnetic field is [25]:

$$H_{\mathrm{SPI}} = g \sum_n \boldsymbol{s}_n \cdot (\boldsymbol{u}_n \times \boldsymbol{p}_n), \tag{1.8}$$

where g is a coupling constant related to the charge and mass of the ions, $\boldsymbol{u}_n$ and $\boldsymbol{p}_n$ are the displacement and momentum of the n-th ion, respectively. With external magnetic field, the time-reversal symmetry is broken, therefore, the Kramers doublet

is not degenerate any more and there will be a magnetization $\boldsymbol{M}$. Assuming isotropy in the SPI, the mean-field approximation gives $\langle \boldsymbol{s}_n \rangle = c\boldsymbol{M}$. Thus the SPI can be rewritten as:

$$H_{\mathrm{SPI}} = \boldsymbol{h} \cdot \sum_n \boldsymbol{u}_n \times \boldsymbol{p}_n. \tag{1.9}$$

Here, $\boldsymbol{h} = gc\boldsymbol{M}$.

SPI was mostly applied to study the magnetic properties and longitudinal thermal transport behaviors of the system previously. In the last decade, it was noticed that SPI could also play a role in the PHE [25]. Although the SPI itself is not particularly small, its induced PHE in the proposed theoretical model was somehow weak compared with the experiments. One of the possible reasons is the isotropic assumption. In real ionic materials, there are no free charges, instead, the charge properties are described by Born effective charge tensor. Therefore, the form of the SPI should be modified according to the real charge distribution. We also note STO is not magnetic, so we cannot expect SPI in STO.

1.6 Perovskite

Perovskite, named in honor of the Russian mineralogist Lev Perovski, originally refers to calcium titanium ($CaTiO_3$). With more minerals similar to the $CaTiO_3$ found, perovskite now refers to this fascinating family of materials with many fantastic properties. All the compounds in this family have the same general formula ABO_3 and orthorhombic crystal structure shown in Fig. 1.4. In the formula, trivalant cation A at eight corner positions usually is a rare earth ion such as Pr, La, Gd, or divalent alkaline earth, *e.g.* Ca, Sr, Ba, *etc.* Cation B at the central position

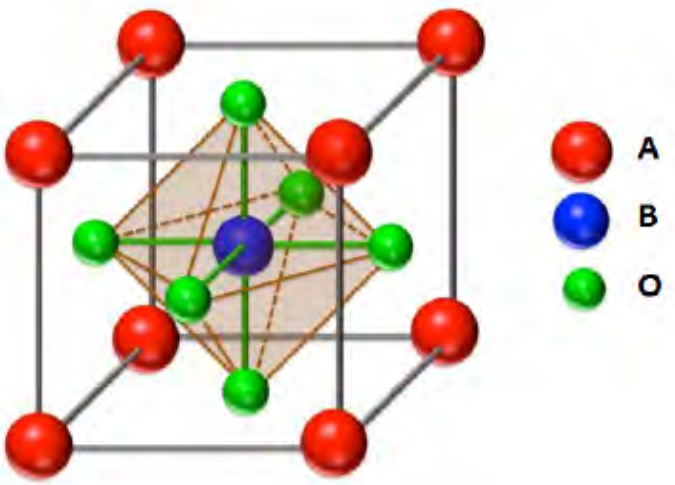

Figure 1.4: Crystal structure of general perovskite.

typically is a transition metal ion, *e.g.* Mn, Ti, Co, Fe, *etc.* O locating at the face center usually is the oxygen anion and six of them form an octahedral cage. The octahedron in the center could be easily distorted, and the distortions will greatly affect the properties of the material, which is the main reason that perovskite has that diversity in electrical, magnetic, and optical properties. Therefore, perovskite has been widely studied in various applications especially in solar cells [38, 39].

1.6.1 Barium Titanate and Strontium Titanate

Alkaline earth titanate is one of the important subfamilies in the perovskite due to their electrical properties. In this thesis, we mainly focus on two of them: $BaTiO_3$ (BTO) and $SrTiO_3$ (STO). One of the important properties of these two materials is that they both go through phase transitions during temperature decreasing

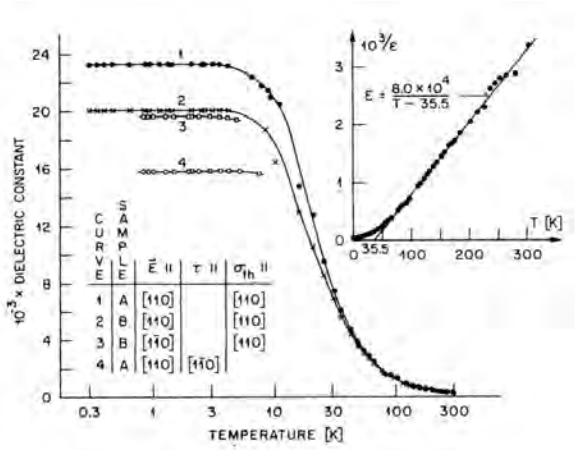

Figure 1.5: Dielectric constant of STO versus temperature. Reprinted figure with permission from [40]. Copyright 2021 by the American Physical Society.

process. Above 400 K for BTO, and above 105 K for STO, both of them are cubic. When temperature decreases to lower than those critical value, they will experience a phase transition. In this transition, the TiO_6 octahedron will be distorted so that they transform to tetragonal structure. Moreover, if the temperature keeps decreasing, further transition sequence could happen: tetragonal $\rightarrow$ orthorhombic $\rightarrow$ rhombohedral. In cubic phase, BTO and STO are paraelectric, while in tetragonal phase, they become ferroelectric. Both BTO and STO has large dielectric constant in ferroelectric phase, however, dielectric constant of the BTO decreases to 0 when temperature goes to 0 [41] while the STO's dielectric constant remains to be an almost constant large value (around 10^4 in SI units) when temperature < 4 K, which is shown in Fig. 1.5. The surprising behavior of STO at extremely low temperature, called quantum paraelectric, was attributed to the quantum fluctuation [40].

Due to the complex structures, BTO and STO are highly anharmonic so that we cannot use the traditional harmonic oscillators to describe their lattice vibrations. To

overcome the shortage of the harmonic potential, a quartic potential was introduced to address the instability of the system [42], which is called the polarizability model. With the extra quartic term, the Hamiltonian is fairly like the free energy in Ginzburg–Landau theory. Applying the mean-field approximation, this model can be solved self-consistently. Although the polarizability model could qualitatively explain the ferroelectricity in perovskite and discover soft optical modes, it is rather parameters-dependent. First-principles calculations have also been implemented in recent years [43, 44, 45, 46] trying to match the measurements. However, the computational results are still not good enough so far. Besides, the large dielectric constants in STO raised by the soft optical modes could also contribute to its large PHE [30]. Therefore, even current first-principles calculations are not perfect, it deserves to try to combine it with the microscopic theory for PHE.

1.7 Objectives

The objectives of this thesis can be divided into two parts, one for the electron dynamics, and the other for the phonon dynamics, which are coupled through electron-phonon interaction. To calculate the transport quantities, one usual method is the non-equilibrium Green's function method (NEGF), which has been developed very well so far [47]. However, NEGF can only deal with small open system, to overcome this shortage, we can combine it with MD method. It has been showed that as long as the electron density is low, it is valid [48]. Therefore, the first objective of this thesis is to numerically calculate the charge transport behaviors in organic polymers using the combined method. Boltzmann transport equation (BTE)

method is another widely used one once the electron and phonon structure of the materials is obtained from first-principles calculations. However, the validity of this method for one dimensional case has not been strictly proved. Thus comparing with the BTE method is the second objective of this thesis.

For phonon dynamics, the thesis focuses on the PHE. Current proposed mechanisms of the PHE all requires significant magnetic field, while according to the general theory for PHE [2], magnetic field is not necessary. Therefore, The third objective of this thesis is to propose a mechanism of PHE induced by electric current and explore its properties. Moreover, there is still a gap between the experiments and theoretical research for PHE. To bridge this gap, this thesis implements a further exploration with the first-principles calculations trying to understand the PHE observed in complex materials, which is the final objective of the thesis.

The thesis may provide insights to understand the electron and phonon dynamics within the electron-phonon interaction. The rest of this thesis is organized as follows. In Chapter 2, NEGF and other methods used in this thesis are provided. Chapter 3 explores the charge transport behaviors in organic polymers. Chapter 4 gives a general description and derivation for the PHE, with which a current-induced PHE is proposed. Based on the research in Chapter 4, first-principles calculations are implemented in Chapter 5. At last, a conclusion of this thesis and an outlook are given in Chapter 6.

Chapter 2

Methods

In this thesis, to explore transport properties in electron and phonon dynamics, NEGF, BTE method and Green-Kubo formula are employed. To figure out the topological structure of an eigensystem, explicit and geometric formulas for Berry curvatures are applied. Moreover, we borrow the density functional theory to implement first-principles calculations for complex materials.

2.1 Nonequilibrium Green's Function Method

The Nonequilibrium Green's Function method, an elegant method handling the nonequilibrium transport problems, was firstly introduced by Schwinger in 1951 [49, 50], and initially applied to solve the Brownian motion problem for a quantum oscillator [51]. Subsequently, Kadanoff and Baym [52], and Keldysh [53] developed equation of motion method and diagrammatic approach, respectively. With the foundation built by them, the NEGF method has been applied in electrical and thermal transport problems [54, 55, 56, 57, 58, 59]. The NEGF method for electron and phonon are similar except for different statistics they obey. Since in this thesis, phonon matters most, we briefly introduce the NEGF method for phonon following

the discipline in the review by Wang *et al.* [60].

2.1.1 Green's Functions for Harmonic Oscillator in Equilibrium

We start with a quantum harmonic oscillator to introduce the definitions of the six Green's functions. By second quantization, a harmonic oscillator can be expressed as follows:

$$H = \frac{1}{2}\dot{u}^2 + \frac{1}{2}\Omega^2 u^2 = \hbar\Omega(a^\dagger a + \frac{1}{2}), \tag{2.1}$$

where $u \equiv \sqrt{m}x = \sqrt{\frac{\hbar}{2\Omega}}(a + a^\dagger)$ with m and x being the mass and the displacement, respectively. $a^\dagger$ and a are the creation and annihilation operators having $[a, a^\dagger] = 1$. The Heisenberg equation determines the evolution of a:

$$\dot{a}(t) = \frac{1}{i\hbar}[a(t), H] = -i\Omega a(t), \tag{2.2}$$

which has the simple solution $a(t) = ae^{-i\Omega t}$. In statistical mechanics, we use the canonical ensemble to describe the equilibrium system where there are many states with corresponding probabilities. The probabilities are given by the density operator $\rho = e^{\beta H}/\mathrm{Tr}(e^{-\beta H})$, $\beta = 1/(k_B T)$. Here k_B is the Boltzmann constant, T is the temperature. With $|n\rangle$ representing the orthonormal basis of the energy eigenstates, we have the typical results in many textbooks,

$$\begin{aligned} &a|n\rangle = \sqrt{n}|n-1\rangle,\ a^\dagger|n\rangle = \sqrt{n+1}|n+1\rangle, \\ &\langle aa\rangle = 0,\ \langle a^\dagger a^\dagger\rangle = 0, \\ &\langle a^\dagger a\rangle = n, \langle aa^\dagger\rangle = 1+n, \end{aligned} \tag{2.3}$$

where $\langle\cdots\rangle = \mathrm{Tr}(\rho\cdots)$ is the ensemble average, and $n = 1/[e^{\beta\hbar\Omega} - 1]$ is the Bose-Einstein distribution function.

Usually, Green's functions are defined with the creation and annihilation operators, but in phonon system, for convenience, we can define the six Green's functions using the u operator directly as follows:

$$\begin{aligned}
&G^{>}(t,t') = -\frac{i}{\hbar}\langle u(t)u(t')^T\rangle,\ G^{<} = -\frac{i}{\hbar}\langle u(t')u(t)^T\rangle^T,\\
&G^{t}(t,t') = \theta(t-t')g^{>}(t,t') + \theta(t'-t)g^{<}(t,t'),\\
&G^{\bar{t}}(t,t') = \theta(t'-t)g^{>}(t,t') + \theta(t-t')g^{<}(t,t'),\\
&G^{r}(t,t') = -\frac{i}{\hbar}\theta(t-t')\langle[u(t),u(t')^T]\rangle,\ G^{a}(t,t') = \frac{i}{\hbar}\theta(t'-t)\langle[u(t),u(t')^T]\rangle.
\end{aligned} \tag{2.4}$$

Here $G^{>}$, $G^{<}$ are called greater and lesser Green's functions, respectively. Combining the greater and lesser Green's functions with a time step function $\theta(t) = 1$ if $t \geqslant 0$ else 0, we obtain time-ordered Green's function G^t and anti-time-ordered Green's function $G^{\bar{t}}$. Furthermore, the commutator between $u(t)$ and $u(t')$ together with the step function forms retarded Green's function G^r and advanced Green's function G^a. T as a superscript indicates matrix transpose, and $\langle[u(t),u(t')^T]$ should be interpreted as $\langle u(t)u(t')^T\rangle - \langle u(t')u(t)^T\rangle^T$. We can easily discover that these six Green's functions are related to each other:

$$\begin{aligned}
G^r - G^a &= G^{>} - G^{<},\\
G^t + G^{\bar{t}} &= G^{>} + G^{<},\\
G^t - G^{\bar{t}} &= G^r + G^a.
\end{aligned} \tag{2.5}$$

These relations hold in both time domain and frequency domain with a Fourier transform defined as $G[\omega] = \int_{-\infty}^{\infty} G(t)e^{i\omega t}dt$. Moreover, in frequency domain, we

have the following relations:

$$\begin{aligned} &G^r[-\omega] = G^r[\omega]^*,\ G^a[\omega] = G^r[\omega]^\dagger, \\ &G^<[\omega]^\dagger = -G^<[\omega],\ G^<[\omega] = G^>[\omega]^T = -G^<[\omega]^* + G^r[\omega]^T - G^r[\omega]^*. \end{aligned} \tag{2.6}$$

These relations can be easily checked by substituting the definitions of the Green's functions.

As an example, we apply these formulas to the harmonic oscillator in equilibrium. With the solution of $a(t)$, the Green's functions are

$$\begin{aligned} G^<(t,t') &= -\frac{i}{2\Omega}\Big[ne^{-i\Omega(t-t')} + (1+n)e^{i\Omega(t-t')}\Big], \\ G^r(t,t') &= -\theta(t-t')\frac{\sin(\Omega t - \Omega t')}{\omega}. \end{aligned} \tag{2.7}$$

The reason they are called the Green's functions is that the retarded Green's function is the solution of the equation

$$\ddot{G}^r(t) + \Omega^2 G^r(t) = -\delta(t), \tag{2.8}$$

where $\delta(t)$ is the Dirac δ function. This is coincident with the original definition of the Green's functions in mathematics. Switching into frequency domain, the Green's functions become

$$\begin{aligned} G^<[\omega] &= -\frac{i\pi}{\Omega}\Big[n\delta(\omega-\Omega) + (n+1)\delta(\omega+\Omega)\Big], \\ G^r[\omega] &= \frac{1}{(\omega+i\eta)^2 - \Omega^2},\ \eta \to 0^+, \end{aligned} \tag{2.9}$$

where η is a positive damping factor to force the integral converge. With the help of the Plemelj formula, which is

$$\frac{1}{x+i\eta} = P\frac{1}{x} - i\pi\delta(x), \tag{2.10}$$

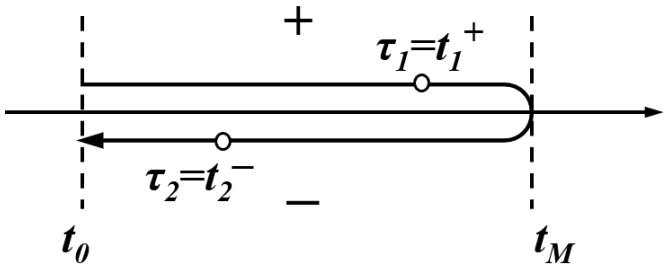

Figure 2.1: Schwinger-Keldysh contour.

where P means the Cauchy principle value, we can further relate the $G^r[\omega]$, $G^a[\omega]$ with the $G^<[\omega]$ that

$$G^<[\omega] = (G^r[\omega] - G^a[\omega])n(\omega). \tag{2.11}$$

Therefore, in equilibrium system, there in fact is only one independent Green's function and usually, we choose the retarded one.

2.1.2 Nonequilibrium Contour-ordered Green's Functions

Nonequilibrium simply means the density operator of the system is not proportional to the canonical distribution $e^{-\beta H}$ any more, therefore, the corresponding six Green's functions have the same forms as we defined in equilibrium. In the six Green's functions, evolution direction in time plays an important role in distinguishing them. Therefore, a new type of Green's functions, contour-ordered Green's functions, is proposed. Since the quantum evolution, represented by the evolution operator $U(t, t')$, can either go forward or backward, we can always treat it as a segment of the contour from $-\infty$ to ∞, then back to $-\infty$ from ∞ [60], as Fig. 2.1 shows. In this way, we define the contour-ordered Green's function as follows:

$$G(\tau, \tau') = -\frac{i}{\hbar}\mathrm{Tr}\Big[\rho(t_0)T_\tau u(\tau)u(\tau')^T\Big], \tag{2.12}$$

where t_0 is a reference time which could be $-\infty$, τ stands for combination of two indices (t, σ), $\sigma = +(-)$ indicates the upper branch (lower branch) of the Schwinger-Keldysh contour shown in Fig. 2.1. T_τ is a contour-order operator ordering the operators along the contour. There are several special rules for calculus and derivative along the contour which should be noted in application [60]:

$$\begin{aligned} &\frac{d}{d\tau} \to \frac{d}{dt}, \frac{df(\tau)}{d\tau} \to \frac{df^\sigma(t)}{dt}, \\ &\int_{\mathcal{C}} d\tau = \int_{-\infty^+}^{\infty} dt^+ + \int_{\infty}^{-\infty^-} dt^- = \sum_{\sigma=\pm} \int_{-\infty}^{\infty} \sigma dt, \\ &\delta(\tau, \tau') = \frac{\partial \theta(\tau, \tau')}{\partial \tau} \to \sigma \delta_{\sigma\sigma'} \delta(t - t'). \end{aligned} \tag{2.13}$$

Exhausting the four combinations of τ, we can map the contour-ordered Green's functions to previously defined Green's functions:

$$G = \begin{pmatrix} G^t & G^< \\ G^> & G^{\bar{t}} \end{pmatrix}. \tag{2.14}$$

With this map, the convolution including contour-ordered Green's functions, for example,

$$C(\tau, \tau') = \int d\tau_1 A(\tau, \tau_1) B(\tau_1, \tau'), \tag{2.15}$$

can be treated as matrix multiplication so that $C^{<,>} = A^r B^{<,>} + A^{<,>} B^a$. More general results are known as the Langreth theorem [61].

2.1.3 Equation of Motion Method

Equation of motion method is an efficient method to start NEGF calculation in coupled system comparing with diagrammatic method. The idea can be illustrated in a coupled harmonic system with a standard Hamiltonian

$$H = \frac{1}{2} p^T p + \frac{1}{2} u^T K u, \tag{2.16}$$

where u is the stack of the displacement of each harmonic oscillator, p is the conjugate momentum vector, and K is the spring constant matrix which is symmetric and positive definite. The first-order equation of motion can be derived according to the previous derivative rules:

$$\frac{\partial G(\tau,\tau')}{\partial \tau} = -\frac{i}{\hbar}\langle T_\tau \dot{u}(\tau) u(\tau')^T\rangle - \frac{i}{\hbar}\delta(\tau,\tau')\langle[u(\tau), u(\tau')^T]\rangle. \tag{2.17}$$

The $\dot{u}(\tau)$ cannot be determined, therefore, we apply one more derivative to both sides, which results in

$$\frac{\partial^2 G(\tau,\tau')}{\partial \tau^2} = -\frac{i}{\hbar}\langle T_\tau \ddot{u}(\tau) u(\tau')^T\rangle - \frac{i}{\hbar}\delta(\tau,\tau')\langle[\dot{u}(\tau), u(\tau')^T]\rangle. \tag{2.18}$$

According to the Heisenberg equation $\ddot{u} = -Ku$ and the commutator $[u(\tau), p(\tau')^T] = i\hbar\delta(\tau,\tau')I$, the second-order equation of motion can be simplified to be

$$\frac{\partial^2 G(\tau,\tau')}{\partial \tau^2} + KG(\tau,\tau') = -\delta(\tau,\tau')I. \tag{2.19}$$

To solve this equation of motion, we treat the system as an open system: a central region with left and right leads. Moreover, we extract the decoupled harmonic oscillators so that the spring constant matrix can be rewritten as follows:

$$K = \begin{pmatrix} K^L & V^{LC} & 0 \\ V^{CL} & K^C & V^{CR} \\ 0 & V^{RC} & K^R \end{pmatrix}, \tag{2.20}$$

where V represents the coupling. We label the contour-ordered Green's functions of the decoupled harmonic oscillators as $g(\tau,\tau') = \mathrm{diag}\{g^L, g^C, g^R\}$, which satisfies the equation of motion,

$$\frac{\partial^2 g^{L,C,R}(\tau,\tau')}{\partial \tau^2} + K^{L,C,R} g(\tau,\tau') = -\delta(\tau,\tau')I. \tag{2.21}$$

It is easy to derive the following Dyson equation:

$$G(\tau,\tau') = g(\tau,\tau') + \int d\tau_1 \int d\tau_2 g(\tau,\tau_1)\Sigma(\tau_1,\tau_2)G(\tau_2,\tau'), \tag{2.22}$$

where Σ is the off-diagonal part of the K [60].

2.2 Boltzmann Transport Equation

Boltzmann transport equation (BTE) is a semi-classical equation proposed by Ludwig Boltzmann in 1872 to describe the statistical behaviors in nonequilibrium thermodynamics [62]. Although it is semi-classical, it is rather powerful which is still widely used in exploring electron and phonon dynamics in various materials. The kernel idea of the BTE is to greatly reduce the enormous degrees of freedom in analyzing the positions and momenta of each particle by employing probability distributions of particles. In this way, the effect of uncountable collisions among particles can be described by some macroscopic values, *e.g.* the relaxation time.

Consider a distribution $f_{\boldsymbol{k}}(\boldsymbol{r})$ measuring the amount of particles in the infinitesimal neighbourhood of $\boldsymbol{r}$ with state $\boldsymbol{k}$, when the system is in nonequilibrium, obviously the distribution varies in time. There are three mechanisms that can affect the distribution [62]: drift, external fields and scattering. Drift refers to particles' entering to state $\boldsymbol{r}$ from adjacent regions and particles' leaving from current position at the same time. Therefore, this mechanism must be related to the velocities of particles,

$$\dot{f}_{\boldsymbol{k}}|_{\text{drift}} = -\boldsymbol{v}_{\boldsymbol{k}} \cdot \frac{\partial f_{\boldsymbol{k}}}{\partial \boldsymbol{r}}. \tag{2.23}$$

External fields can change the state $\boldsymbol{k}$ of particles by the electromagnetic interaction,

and the rate of the change is

$$\dot{\boldsymbol{k}} = \frac{e}{\hbar}(\boldsymbol{E} + \boldsymbol{v}_{\boldsymbol{k}} \times \boldsymbol{B}). \tag{2.24}$$

Due to $\dot{\boldsymbol{k}}$, the distribution will change at the rate

$$\dot{f}_{\boldsymbol{k}}|_{\text{field}} = -\frac{e}{\hbar}(\boldsymbol{E} + \boldsymbol{v}_{\boldsymbol{k}} \times \boldsymbol{B}) \cdot \frac{\partial f_{\boldsymbol{k}}}{\partial \boldsymbol{k}}. \tag{2.25}$$

Scattering, labelled as $\dot{f}_{\boldsymbol{k}}|_{\text{scatt}}$, is a net effect containing all the microscopic collisions in the system, and we cannot rigorously address it without appropriate approximations.

Combining all the three terms, we obtain the general BTE,

$$\frac{\partial f_{\boldsymbol{k}}}{\partial t} + \boldsymbol{v}_{\boldsymbol{k}} \cdot \frac{\partial f_{\boldsymbol{k}}}{\partial \boldsymbol{r}} + \frac{e}{\hbar}(\boldsymbol{E} + \boldsymbol{v}_{\boldsymbol{k}} \times \boldsymbol{B}) \cdot \frac{\partial f_{\boldsymbol{k}}}{\partial \boldsymbol{k}} = \frac{\partial f_{\boldsymbol{k}}}{\partial t}|_{\text{scatt}}. \tag{2.26}$$

In the steady state, the first term must vanish. In equilibrium, the distribution function $f_{\boldsymbol{k}} \to f^0_{\boldsymbol{k}}$ is the Bose-Einstein or Fermi-Dirac distribution.

2.2.1 Linearized BTE and Single-mode Relaxation-time Approximation

The difficulty to solve the BTE is the complexity of the scattering term. If we assume the deviation from equilibrium is small, we may only keep the lowest order of the change $(f_{\boldsymbol{k}} - f^0_{\boldsymbol{k}})$ in the scattering term while replace $f_{\boldsymbol{k}}$ with $f^0_{\boldsymbol{k}}$ for all other terms. In this way, the scattering can be simplified to be the integrated probability of the particles jumping from one state to another,

$$\begin{aligned} \dot{f}_{\boldsymbol{k}}|_{\text{scatt}} &= \int [f_{\boldsymbol{k}'}(1 - f_{\boldsymbol{k}}) - f_{\boldsymbol{k}}(1 - f_{\boldsymbol{k}'})] P(\boldsymbol{k} \to \boldsymbol{k}') d\boldsymbol{k}' \\ &\approx \int (f_{\boldsymbol{k}'} - f_{\boldsymbol{k}}) P(\boldsymbol{k} \to \boldsymbol{k}') d\boldsymbol{k}', \end{aligned} \tag{2.27}$$

where we have used the principle of microscopic reversibility $P(\boldsymbol{k} \to \boldsymbol{k}') = P(\boldsymbol{k}' \to \boldsymbol{k})$. Therefore, the linearized BTE is

$$\boldsymbol{v}_{\boldsymbol{k}} \cdot \frac{\partial f^0_{\boldsymbol{k}}}{\partial \boldsymbol{r}} + \frac{e}{\hbar}(\boldsymbol{E} + \boldsymbol{v}_{\boldsymbol{k}} \times \boldsymbol{B}) \cdot \frac{\partial f^0_{\boldsymbol{k}}}{\partial \boldsymbol{k}} = \int (f_{\boldsymbol{k}'} - f_{\boldsymbol{k}}) P(\boldsymbol{k} \to \boldsymbol{k}') d\boldsymbol{k}'. \tag{2.28}$$

Moreover, with further assumptions, linearized BTE could have explicit solutions. First, we assume the distribution may only rely on the energy of particles $\varepsilon_{\boldsymbol{k}}$ and the energy surface is spherical, *i.e.* $\varepsilon_{\boldsymbol{k}} \propto k^2$. Second, the probability should only depend on the angle between two vectors so that the integral can be extracted out to be a mode-dependent value, labelled as $1/\tau(k)$, the single-mode relaxation time. Thereafter, the BTE becomes

$$\boldsymbol{v}_{\boldsymbol{k}} \cdot \Big[\frac{\partial f^0_{\boldsymbol{k}}}{\partial \boldsymbol{r}} + e(\boldsymbol{E} + \boldsymbol{v}_{\boldsymbol{k}} \times \boldsymbol{B}) \cdot \frac{\partial f^0_{\boldsymbol{k}}}{\partial \varepsilon_{\boldsymbol{k}}}\Big] = -\frac{f_{\boldsymbol{k}} - f^0_{\boldsymbol{k}}}{\tau(k)}. \tag{2.29}$$

Once we have solved the BTE, we can calculate many transport observables, for example, the electrical conductivity. The electric current $\boldsymbol{J}$, by definition, is $\int e\boldsymbol{v}_{\boldsymbol{k}} f_{\boldsymbol{k}} d\boldsymbol{k}$. Substituting the solution of $f_{\boldsymbol{k}}$, we obtain [62]

$$\boldsymbol{J} = -e^2 \int \boldsymbol{v}_{\boldsymbol{k}} \boldsymbol{v}_{\boldsymbol{k}} \cdot \frac{\partial f^0_{\boldsymbol{k}}}{\partial \varepsilon_{\boldsymbol{k}}} \boldsymbol{E} \tau(k) d\boldsymbol{k}. \tag{2.30}$$

Since $\boldsymbol{J} = \sigma \boldsymbol{E}$, the electrical conductivity tensor can be extracted out.

2.3 Berry Curvature

Berry curvatures contain information of the parameter space and determine its topological structure. Moreover, Berry curvatures are closely related some physical observables, for example, electrical conductivity in quantum Hall effect where $\sigma_{xy} = -\frac{e^2}{\hbar}\Omega_{xy}$. In PHE, Berry curvatures are also the key ingredients to

calculate the phonon Hall conductivity. Therefore, in this section, two methods to calculate Berry curvatures are given.

The first one is by explicit derivation starting from the eigen equation. Recall our introduction for Berry phase in Chapter 2, the Berry curvatures are defined as follows:

$$\Omega_{\mu\nu} = -\mathrm{Im}\Big[\langle\frac{\partial n(\boldsymbol{R})}{\partial R^{\mu}}|\frac{\partial n(\boldsymbol{R})}{\partial R^{\nu}}\rangle - (\mu \leftrightarrow \nu)\Big]. \tag{2.31}$$

Since $H(\boldsymbol{R})|n(\boldsymbol{R})\rangle = E_n|n(\boldsymbol{R})\rangle$, applying partial derivative to both sides, we obtain

$$\frac{\partial H(\boldsymbol{R})}{\partial R^{\nu}}|n(\boldsymbol{R})\rangle + H(\boldsymbol{R})|\frac{\partial n(\boldsymbol{R})}{\partial R^{\nu}}\rangle = \frac{\partial E_n(\boldsymbol{R})}{\partial R^{\nu}}|n(\boldsymbol{R})\rangle + E_n(\boldsymbol{R})|\frac{\partial n(\boldsymbol{R})}{\partial R^{\nu}}\rangle. \tag{2.32}$$

Afterwards, we multiply $\langle m(\boldsymbol{R})|$ to the left on both sides so that

$$\langle m(\boldsymbol{R})|\frac{\partial H(\boldsymbol{R})}{\partial R^{\nu}}|n(\boldsymbol{R})\rangle = (E_n - E_m)\langle m(\boldsymbol{R})|\frac{\partial n(\boldsymbol{R})}{\partial R^{\nu}}\rangle + \frac{\partial E_n(\boldsymbol{R})}{\partial R^{\nu}}\delta_{mn}. \tag{2.33}$$

Inserting the identity $\sum\limits_{m}|m(\boldsymbol{R})\rangle\langle m(\boldsymbol{R})| = I$ into the Eq. (2.31), the Berry curvatures becomes

$$\begin{aligned}\Omega_{\mu\nu} &= -\mathrm{Im}\Big[\sum_{m}\langle\frac{\partial n(\boldsymbol{R})}{\partial R^{\mu}}|m(\boldsymbol{R})\rangle\langle m(\boldsymbol{R})|\frac{\partial n(\boldsymbol{R})}{\partial R^{\nu}}\rangle - (\mu \leftrightarrow \nu)\Big] \\ &= -\mathrm{Im}\Big[\sum_{m\neq n}\frac{\langle n(\boldsymbol{R})|\frac{\partial H(\boldsymbol{R})}{\partial R^{\mu}}|m(\boldsymbol{R})\rangle\langle m(\boldsymbol{R})|\frac{\partial H(\boldsymbol{R})}{\partial R^{\nu}}|n(\boldsymbol{R})\rangle}{(E_n(\boldsymbol{R}) - E_m(\boldsymbol{R}))^2} - (\mu \leftrightarrow \nu)\Big].\end{aligned} \tag{2.34}$$

The $m = n$ case is excluded because it is real: $\langle n(\boldsymbol{R})|n(\boldsymbol{R})\rangle = 1 \rightarrow \langle n(\boldsymbol{R})|\frac{\partial n(\boldsymbol{R})}{\partial R^{\nu}}\rangle = -(\langle n(\boldsymbol{R})|\frac{\partial n(\boldsymbol{R})}{\partial R^{\nu}}\rangle)^*$. In this way, the partial derivative now is applied to the Hamiltonian, which is much easier to calculate in practice.

The second method is a geometric method, which is usually used in lattice system. The definition of the Berry phase is the net phase in the evolution of a state through a closed loop, therefore, we can split the loop into infinitesimal segments and extract

the Berry phase from a sequence of the inner products [16],

$$\gamma_n = -\mathrm{Im}\Big[\ln\Big(\langle n_0|n_1\rangle\langle n_1|n_2\rangle\cdots\langle n_{N-1}|n_0\rangle\Big)\Big], \tag{2.35}$$

where the subscript $i = 0, 1, \cdots, N-1$ represents $\boldsymbol{R}_0, \boldsymbol{R}_1, \cdots, \boldsymbol{R}_{N-1}$. This expression can be easily related to the continuum formula of the Berry phase by Taylor expansion up to the first order,

$$\begin{aligned}\ln\langle n(\boldsymbol{R})|n(\boldsymbol{R}+d\boldsymbol{R})\rangle &= \ln\langle n(\boldsymbol{R})|\Big(|n(\boldsymbol{R})\rangle + \frac{\partial|n(\boldsymbol{R})\rangle}{\partial\boldsymbol{R}}\cdot d\boldsymbol{R}+\cdots\Big)\\ &= \ln\Big(1+\langle n(\boldsymbol{R})|\partial_{\boldsymbol{R}}|n(\boldsymbol{R})\rangle\cdot d(\boldsymbol{R})+\cdots\Big)\\ &= \langle n(\boldsymbol{R})|\partial_{\boldsymbol{R}}|n(\boldsymbol{R})\rangle\cdot d(\boldsymbol{R})+\cdots .\end{aligned} \tag{2.36}$$

After taking the continuum limit, the higher order terms can be discarded so that $\gamma_n = -\mathrm{Im}\int_{\mathcal{C}}\langle n(\boldsymbol{R})|\partial_{\boldsymbol{R}}|n(\boldsymbol{R})\rangle\cdot d(\boldsymbol{R})$. Since Berry phase can also be regarded as a surface integral of the Berry curvatures over the area enclosed by the loop path $\mathcal{C}$ using the Stokes' theorem, the Berry curvatures can be approximated to be the Berry phase through an infinitesimal loop divided by the area it suspends,

$$\boldsymbol{\Omega}_n(\boldsymbol{R}) \approx \frac{\gamma_n}{d\boldsymbol{S}}, \tag{2.37}$$

where vector $d\boldsymbol{S}$ points to the direction of the normal vector of the area dS. In the continuum limit, it has been proved this simple formula can produce correctly the Berry curvatures [63].

The explicit formula is elegant enough to be used in calculation for simple models, while for more complicated Hamiltonian or a numerical one, it could be troublesome and inefficient. Therefore, geometric method is more suitable in complex system.

2.4 Green-Kubo formula

Green-Kubo formula is a widely used formula to study transport phenomena which generally describes the response of a system to an external perturbation up to the first order. Since it only considers the first order perturbation, it is named as the *linear response* theory and not rigorous. However, it is proven to be rather convincing in a large number of applications, for example, the calculation of thermal conductivity. This formula was developed by Melville Green in 1954 [64] and Royogo Kubo in 1957 [65].

Consider a system with a time-dependent perturbation: $H(t) = H_0 + H'(t)$, where $H'(t)$ is an adiabatic perturbation turned on at time 0. Under this perturbation, the expectation of an observable A will vary from its value in equilibrium:

$$\Delta\langle A\rangle_t = \langle A\rangle_t - \langle A\rangle_0 = \mathrm{Tr}[\rho(t)A] - \mathrm{Tr}(\rho_0 A), \tag{2.38}$$

where $\rho_0 = \frac{1}{\mathcal{Z}} e^{-\beta\mathcal{H}}$ is the density matrix in equilibrium, $\rho(t)$ is the density matrix at time t, $\beta = 1/k_B T$, T is the temperature, and $\mathcal{H} = H(t) - \mu N$ in general if the system has a chemical potential μ. We define $\rho(t) = \rho_0 + \delta\rho(t)$, then according to its equation of motion within the Schrödinger picture,

$$\frac{d\delta\rho(t)}{dt} = \frac{1}{i\hbar}\Big([\mathcal{H}_0, \rho_0] + [\mathcal{H}_0, \delta\rho(t)] + [H'(t), \rho_0] + [H'(t), \delta\rho(t)]\Big), \tag{2.39}$$

where $\mathcal{H}_0 = H_0 - \mu N$. Note that $[\mathcal{H}_0, \rho_0] = 0$ and $[H'(t), \delta\rho(t)]$ is a second order correction. Therefore, if we keep only the terms up to first order, the equation becomes

$$i\hbar\frac{d\delta\rho(t)}{dt} - [\mathcal{H}_0, \delta\rho(t)] = [H'(t), \rho_0]. \tag{2.40}$$

For convenience, we switch to interaction picture such that

$$\delta\rho_I(t) = e^{\frac{i}{\hbar}\mathcal{H}_0 t}\delta\rho(t)e^{-\frac{i}{\hbar}\mathcal{H}_0 t}, H'_I(t) = e^{\frac{i}{\hbar}\mathcal{H}_0 t}H'(t)e^{-\frac{i}{\hbar}\mathcal{H}_0 t}. \tag{2.41}$$

Then the equation is further simplified to be

$$i\hbar\frac{d\delta\rho_I(t)}{dt} = [H'_I(t), \rho_0], \tag{2.42}$$

with the solution $\delta\rho_I(t) = -\frac{i}{\hbar}\int_0^t dt'[H'_I(t'), \rho_0]$. If we switch back to Schrödinger picture, and assume the perturbation is $H'(t) = Bf(t)$, where $f(t)$ is a real function, the deviation of the expectation of the observable A is

$$\Delta\langle A\rangle_t = -\frac{i}{\hbar}\int_0^t dt' \mathrm{Tr}\{e^{\frac{i}{\hbar}\mathcal{H}_0(t'-t)}[B, \rho_0]e^{-\frac{i}{\hbar}\mathcal{H}_0(t'-t)}A\}f(t'). \tag{2.43}$$

Defining $A(t) \equiv e^{\frac{i}{\hbar}\mathcal{H}_0 t}Ae^{-\frac{i}{\hbar}\mathcal{H}_0 t}, B(t) \equiv e^{\frac{i}{\hbar}\mathcal{H}_0 t}Be^{-\frac{i}{\hbar}\mathcal{H}_0 t}$ and applying the identity of the commutator, $\mathrm{Tr}\{[B, \rho_0]A\} = \mathrm{Tr}\{\rho_0[A, B]\}$, we obtain

$$\Delta\langle A\rangle_t = -\frac{i}{\hbar}\int_0^t dt' \mathrm{Tr}\{\rho_0[A(t), B(t')]\}f(t'). \tag{2.44}$$

Furthermore, we can define a response function,

$$\chi_{AB}(t - t') \equiv -\frac{i}{\hbar}\theta(t - t')\mathrm{Tr}\{\rho_0[A(t), B(t')]\} \tag{2.45}$$

so that

$$\Delta\langle A\rangle_t = \int_0^t dt'\chi_{AB}(t - t')f(t'). \tag{2.46}$$

2.4.1 Kubo Identity

Define the canonical correlator as follows:

$$\langle A(t); B(t')\rangle \equiv \frac{1}{\beta}\int_0^\beta d\lambda \mathrm{Tr}\Big[\rho_0 e^{\lambda\mathcal{H}_0}A(t)e^{-\lambda\mathcal{H}_0}B(t')\Big]. \tag{2.47}$$

Then the Kubo identity says

$$\begin{aligned}
\langle \dot{A}(t); B(t')\rangle &= \frac{1}{\beta}\mathrm{Tr}\{\rho_0 \int_0^\beta d\lambda e^{\lambda\mathcal{H}_0}\dot{A}(t)e^{-\lambda\mathcal{H}_0}B(t')\} \\
&= \frac{i}{\hbar\beta}\mathrm{Tr}\{\rho_0 \int_0^\beta d\lambda e^{\lambda\mathcal{H}_0}[\mathcal{H}_0, A(t)]e^{-\lambda\mathcal{H}_0}B(t')\} \\
&= \frac{i}{\hbar\beta}\mathrm{Tr}\{\rho_0 \int_0^\beta d\lambda \frac{d}{d\lambda}[e^{\lambda\mathcal{H}_0}A(t)e^{-\lambda\mathcal{H}_0}]B(t')\} \\
&= \frac{i}{\hbar\beta}\mathrm{Tr}\{\rho_0[e^{\beta\mathcal{H}_0}A(t)e^{-\beta\mathcal{H}_0} - A(t)]B(t')\} \\
&= \frac{i}{\hbar\beta}\mathrm{Tr}\{[A(t), \rho_0]B(t')\} \\
&= \frac{1}{\beta}\Big(- \frac{i}{\hbar}\mathrm{Tr}\{\rho_0[A(t), B(t')]\}\Big),
\end{aligned} \tag{2.48}$$

where we have used the fact that $\dot{A}(t) = \frac{i}{\hbar}[\mathcal{H}_0, A(t)]$. Therefore, the response function can be rewritten as

$$\chi_{AB}(t - t') = \beta\langle \dot{A}(t); B(t')\rangle. \tag{2.49}$$

2.5 Density Functional theory

Density functional theory (DFT) is a remarkable theory that make it possible to calculate complicated structures in various real materials. Instead of solving the Schrödinger equation of the N-electron wave function, DFT follows a new scheme handling the electron density $n(\boldsymbol{r})$ where $\boldsymbol{r}$ is the coordinates of electrons.

Generally, the non-relativistic Hamiltonian for a molecule is

$$\begin{aligned}
H &= T_N(\boldsymbol{R}) + T_e(\boldsymbol{r}) + U_{eN}(\boldsymbol{r}, \boldsymbol{R}) + U_{ee}(\boldsymbol{r}) + U_{NN}(\boldsymbol{R}) \\
&= -\sum_i \frac{\hbar^2}{2M_i}\nabla^2_{\boldsymbol{R}_i} - \frac{\hbar^2}{2m_e}\nabla^2_{\boldsymbol{r}_i} - \sum_i\sum_j \frac{Z_i e^2}{4\pi\epsilon_0}|\boldsymbol{R}_i - \boldsymbol{r}_j| \\
&+ \sum_i\sum_{j>i} \frac{e^2}{4\pi\epsilon_0|\boldsymbol{r}_i - \boldsymbol{r}_j|} + \sum_i\sum_{j>i} \frac{Z_i Z_j e^2}{4\pi\epsilon_0|\boldsymbol{R}_i - \boldsymbol{R}_j|},
\end{aligned} \tag{2.50}$$

where i, j label the electrons and nuclei, $\boldsymbol{R}$ and $\boldsymbol{r}$ are the coordinates for electrons and nuclei, respectively, M_i refers to the mass of each nucleus with Z_i being the associated charge. T_N and T_e are the kinetic energies of electrons and nuclei. U_{NN} and U_{ee} are the corresponding potential energies. U_{eN} represents the Coulombic attraction among electrons and nuclei, which mixes the electronic and nuclear coordinates so that we can not use the product of electronic and nuclear wavefunction to obtain the total wavefunction. To separate the mixed coordinates, the Born-Oppenheimer approximation is assumed under the fact that a nucleus is much heavier than an electron. Therefore, with this approximation, the nuclear coordinates $\boldsymbol{R}$ could be regarded as parameters in electronic wavefunction, *i.e.* the total wavefunction can be separated as $\Psi_{\text{total}} = \psi_e(\boldsymbol{r}; \boldsymbol{R})\psi_N(\boldsymbol{R})$. In this way, nuclei are just parametrically distributed in the space with electrons moving around.

Having made the Born-Oppenheimer approximation, from the electrons' perspective, the T_n can be neglected and the U_{nn} can also be excluded since it only contributes a constant. Therefore, the Schrödinger equation for electrons can be written as

$$H_e\psi_e(\boldsymbol{r}; \boldsymbol{R}) = [T_e(\boldsymbol{r}) + U_{eN}(\boldsymbol{r}, \boldsymbol{R}) + U_{ee}(\boldsymbol{r})]\psi_e(\boldsymbol{r}; \boldsymbol{R}) = E_e\psi_e(\boldsymbol{r}; \boldsymbol{R}). \tag{2.51}$$

The total eigen equation is

$$\begin{aligned} H\Psi_{\text{total}}(\boldsymbol{r}, \boldsymbol{R}) = {} & [T_N + U_{NN} + E_e]\Psi_{\text{total}}(\boldsymbol{r}, \boldsymbol{R}) \\ & - \sum_i \frac{\hbar^2}{2M_i}[2\boldsymbol{\nabla}_{\boldsymbol{R}_i}\psi_e(\boldsymbol{r}; \boldsymbol{R}) \cdot \boldsymbol{\nabla}_{\boldsymbol{R}_i}\psi_N(\boldsymbol{R}) + \psi_N(\boldsymbol{R})\nabla^2_{\boldsymbol{R}_i}\psi_e(\boldsymbol{r}; \boldsymbol{R})]. \end{aligned} \tag{2.52}$$

If we assume the electronic wavefunctions do not vary with respect to the nuclear

coordinates, the nuclear wavefunctions satisfies

$$H\psi_N(\boldsymbol{R}) = [T_N + U_{NN} + E_e]\psi_N(\boldsymbol{R}) \equiv E_{\text{total}}\psi_N(\boldsymbol{R}). \tag{2.53}$$

This equation can be interpreted as the nuclei evolve in an effective potential including the electronic contribution.

Although the Born-Oppenheimer approximation has simplified the total eigen equation, it is still impossible to solve the Eq. (2.51) in general. Therefore, Hartree made a great progress with a self-consistent field method by assuming electrons are independent from each other and the original interacting terms are included in a mean field [66]. In the Hartree's method, the electronic Schrödinger equation can be rewritten as

$$H_e\psi_e(\boldsymbol{r}) = \sum_i [T_e(\boldsymbol{r}_i) + U_{\text{ext}}(\boldsymbol{r}_i) + U_{\text{H}}(\boldsymbol{r}_i)]\psi_e(\boldsymbol{r}) = E_e\psi_e(\boldsymbol{r}). \tag{2.54}$$

Here $U_{\text{ext}}(\boldsymbol{r}_i)$ is the potential from ions and $U_{\text{H}}(\boldsymbol{r}_i)$ is the Hartree potential from averaging all other electrons. Since each electron is independent, the electronic wavefunction should be a sequence of product,

$$\psi_e(\boldsymbol{r}_1, \boldsymbol{r}_2, \cdots, \boldsymbol{r}_n) = \phi_e(\boldsymbol{r}_1)\phi_e(\boldsymbol{r}_2)\cdots\phi_e(\boldsymbol{r}_n). \tag{2.55}$$

Each one-electron wavefunctions $\phi_e(\boldsymbol{r}_i)$ will satisfy corresponding Schrödinger equation: $H_{e,i}\phi_e(\boldsymbol{r}_i) = E_{e,i}\phi_e(\boldsymbol{r}_i)$, where $\sum_i H_{e,i} = H_e$. Obviously, Hartree's method has greatly reduced the complexity of the original many-body problem by converting it into a collection of one-body problems.

2.5.1 Hohenberg-Kohn Theorems

In Hartree's pioneer work, two basic principles in quantum physics, the anti-symmetry principle and the Pauli's exclusion principle, are completely excluded. Therefore, the associated exchange and correlation energies are not considered. Fock came up with a solution to include the missing terms [67]. In the final formulation, the electronic wavefunction is elegantly expressed by Slater determinant containing all possible linear combinations of one-electron wavefunctions. The updated method is called the Hartree-Fock method.

Although the Hartree-Fock method has already succeeded in handling the exchange energy, the method itself is still limited by the number of electrons in practice. Ways to deal with electronic wavefunctions did not achieve great success, new methodology should be considered. Inspired by the earliest scheme proposed by Thomas and Fermi, who dealt with the electron density and energy functional, Hohenberg and Kohn made a great breakthrough in 1964 [68].

The Hohenberg-Kohn theorems redefine the electronic Hamiltonian H_e as the sum of two terms: $F \equiv T_e + U_{ee}$ only accounting for electrons, and the external potential v_{ext} accounting for the electron-ion interaction. For simplicity, we ignore the subscript and all items we discussed in this section are for electrons. The expectation value of the energy and the electron density are obtained as follows:

$$\begin{aligned} E &= \langle \Psi | H | \Psi \rangle \\ n(\boldsymbol{r}) &= \langle \Psi | n(\boldsymbol{r}) | \Psi \rangle, \end{aligned} \tag{2.56}$$

where E contains the external potential $v_{\text{ext}}(\boldsymbol{r})$.There are two theorems in the

Hohenberg-Kohn theorems, one is about the uniqueness of $v_{\text{ext}}(\boldsymbol{r})$ as a functional of $n(\boldsymbol{r})$, the other is the variational principle.

2.5.1.1 The First Hohenberg-Kohn theorem

The first Hohenberg-Kohn theorem says: *the external potential $v_{\text{ext}}(\boldsymbol{r})$, and hence the total energy, is a unique functional of the ground state electron density $n(\boldsymbol{r})$.*

We can prove this theorem by contradiction. Assuming two different external potentials $v^1_{\text{ext}}(\boldsymbol{r})$ and $v^2_{\text{ext}}(\boldsymbol{r})$ produce the same electron density $n_0(\boldsymbol{r})$, the corresponding Hamiltonian H_1 and H_2 will have two different ground states, Ψ_1 and Ψ_2. Ground states have lowest energy, therefore,

$$\begin{aligned} E^1_0 &= \langle\Psi_1|H_1|\Psi_1\rangle < \langle\Psi_2|H_1|\Psi_2\rangle = \langle\Psi_2|H_2|\Psi_2\rangle + \langle\Psi_2|(H_1 - H_2)|\Psi_2\rangle \\ E^1_0 &< E^2_0 + \int n_0(\boldsymbol{r})[v^1_{\text{ext}}(\boldsymbol{r}) - v^2_{\text{ext}}(\boldsymbol{r})]d\boldsymbol{r}. \end{aligned} \tag{2.57}$$

Equivalently, we also have

$$E^2_0 < E^1_0 + \int n_0(\boldsymbol{r})[v^2_{\text{ext}}(\boldsymbol{r}) - v^1_{\text{ext}}(\boldsymbol{r})]d\boldsymbol{r}. \tag{2.58}$$

Combining the Eq. (2.57) and Eq. (2.58), we obtain a contradiction: $E^1_0 + E^2_0 < E^1_0 + E^2_0$. Therefore, the external potential $v_{\text{ext}}(\boldsymbol{r})$ is indeed uniquely determined by the ground state density.

2.5.1.2 The Second Hohenberg-Kohn theorem

The second Hohenberg-Kohn theorem says: *the ground state energy can be obtained variationally: the density that minimizes the total energy is the exact ground state density.*

The first theorem indicates the ground state wavefunction Ψ and the expectation value of the Hamiltonian E are functional of $n(\boldsymbol{r})$. A density that is the ground-state

of some external potential is known as v-representable. If there is another density $n(\boldsymbol{r})$ with which the energy reaches the minimum and it is different from the ground state density $n_0(\boldsymbol{r})$, then one has

$$E_0 = E_{v_{\text{ext}}}[n_0] > E_{v_{\text{ext}}}[n] = \langle \Psi | H_0 | \Psi \rangle. \tag{2.59}$$

However, according to the Rayleigh-Ritz variational principle, $\langle \Psi | H_0 | \Psi \rangle >= E_0$ for any trial wavefunction Ψ. Therefore, the second Hohenberg-Kohn theorem is valid.

For any given $v_{\text{ext}}(\boldsymbol{r})$, we have

$$E_{\text{ext}}[n] = F_{\text{HK}}[n] + \int n(\boldsymbol{r}) U_{\text{ext}}(\boldsymbol{r}) d\boldsymbol{r}, \tag{2.60}$$

where $F_{\text{HK}}[n] = \langle \Psi_0(n) | F | \Psi_0(n) \rangle$. Minimizing the energy by varying the density, we can approach the ground state energy.

2.5.2 Kohn-Sham Equation

Although Hohenberg-Kohn theorems enable us calculate the ground state energy by varying the electron density to minimize the energy, they do not provide a practical method. Subsequently, Kohn and Sham constructed a fictitious system of non-interacting particles generating the same density as any interacting system [69]. In this system, they map the interactions into an effective single-particle potential U_{eff}, the Kohn-Sham potential, to obtain the one-electron Schrödinger equation, which is known as the Kohn-Sham Equation. This equation greatly boosts the numerical calculations for real materials.

Kohn-Sham method regroups the Hamiltonian in the Eq. (2.60) to form an

exchange-correlation energy $E_{\rm xc}$:

$$\begin{aligned} E_{\rm ext}[n] &= F_{\rm HK}[n] + \int n(\boldsymbol{r}) U_{\rm ext}(\boldsymbol{r}) d\boldsymbol{r} \\ &= T_{\rm non}[n] + E_{\rm H}[n] + E_{\rm xc}[n] + \int n(\boldsymbol{r}) U_{\rm ext}(\boldsymbol{r}) d\boldsymbol{r}. \end{aligned} \tag{2.61}$$

Here the exchange-correlation energy $E_{\rm xc}[n]$ is defined as follows:

$$\begin{aligned} E_{\rm xc}[n] &= T[n] - T_{\rm non}[n] + E_{\rm ee}[n] - E_{\rm H}[n] \\ &\equiv T_{\rm int}[n] + E_{\rm x}[n] + E_{\rm int}[n] \\ &\equiv E_{\rm x}[n] + E_{\rm c}[n], \end{aligned} \tag{2.62}$$

where the kinetic energy $T[n]$ is divided into the non-interacting $T_{\rm non}[n]$ and interacting $T_{\rm int}[n]$, $E_{\rm x}$ and $E_{\rm int}[n]$ represent the exchange energy and correlations among different electrons, respectively, $E_{\rm c}$ contains all the correlation energies. The extracted $E_{\rm H}[n]$ is the Hartree (electrostatic) energy of the electrons,

$$E_{\rm H}[n(\boldsymbol{r})] = \frac{1}{2} \int \int \frac{n(\boldsymbol{r}) n(\boldsymbol{r}')}{|\boldsymbol{r} - \boldsymbol{r}'|} d\boldsymbol{r} d\boldsymbol{r}'. \tag{2.63}$$

For a system with the total number of the electrons fixed as N, according to the second Hohenberg-Kohn theorem, we need to solve a variational problem which is

$$\delta \Big[F[n] + \int U_{\rm ext}(\boldsymbol{r}) n(\boldsymbol{r}) d\boldsymbol{r} - \mu \Big(\int n(\boldsymbol{r}) d\boldsymbol{r} - N \Big) \Big] = 0, \tag{2.64}$$

where μ is the chemical potential. The associated Euler-Lagrange equation is

$$\mu = \frac{\delta F[n(\boldsymbol{r})]}{\delta n(\boldsymbol{r})} + U_{\rm ext}(\boldsymbol{r}) \equiv \frac{\delta T_{\rm non}[n(\boldsymbol{r})]}{\delta n(\boldsymbol{r})} + U_{\rm eff}(\boldsymbol{r}). \tag{2.65}$$

Here the Kohn-Sham potential, $U_{\rm eff}(\boldsymbol{r}) \equiv U_{\rm ext}(\boldsymbol{r}) + U_{\rm H}(\boldsymbol{r}) + U_{\rm xc}(\boldsymbol{r})$. The Hartree potential and the exchange-correlation potential can be written as

$$\begin{aligned} U_{\rm H}(\boldsymbol{r}) &= \frac{\delta E_{\rm H}[n(\boldsymbol{r})]}{\delta n(\boldsymbol{r})} = \int \frac{n(\boldsymbol{r}')}{|\boldsymbol{r} - \boldsymbol{r}'|} d\boldsymbol{r}', \\ U_{\rm xc}(\boldsymbol{r}) &= \frac{\delta E_{\rm xc}[n(\boldsymbol{r})]}{\delta n(\boldsymbol{r})}. \end{aligned} \tag{2.66}$$

Then the effective non-interacting Schrödinger equation for the orthonormal single-electron states ϕ_i is

$$\Big[-\frac{1}{2}\nabla^2 + U_{\text{eff}}(\boldsymbol{r})\Big]\phi_i(\boldsymbol{r}) = \varepsilon_i\phi_i(\boldsymbol{r}), \tag{2.67}$$

where ε_i are the corresponding Lagrange multipliers. The density can be constructed by summing over all the states up to Fermi energy:

$$n(\boldsymbol{r}) = \sum_i^N |\phi(\boldsymbol{r})|^2, \tag{2.68}$$

and the total ground state wavefunction of this system is constructed by a Slater determinant of $\phi_i(\boldsymbol{r}_i)$:

$$\Psi_{\text{KS}} = \frac{1}{\sqrt{(N!)}}\det[\phi_1(\boldsymbol{r}_1)\phi_2(\boldsymbol{r}_2)\cdots\phi_N(\boldsymbol{r}_N)]. \tag{2.69}$$

So far we have built up the base of the DFT. The only left problem is that the exact form of the exchange-correlation potential U_{xc} is unknown and approximations must be applied. There are many successful approximations, such as the local density approximation (LDA) [69] made by Kohn-Sham themselves, generalized gradient approximation (GGA) [70], and other complex approximations. Although they are still approximations, the obtained results are in good agreement with experiments for many materials making the DFT a powerful method in modern physics. Moreover, many textbooks and developed software packages focusing on the practical applications of the DFT have greatly deepen our understanding in condensed mater physics.

Chapter 3

Charge Transport in Organic Polymers

In this chapter, we combine the NEGF method with the MD method to numerically calculate the charge transport behaviors in the organic polymer, and as an initial proof of concept, we apply it to a famous one-dimensional (1-D) model, the Su-Schrieffer-Heeger (SSH) model [4], which describes trans-polyacetylene, one kind of organic polymer. Besides, we follow the standard routine to explicitly calculate the diffusion constant for the SSH model based on the BTE method and compare the two results. Furthermore, based on the first-principles calculations [71], we implement a similar simulation for another kind of polymer, poly(nickel-ethylenetetrathiolate), *i.e.* poly(Ni-C_2S_4), which is treated as a quasi 1-D chain with phonons being three-dimensional and electrons being one-dimensional.

3.1 Nonlinear Schrödinger Equation

Let us consider a typical Left-Central-Right (L-C-R) structure with electrons and phonons coupled in central part and two semi-infinite phonon baths (no electrons) on the two ends. These two leads are in equilibrium which can be characterized

by temperature. Under this assumption, the Hamiltonian of this system is, $H_{\text{tot}} = H_{\text{e}} + H_{\text{ph}} + H_{\text{epi}}$. The electron part is

$$H_{\text{e}} = c^{\dagger} T c, \tag{3.1}$$

which is a traditional tight-binding model with transferring matrix T. The phonon part is

$$\begin{aligned} H_{\text{ph}} = \sum_{\alpha=L,C,R} \frac{1}{2}(\dot{u}^{\alpha})^{T} u^{\alpha} + \frac{1}{2}(u^{\alpha})^{T} K^{\alpha} u^{\alpha} \\ + (u^{L})^{T} V_{\text{ph}}^{LC} u^{C} + (u^{C})^{T} V_{\text{ph}}^{CR} u^{R}, \end{aligned} \tag{3.2}$$

where u^{α} is a column vector of atom displacements which are multiplied by square root of the atom mass, $u^{\alpha} = \sqrt{m} x^{\alpha}$ (therefore all other quantities should be adjusted accordingly), $\dot{u}^{\alpha}$ is the corresponding momentum, K^{α} is the spring constant matrix of this phonon system (we assume all three parts share a same spring constant matrix), and V_{ph}^{LC}, V_{ph}^{CR} are the coupling matrices between baths and central part with $V_{\text{ph}}^{LC} = (V_{\text{ph}}^{CL})^{T}$, $V_{\text{ph}}^{RC} = (V_{\text{ph}}^{CR})^{T}$. For the EPI, we assume it is in the form of

$$H_{\text{epi}} = \sum_{i,j,k} c_i^{\dagger} M_{ij}^{k} c_j u_k, \tag{3.3}$$

where M_{ij}^{k} is the coupling tensor. Working in the Heisenberg picture, we can obtain the equations of motion for electrons and phonons, respectively, through the Heisenberg equation. For electrons,

$$i\hbar \dot{c} = Tc + \sum_{k} M^{k} u_k c. \tag{3.4}$$

For phonons,

$$\begin{aligned} \ddot{u}^{C} &= -K^{C} u^{C} - c^{\dagger} M c - V_{\text{ph}}^{CL} u^{L} - V_{\text{ph}}^{CR} u^{R} \\ \ddot{u}^{\alpha} &= -K^{\alpha} u^{\alpha} - V_{\text{ph}}^{\alpha C} u^{C}, \;\; \alpha = L, R \end{aligned} \tag{3.5}$$

The solution of the leads' phonons is

$$\begin{aligned} u^{\alpha}(t) = &\int_{t_0}^{t} D_{\alpha}^{r}(t,t')V_{ph}^{\alpha C}(t')dt' + \frac{\partial D_{\alpha}^{r}(t,t_0)}{\partial t_0}u^{\alpha}(t_0) \\ &-D_{\alpha}^{r}(t,t_0)\dot{u}^{\alpha}(t_0), \;\; \alpha = L,R \end{aligned} \tag{3.6}$$

where $D_{\alpha}^{r}(t,t_0) = -i\theta(t-t_0)\langle[u^{\alpha}(t), u^{\alpha}(t_0)^{T}]\rangle$ is the retarded Green's function of leads' phonons, and it satisfies the following equation:

$$\frac{\partial^2 D_{\alpha}^{r}(t,t')}{\partial t'^2} + D_{\alpha}^{r}(t,t')K^{\alpha} = -\delta(t-t')I. \tag{3.7}$$

Based on this solution, we can obtain the equation of motion for central phonons,

$$\begin{aligned} \ddot{u}^{C} = &- K^{C}u^{C} - c^{\dagger}Mc - \int_{t_0}^{t}\Big[V_{\mathrm{ph}}^{CL}D_{L}^{r}(t,t')V_{\mathrm{ph}}^{LC} \\ &+ V_{\mathrm{ph}}^{CR}D_{R}^{r}(t,t')V_{\mathrm{ph}}^{RC}\Big]u^{C}(t')dt' + \xi, \end{aligned} \tag{3.8}$$

where

$$\begin{aligned} &\xi = \sum_{\alpha=L,R}\xi_{\alpha}, \\ &\xi_{\alpha}(t) \equiv V_{\mathrm{ph}}^{C\alpha}\Big[D_{\alpha}^{r}(t,t_0)\dot{u}^{\alpha}(t_0) - \dot{D}_{\alpha}^{r}(t,t_0)u^{\alpha}(t_0)\Big]. \end{aligned} \tag{3.9}$$

For simplicity, we define the self energy of phonon baths as follows:

$$\begin{aligned} &\Pi_{\alpha}^{r}(t,t') \equiv V_{\mathrm{ph}}^{C\alpha}D_{\alpha}^{r}(t,t')V_{\mathrm{ph}}^{\alpha C}, \alpha = L,R, \\ &\Pi^{r} \equiv \Pi_{L}^{r} + \Pi_{R}^{r}. \end{aligned} \tag{3.10}$$

Then the solution can be rewritten as

$$\ddot{u}^{C} = -K^{C}u^{C} - c^{\dagger}Mc - \int_{t_0}^{t}\Pi^{r}(t,t')u^{C}(t')dt' + \xi \tag{3.11}$$

We can prove that the noise ξ satisfies the fluctuation-dissipation relation,

$$\langle\xi_{\alpha}(t)\xi_{\alpha}(t')^{T}\rangle = i\hbar\overline{\Pi}_{\alpha}(t,t') \tag{3.12}$$

where $\overline{\Pi}_{\alpha}(t,t') = \frac{1}{2}V_{\mathrm{ph}}^{C\alpha}(D_{\alpha}^{>}(t,t') + D_{\alpha}^{<}(t,t'))V_{\mathrm{ph}}^{\alpha C}$.

In normal mode space, we have

$$\begin{aligned} D^r_\alpha(t,t_0) &= -\theta(t-t_0)U_\alpha \frac{\sin\Big(\Omega_\alpha(t-t_0)\Big)}{\Omega_\alpha} U^T_\alpha, \\ u^\alpha(t_0) &= \sqrt{\frac{\hbar}{2\Omega_\alpha}}(ae^{-i\Omega_\alpha t_0} + a^\dagger e^{i\Omega_\alpha t_0}), \end{aligned} \tag{3.13}$$

where Ω_α and U_α are the normal mode eigenvalue and eigenvector matrices, respectively, and $U_\alpha U^T_\alpha = I$. At time t_0, leads are in equilibrium, therefore, $\langle a^\dagger a\rangle = n(\Omega_\alpha) = 1/[e^{\hbar\Omega_\alpha/k_BT_\alpha} - 1]$, the Bose-Einstein distribution, T_α is the temperature of leads. Substituting these formulas into the correlation $\langle \xi_\alpha(t)\xi_\alpha(t')^T\rangle$, we obtain

$$\begin{aligned} \langle \xi_\alpha(t)\xi_\alpha(t')^T\rangle = V^{C\alpha}_{\rm ph}U_\alpha\Big[&\frac{\hbar}{2\Omega_\alpha}\cos\Big(\Omega_\alpha(t-t')\Big)\Big(2n(\Omega_\alpha)+1\Big) \\ &- \frac{i\hbar}{2\Omega_\alpha}\sin\Big(\Omega_\alpha(t-t')\Big)\Big]U^T_\alpha V^{\alpha C}_{\rm ph}. \end{aligned} \tag{3.14}$$

Note that the greater Green's function in normal mode space can be expressed as

$$D^>_\alpha = U_\alpha\Big[-\frac{i}{2\Omega_\alpha}\cos\Big(\Omega_\alpha(t-t')\Big)\Big(2n(\Omega_\alpha)+1\Big) - \frac{1}{2\Omega_\alpha}\sin\Big(\Omega_\alpha(t-t')\Big)\Big]U^T_\alpha. \tag{3.15}$$

Therefore, $\langle \xi_\alpha(t)\xi_\alpha(t')^T\rangle = i\hbar V^{C\alpha}_{\rm ph}D^>_\alpha V^{\alpha C}_{\rm ph}$. Similarly, $\langle \xi_\alpha(t')\xi_\alpha(t)^T\rangle = i\hbar V^{C\alpha}_{\rm ph}D^<_\alpha V^{\alpha C}_{\rm ph}$. We define the symmetrized correlation function as

$$\langle \xi_\alpha(t)\xi_\alpha(t')^T\rangle \equiv \frac{1}{2}\langle \xi_\alpha(t)\xi_\alpha(t')^T + \xi_\alpha(t')\xi_\alpha(t)^T\rangle. \tag{3.16}$$

Then we obtain the fluctuation-dissipation relation: $\langle \xi_\alpha(t)\xi_\alpha(t')^T\rangle = i\overline{\Pi}_\alpha(t,t')$.

Now we have obtained the equations of motion for both the central electrons and phonons, and this approach is borrowed from Lü and Wang [72]. For convenience, we can just drop the superscript identifying the central part. As for now, what we have done is accurate in quantum level. However, it is difficult to numerically simulate a totally quantum many-body system, so we have to make some classical

approximations: we interpret the operators c and u as complex wave function and real variable respectively. If there is only one electron in the central part, regarding c as a complex wave function is not an approximation, but replacing u with real variable is indeed a classical approximation. Under this assumption, we can implement a molecular dynamic simulation right away. In addition, we can also try to solve the phonons' equation of motion formally:

$$u(t) = -\int_{-\infty}^{t} D^r(t,t')\Big[\xi(t') - c^\dagger(t')Mc(t')\Big]dt', \tag{3.17}$$

where $D^r(t,t')$ is the central phonons' retarded Green's function, and it satisfies

$$(\frac{\partial^2}{\partial t^2} + K)D^r(t,t') + \int_{-\infty}^{t} \Pi^r(t,t'')D^r(t'',t')dt'' = -\delta(t-t')I. \tag{3.18}$$

In the frequency domain, it becomes: $\tilde{D}^r[\omega] = \Big((\omega+i\eta)^2 - K - \tilde{\Pi}^r[\omega]\Big)^{-1}$. Substituting the Eq. (3.17) back to the Eq. (3.4), we obtain:

$$\begin{aligned} i\hbar\dot{c} = Tc &- \Big(\sum_{k,k'}\int_{-\infty}^{t} M^k D^r_{kk'}(t,t')\xi_{k'}(t')\Big)c(t) \\ &+ \Big(\sum_{k,k'}\int_{-\infty}^{t} M^k D^r_{kk'}(t,t')\sum_{ij}\Big[c_i^\dagger(t')M^{k'}_{ij}c_j(t')\Big]\Big)c(t) \end{aligned} \tag{3.19}$$

It is similar to a Schrödinger equation except that it is nonlinear, so we call it the nonlinear Schrödinger equation. However, the cost of eliminating phonons from single electron's equation of motion is much more expensive than solving the coupled equations of motion, therefore in our MD simulation, we still solve the Eq. (3.4) and Eq. (3.11) directly.

3.2 Numerical Simulation for the SSH Model

3.2.1 Model and simulation details

As an illustration, we apply our method to the SSH model with the L-C-R structure. The Hamiltonian of this model is

$$\begin{aligned} H_{\mathrm{e}} &= -\sum_j \gamma c_j^\dagger c_{j+1} + \mathrm{h.c.}, \\ H_{\mathrm{ph}} &= \frac{1}{2}\sum_j K(u_{j+1}-u_j)^2 + \frac{1}{2}\sum_j \dot{u}_j^2, \\ H_{\mathrm{epi}} &= \sum_j \alpha c_j^\dagger c_{j+1}(u_{j+1}-u_j) + \mathrm{h.c.}, \end{aligned} \tag{3.20}$$

where γ is the hopping constant of the electron tight binding model, K is the spring constant, and α is the electron-phonon coupling constant. Compared with the original SSH model, there is no dimerization in our model for we only put one electron into the system, which can not be dimerized. Based on the Hamiltonian, we can derive its equations of motion. The time-dependent Schrödinger equation for the electron is

$$i\dot{c}_j = [-\gamma + \alpha(u_{j+1}-u_j)]c_{j+1} + [-\gamma + \alpha(u_j - u_{j-1})]c_{j-1}, \tag{3.21}$$

and for phonons,

$$\ddot{u}_j = -K(2u_j - u_{j+1} - u_{j-1}) + \alpha(c_j^\dagger c_{j+1} + c_{j+1}^\dagger c_j) - \alpha(c_{j-1}^\dagger c_j + c_j^\dagger c_{j-1}). \tag{3.22}$$

We use the 4th-order Runge-Kutta method to solve the time-dependent Schrödinger equation, and use the central difference method to solve phonons' equation of motion. The size of the central part is chosen to be 999 unit cells in our simulation, and the single electron locates at the center of the central part initially. We do not allow

the electron to move into the two leads or the other end point, thus it is a hard wall boundary condition and it will cause a size effect, which should be eliminated correctly. The initial displacements of phonons can be obtained using the Eq. (3.17) with no electron, which is

$$u(t) = -\int_{-\infty}^{t} D^r(t,t')\xi(t')dt' = -\Big(\mathcal{F}^{-1}\Big(\tilde{D}^r[\omega]\tilde{\xi}[\omega]\Big)\Big)(t), \tag{3.23}$$

where the convolution theorem is applied, and we only pick some initial values. To generate the noise from the baths, we use the Box-Muller method to produce the distribution we want in the frequency domain, then we switch it into the time domain by the Fourier transform.

Transferring into the frequency domain, the Eq. (3.12) becomes

$$\langle\tilde{\xi}_\alpha(\omega)\tilde{\xi}_\alpha(\omega')^\dagger\rangle = 2\pi\delta(\omega-\omega')\tilde{\overline{\Pi}}_\alpha[\omega] = -i\hbar\pi\delta(\omega-\omega')\Big[2n(\omega)+1\Big]\mathrm{Im}\Pi^r_\alpha[\omega], \tag{3.24}$$

where

$$\begin{aligned}\tilde{\xi}_\alpha[\omega] &= \int_{-\infty}^{\infty}\xi_\alpha(t)e^{i\omega t}dt,\\ \tilde{\overline{\Pi}}_\alpha(\omega) &= \int_{-\infty}^{\infty}\overline{\Pi}_\alpha(t)e^{i\omega t}dt.\end{aligned} \tag{3.25}$$

We split the $\tilde{\xi}_\alpha(\omega)$ to be: $\tilde{\xi}_\alpha(\omega) = a(\omega) + ib(\omega)$, and demand that

$$\begin{aligned}&\langle a(\omega)a(\omega')\rangle = \langle b(\omega)b(\omega')\rangle = \pi\delta(\omega-\omega')\tilde{\overline{\Pi}}_\alpha(\omega),\\ &\langle a(\omega)b(\omega')\rangle = \langle b(\omega)a(\omega')\rangle = 0,\end{aligned} \tag{3.26}$$

i.e., $a(\omega)$ and $b(\omega)$ are two independent variables obeying a normal distribution with mean 0 and variance $\pi\tilde{\overline{\Pi}}_\alpha(\omega)$. The Box-Muller transform is a random number sampling method to generate a pair of independent, normally distributed variables. Consider a pair of continuous variables (x, y) which satisfy the following normal

distribution:

$$\begin{aligned} p(x,y)dxdy &= \frac{1}{2\pi\sigma^2}e^{-\frac{x^2+y^2}{2\sigma^2}}dxdy \\ &= \frac{1}{2\pi\sigma^2}e^{-\frac{r^2}{2\sigma^2}}drd\theta, \\ &\equiv \frac{1}{2\pi}d\theta e^{-z}dz, \end{aligned} \tag{3.27}$$

where r and θ are corresponding polar variables, $z \equiv \frac{r^2}{2\sigma^2}$. The mean of the two variables is 0, and the variance is σ^2. Given two uniformly distributed variables U_1 and U_2, we can generate the θ and z by $2\pi U_1$ and $-\ln U_2$, respectively. Thereafter, the original variables are obtained as follows:

$$\begin{aligned} x &= \sigma\sqrt{-2\ln U_2}\cos 2\pi U_1, \\ y &= \sigma\sqrt{-2\ln U_2}\sin 2\pi U_1. \end{aligned} \tag{3.28}$$

Besides the noise, retarded Green's functions of phonons are required. Generally, the Green's functions for an open system can be calculated with the help of the surface Green's functions, labeled as g_0^r in this subsection, which can be obtained numerically by a recursive method developed by M.P. Lopez Sancho *et al.*[73]. To illustrate this method, let us consider a harmonic L-C-R leads system with the spring constant matrices,

$$\tilde{K} = \begin{pmatrix} K^L & V^{LC} & 0 \\ V^{CL} & K^C & V^{CR} \\ 0 & V^{RC} & K^R \end{pmatrix}, \tag{3.29}$$

where

$$K^L = \begin{pmatrix} \ddots & & & \\ & k_{10} & k_{00} & k_{01} \\ & & k_{10} & k_{00} \end{pmatrix},$$

$$K^C = \begin{pmatrix} k_{00} & k_{01} & & & & \\ k_{10} & k_{00} & k_{01} & & & \\ & & & \ddots & & \\ & & & & k_{10} & k_{00} \end{pmatrix}, \tag{3.30}$$

$$K^R = \begin{pmatrix} k_{00} & k_{01} & & \\ k_{10} & k_{00} & k_{01} & \\ & & & \ddots \end{pmatrix}.$$

Here we assume $k_{00} = k_{11} = \cdots$, $k_{01} = k_{12} = \cdots$, $k_{10} = k_{21} = \cdots$ for simplicity (not necessary), and k_{00}, k_{01}, k_{10} can be block matrices. For simplicity, we temporarily write the right lead's retarded Green's function in the frequency domain as g^R, and it satisfies

$$(\omega^2 - K^R)g^R = I. \tag{3.31}$$

We restrict the couplings between the leads and the central part are only nonzero for corner elements (nearest neighbors) so that we only need g^R_{00}. For the first column

elements in g^R, the sequence of equations are

$$\begin{cases} (\omega^2 - k_{00})g^R_{00} - k_{01}g^R_{10} = I, \\ -k_{10}g^R_{00} + (\omega^2 - k_{11})g^R_{00} - k_{01}g^R_{20} = I, \\ \cdots \\ -k_{10}g^R_{n-10} + (\omega^2 - k_{nn})g^R_{n0} - k_{01}g^R_{n+10} = I, \quad n >= 1. \end{cases} \tag{3.32}$$

Eliminating all odd indices, we obtain

$$\begin{cases} \Big[(\omega^2 - \varepsilon^s_1\Big]g^R_{00} = I + \alpha_1 g^R_{20}, \\ \cdots \\ \Big[(\omega^2 - \varepsilon_1\Big]g^R_{n0} = \beta_1 g^R_{n-20} + \alpha_1 g^R_{n+20}, n >= 2, \end{cases} \tag{3.33}$$

where we define

$$\begin{cases} \alpha_1 \equiv k_{01}(\omega^2 - k_{00})^{-1}k_{01}, \\ \beta_1 \equiv k_{10}(\omega^2 - k_{00})^{-1}k_{10}, \\ \varepsilon^s_1 \equiv k_{00} + k_{01}(\omega^2 - k_{00})^{-1}k_{10}, \\ \varepsilon_1 \equiv k_{00} + k_{10}(\omega^2 - k_{00})^{-1}k_{01} + k_{01}(\omega^2 - k_{00})^{-1}k_{10}. \end{cases} \tag{3.34}$$

This operation effectively doubles the lattice constant. If we keep applying this operation, we can construct an iterative sequence as follows:

$$\begin{cases} \alpha_l = \alpha_{l-1}(\omega^2 - \varepsilon_{l-1})^{-1}\alpha_{l-1}, \\ \beta_l = \beta_{l-1}(\omega^2 - \varepsilon_{l-1})^{-1}\beta_{l-1}, \\ \varepsilon^s_l = \varepsilon^s_{l-1} + \alpha_{l-1}(\omega^2 - \varepsilon_{l-1})^{-1}\beta_{l-1}, \\ \varepsilon_l = \varepsilon_{l-1} + \alpha_{l-1}(\omega^2 - \varepsilon_{l-1})^{-1}\beta_{l-1} + \beta_{l-1}(\omega^2 - \varepsilon_{l-1})^{-1}\alpha_{l-1}, \end{cases} \tag{3.35}$$

with $\varepsilon_0 = \varepsilon_0^s = k_{00}$, $\alpha_0 = k_{01}$, $\beta_0 = k_{10}$. Repeating this iteration until α_l and β_l are small enough so that $\varepsilon_l \approx \varepsilon_{l-1}$ and $\varepsilon_l^s \approx \varepsilon_{l-1}^s$, we obtain

$$g_{00}^R \approx (\omega^2 - \varepsilon_l^s)^{-1}. \tag{3.36}$$

This Green's function is known as the surface Green's function g_{0R}^r. We can obtain g_{0L}^r in the same way. With the left and right surface Green's functions, the self energy is simply:

$$\tilde{\Pi}^r[\omega] = V^{CL} g_{0L}^r V^{LC} + V^{CR} g_{0R}^r V^{RC}. \tag{3.37}$$

Fortunately, exact solutions are feasible for a uniform and harmonic1-D chain [74]. In the frequency domain, the retarded Green's function satisfies

$$\omega^2 \tilde{D}^r[\omega] - \begin{pmatrix} \ddots & & & & & \\ & -K & 2K & -K & & \\ & & -K & 2K & -K & \\ & & & & & \ddots \end{pmatrix}_{\infty\times\infty} \tilde{D}^r[\omega] = I. \tag{3.38}$$

In elements, it is

$$(\omega^2 - 2K)\tilde{D}_{jj'}^r[\omega] + K\tilde{D}_{j-1j'}^r[\omega] + K\tilde{D}_{j+1j'}^r[\omega] = \delta_{jj'}. \tag{3.39}$$

We assume the solution is: $\tilde{D}_{jj'}^r[\omega] = C\lambda^{|j-j'|}$, and $j > j'$ without loss of generality. $|\lambda| < 1$ must be required to make sure the $\tilde{D}_{jj'}^r[\omega]$ goes to zero when $|j - j'| \to \infty$. This solution also satisfies the translational symmetry. If $j \neq j'$, the λ can be easily obtained,

$$\begin{aligned} \lambda_{1,2} &= \frac{-(\omega^2 - 2K) \pm \sqrt{(\omega^2 - 2K)^2 - 4K^2}}{2K}, \\ \lambda_1\lambda_2 &= 1, \end{aligned} \tag{3.40}$$

with $|\lambda_1| < 1$ and $|\lambda_2| > 1$. If $j = j'$, the constant C can be determined,

$$C = \frac{1}{\omega^2 - 2K + 2K\lambda} = \frac{1}{K(\lambda_1 - \lambda_2)}. \tag{3.41}$$

Therefore, the complete solution is

$$\tilde{D}^r_{jj'}[\omega] = \frac{\lambda_1^{|j-j'|}}{K(\lambda_1 - \lambda_2)}. \tag{3.42}$$

We can also obtain this solution by breaking the chain into three parts. Since it is a uniform chain, the leads' Green's functions just satisfy the same equations except the indices are semi-infinite, and we only need one surface Green's function. Therefore, the corresponding surface Green's function and self energy are

$$g^r_0[\omega] = -\frac{\lambda_1}{K}, \tilde{\Pi}[\omega] = 2K^2 g^r_0. \tag{3.43}$$

For the parameters, we use the typical SSH model parameter sets: $\gamma = 2.5$ eV, $\alpha = 4.1$ eV/Å, $K = 21.0$ eV/Å^2, $m = 1349.14$ eVfs^2/Å^2, lattice constant $a = 1.22$ Å. For simplicity, in this section, every time when we say α and K, it means $\alpha/\sqrt{m}$ and K/m in atomic units, *i.e.*, $\gamma = 0.09$ hartree, $\alpha/\sqrt{m} = 0.00052$ hartree/a_0, $K/m = 9.1 * 10^{-6}$ hartree/a_0^2, $a = 2.3$ a_0, where a_0 is the Bohr radius. As for the time step, we choose it to be 1.0 a.u., which is about 0.0242 fs.

3.2.2 Results and Discussions

To check the validity of the noise we generate, we can calculate the energy of a pure phonon system according to the Eq. (3.23). The energy of the 1-D chain can

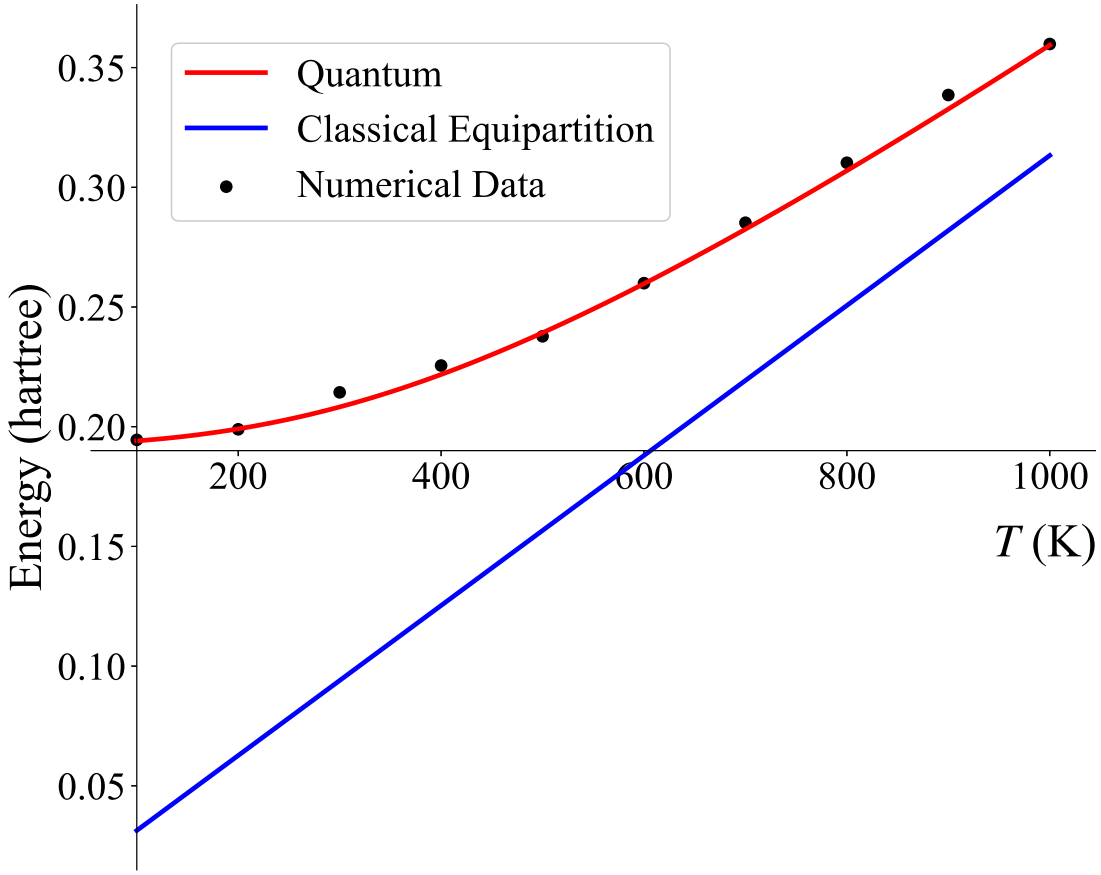

Figure 3.1: Energy of the 1-D lattice vibration with 99 sites. Black dots are numerical results averaged over 1000 time points with 100 ensembles for each time point. Red solid line and blue solid line are quantum and classical equipartition predictions, respectively.

be derived theoretically.

$$\begin{aligned}
\langle E\rangle &= \langle \sum_j \frac{1}{2}\dot{u}_j^2 + \sum_j \frac{1}{2}K(u_{j+1}-u_j)^2\rangle \\
&= \langle \sum_j K(u_{j+1}-u_j)^2\rangle \\
&= \sum_{l=0}^{N-1} \hbar\omega_q\Big(n(\omega_q)+\frac{1}{2}\Big),\ \omega_q = 2\sqrt{K}|\sin\frac{qa}{2}|,\ q=\frac{2\pi l}{Na} \\
&\approx Nk_BT + \frac{1}{2}\sum_{l=0}^{N-1}\hbar\omega_q,\ k_BT \gg \hbar\omega_q.
\end{aligned} \tag{3.44}$$

From the first line to the second, we have used the viral theorem, and the formula in the second line can be used to evaluate the energy in our numerical simulation. The

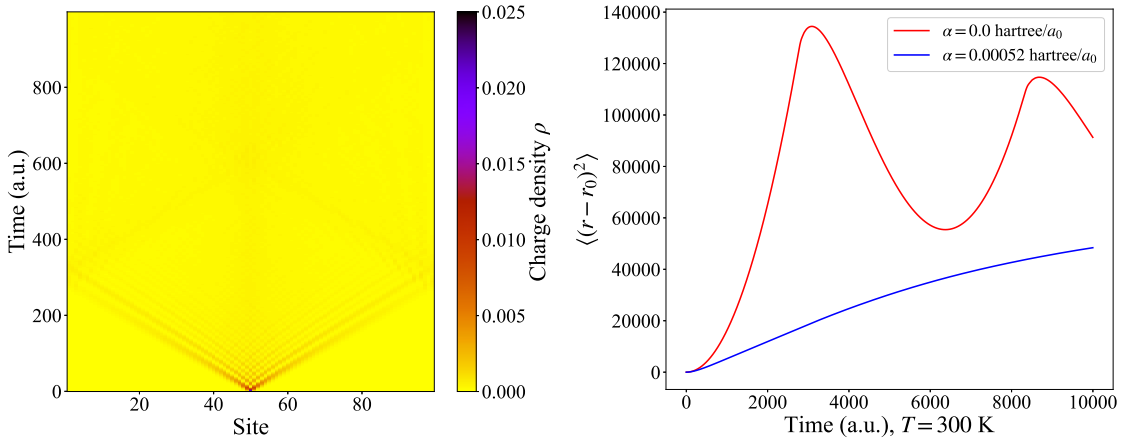

(a) charge density (b) $\langle (r - r_0)^2 \rangle (t)$

Figure 3.2: (a) Evolution of the charge density with central size 99 and total simulation time 1000 in atomic units (about 24.2 fs). α is set to be 0.00052 hartree/a_0. (b) Plot of the ensemble averaged squared displacement versus time at $T = 300$ K with central size 999 and total simulation time 10000 in atomic units (about 242 fs).

third line is the standard result of the 1-D lattice vibration. $n(\omega_q) = 1/[e^{\hbar\omega_q/k_BT} - 1]$ is the Bose-Einstein distribution. If the temperature is high enough, we obtain the classical equipartition result plus a quantum correction, which is the fourth line. We have performed a comparison in Fig. 3.1, from which we can conclude our simulation is consistent with the quantum predictions.

The electron stays at the center initially, then its wave function will spread to both ends due to the hopping terms. The evolution of charge density can be observed in Fig. 3.2(a), and obviously, there is a size effect. To study the electron's motion more quantitatively, we calculate the mean squared displacement of the electron

$$\langle (r - r_0)^2 \rangle (t) = \sum_j (j - j_0)^2 |c(j,t)|^2, \tag{3.45}$$

and take the ensemble average over 10000 ensembles. In Fig. 3.2(b), we illustrate the comparison between two cases, with EPI and without. From this figure, we

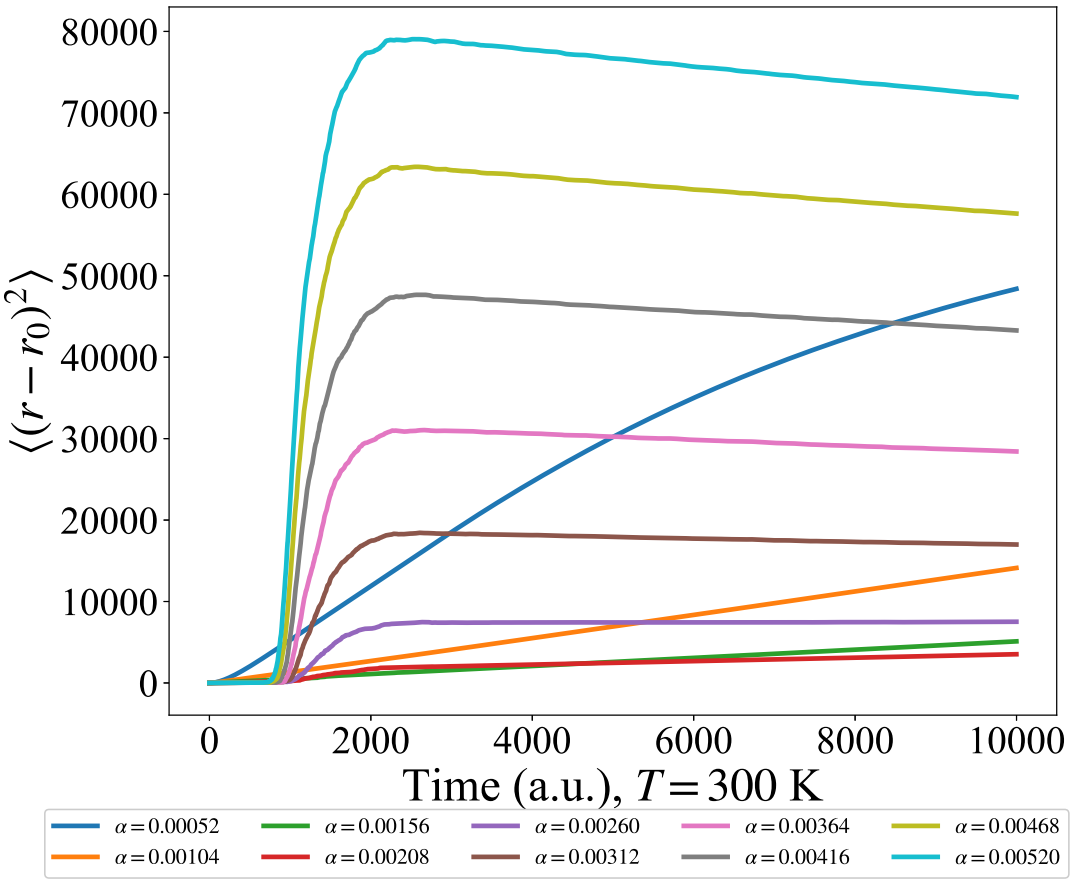

Figure 3.3: Electron's movement for different coupling constant α value at $T = 300$ K. The unit of the α is hartree/a_0, and the total simulation time is 10000 in atomic units (about 242 fs).

can conclude that EPI indeed slows down the movement of the electron, but its effect is not strong enough to go into a diffusive region. Naturally, we increase the value of the coupling constant α to explore the electron's behavior further, which is given in Fig. 3.3. The increased coupling constant causes a further decrease of the displacement of the electron, and as expected, we observe diffusive behavior for suitable large α.

However, there is one issue that if the α is too large, $\langle (r - r_0)^2 \rangle(t)$ will have a sudden increase, which is unreasonable. After analyzing our simulation results,

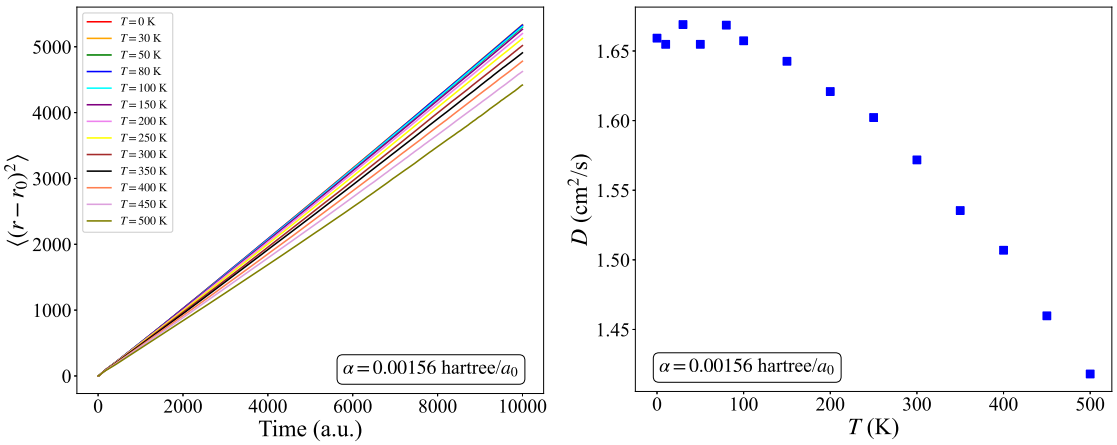

(a) (b)

Figure 3.4: (a) Different slope of $\langle r^2 \rangle$ versus time for different temperature When $\alpha = 0.00156$ hartree/a_0 (3 times of the original α). (b) The relation between diffusion constant and temperature (in SI units) based on Fig. 3.4(a) when $\alpha = 0.00156$ hartree/a_0.

we find that it can be understood that even in the diffusive region, there is still a ballistic part whose velocity is not affected by the EPI, but determined by the hopping parameter. Therefore, when the ballistic part hits two ends, it will be trapped in the vicinity of the ends due to our boundary condition, while the diffusive part is far from the ends at the same time. Although the ballistic part is very weak, the cumulation of this trapping effect will result in a sudden increase in the ensemble averaged squared displacement when α is large. To eliminate this size effect, we separate the $\langle (r - r_0)^2 \rangle(t)$ into two parts:

$$\langle (r - r_0)^2 \rangle(t) = P_{\text{ends}} \langle (r - r_0)^2 \rangle(t) + P_{\text{middle}} \langle (r - r_0)^2 \rangle(t), \tag{3.46}$$

where P_{ends} and P_{middle} represent the corresponding proportions which should be determined through numerical tests. This separation is only applicable for those situations in which the diffusive part takes much longer time to reach the ends than

the ballistic part. In our simulation, the middle part occupies eighty percent of the length and we only use the middle part to study the diffusive behavior. Figure 3.4(a) shows the behavior of $\langle (r - r_0)^2 \rangle$ at different temperature, and the corresponding diffusion constants are given in Fig. 3.4(b). The diffusion constant fluctuates at low temperatures, and then keeps decreasing for increasing temperatures. Using the Einstein relation $\mu = \frac{eD}{k_B T}$, we can immediately know that the increase of temperature will result in a decrease of mobility, which is the feature of bandlike charge transport.

In 2006, Troisi and Orlandi published a paper where they did a similar work as ours but with a slightly different model [75]. In their model, they just treated phonons as independent harmonic oscillators, and they observed diffusive behaviors. Therefore, we have tried to modify the SSH model to be close to Troisi's one by adding an onsite term which is much larger than the off-diagonal terms in phonons' Hamiltonian, and using the same parameters. The results are completely different from theirs, and the electron is almost ballistic under the EPI. However, this difference is expected. In our model, the off-diagonal terms represent the couplings among harmonic oscillators, and as a consequence, there are only acoustic phonons, while in Troisi's model, there are only optical phonons. Even small off-diagonal terms can decrease the scattering rate between the electron and phonons remarkably.

3.2.3 Comparison with Boltzmann Theory

According to the Boltzmann transport theory, the electron states in solids can be described by a distribution function $f(\boldsymbol{r}, \boldsymbol{k}, t)$, which satisfies the BTE,

$$\frac{\partial f}{\partial t} + \boldsymbol{v} \cdot \frac{\partial f}{\partial \boldsymbol{r}} + \boldsymbol{F} \cdot \frac{\partial f}{\partial (\hbar \boldsymbol{k})} = \left. \frac{\partial f}{\partial t} \right|_{\text{scatt}}, \tag{3.47}$$

where $\boldsymbol{v}$ is the velocity, and $\boldsymbol{F}$ is the external force. The scattering part usually is very complicated, therefore, we invoke the relaxation time approximation,

$$\left.\frac{\partial f}{\partial t}\right|_{\text{scatt}} = -\frac{f(\boldsymbol{k}) - f_0}{\tau_{\boldsymbol{k}}} \tag{3.48}$$

We can also evaluate the scattering term by the Fermi's golden rule,

$$P(\boldsymbol{k'} \to \boldsymbol{k}) = \frac{2\pi}{\hbar} \sum_{k'} |M(\boldsymbol{k}, \boldsymbol{k'})|^2 \delta(\varepsilon_{\boldsymbol{k}} - \varepsilon_{\boldsymbol{k'}}), \tag{3.49}$$

where $M(\boldsymbol{k}, \boldsymbol{k'}) = \langle k|\delta U|k'\rangle$ is the scattering matrix, and δU is the interacting potential. Combining these two evaluations, we obtain

$$\frac{1}{\tau_{\boldsymbol{k}}} = \frac{2\pi}{\hbar} \sum_{k'} |M(\boldsymbol{k}, \boldsymbol{k'})|^2 \delta(\varepsilon_{\boldsymbol{k}} - \varepsilon_{\boldsymbol{k'}})(1 - \cos\theta_{\boldsymbol{k}\boldsymbol{k'}}), \tag{3.50}$$

in which the $\theta_{\boldsymbol{k}\boldsymbol{k'}}$ is the angle between $\boldsymbol{k}$ and $\boldsymbol{k'}$ [76]. Therefore, the key point is to work out the scattering matrix $M(\boldsymbol{k}, \boldsymbol{k'})$. In the SSH model, there are only acoustic phonons, so we can use deformation potential method to carry out the scattering matrix, which was firstly developed by Bardeen and Shockley in 1950 [77]. In the deformation potential theory, the shift of the electron band edge caused by the EPI can be attributed to a perturbative effect of a deformation potential. The deformation potential, induced by the lattice distortion, can be written as follows:

$$\delta U = E_1 \Delta V, \tag{3.51}$$

where E_1 is the deformation potential constant, ΔV is the lattice deformation. We assume the displacement of each atom in our model is $u_j \equiv \sqrt{m}\epsilon j a$ with strain constant ϵ , and lattice constant a. Thus the electronic energy dispersion relation is

$$\begin{aligned} E &= -2[\gamma - \alpha(u_{j+1} - u_j)]\cos ka \\ &= -2(\gamma - \sqrt{m}a\alpha\epsilon)\cos ka. \end{aligned} \tag{3.52}$$

Here k is the lattice wave vector. Comparing with the original energy dispersion relation $E = -2\gamma \cos ka$, we can find the E_1,

$$E_1 = 2\sqrt{m}a\alpha \cos ka. \tag{3.53}$$

With the second quantization, the displacement of an atom in this 1-D chain is

$$\begin{aligned} u_j &= \sum_q \sqrt{\frac{\hbar}{2\omega_q N m}}(a_q e^{iqja} + a_q^\dagger e^{-iqja}), \\ \omega_q &= 2\sqrt{K}|\sin\frac{qa}{2}|. \end{aligned} \tag{3.54}$$

The dilation ΔV is defined as $\frac{\partial u_j}{\partial(ja)}$, and the eigenstates of non-interacting tight-binding model is $|k\rangle = \sum_j \frac{1}{\sqrt{N}} e^{ikja}$. Therefore, the scattering element $\langle k|\delta U|k'\rangle$ can be written as

$$\langle k|\delta U|k'\rangle = iE_1 q \sqrt{\frac{\hbar}{2\omega_q N m}}(a_q + a_{-q}^\dagger)\Big|_{q=k-k'}. \tag{3.55}$$

Taking the thermal average of its modular square, we obtain

$$\left\langle |\langle k|\delta U|k'\rangle|^2 \right\rangle = \frac{\hbar E_1^2 q^2}{2\omega_q N m}(2n_q + 1), \tag{3.56}$$

where $n_q = \frac{1}{e^{\beta\hbar\omega_q} - 1}$ is the Bose-Einstein distribution function. Since the deformation potential theory is only applicable for long wave limit, *i.e.*, only for acoustic phonons, we take $q \to 0$ forcing $n_q \to \frac{k_B T}{\hbar\omega_q} \gg 1$ and $\omega_q \to \sqrt{K}qa \equiv cq$. Thereafter, the scattering matrix (in this 1-D case, it is just a number) becomes

$$|M(k,k')|^2 = \left\langle |\langle k|\delta U|k'\rangle|^2 \right\rangle = \frac{k_B T E_1^2}{c_{ii}}, \tag{3.57}$$

where $c_{ii} \equiv Nmc^2$ and c is the lattice wave velocity. Substituting the scattering matrix into the Eq. (3.50), we obtain the explicit formula for the relaxation time,

$$\begin{aligned}\frac{1}{\tau_k} &= \sum_{k'} \frac{2\pi}{\hbar} \frac{k_B T E_1^2}{NmKa^2} \delta(\varepsilon_k - \varepsilon_{k'})(1 - \cos\theta_{kk'}) \\ &\to a \int \frac{dk'}{2\pi} \frac{2\pi}{\hbar} \frac{k_B T E_1^2}{NmKa^2} \frac{1}{\hbar |v_k|} \delta(k - k') \cdot 2 \\ &= \frac{8a\alpha^2 k_B T \cos^2 ka}{\hbar^2 K |v_k|}.\end{aligned} \tag{3.58}$$

Here the factor $1 - \cos\theta_{kk'}$ is replaced with 2 because in 1-D, only when $k = -k'$, this factor equals to 2 with the constraint $\varepsilon_k = \varepsilon_{k'}$, otherwise it is 0. With the relaxation time, the diffusion constant can be worked out [78],

$$D \equiv \frac{\sum\limits_k v_k^2 \tau_k e^{-\beta\varepsilon_k}}{\sum\limits_k e^{-\beta\varepsilon_k}} \to \frac{\int_0^{\frac{\pi}{a}} dk v_k^2 \tau_k e^{-\beta\varepsilon_k}}{\int_0^{\frac{\pi}{a}} dk e^{-\beta\varepsilon_k}} \tag{3.59}$$

We further simplify the formula to be

$$D = \frac{Ka^2\gamma^2}{2\hbar\alpha^2} \frac{\int_{-b}^{b} \frac{(b^2 - x^2)e^x}{x^2} dx}{\int_{-b}^{b} \frac{e^x}{\sqrt{b^2 - x^2}} dx}, \tag{3.60}$$

where $b \equiv 2\beta\gamma$.

Since the BTE method always predicts diffusive behavior, immediately, we are aware that it contradicts with our simulation results for SSH parameters. Therefore, to make further comparison, we calculate the $D-T$ relation using the Eq. (3.60) with $\alpha = 0.00156$ hartree/a_0, which is shown in Fig. 3.5. Compared with our simulation results, values in Fig. 3.5 are much smaller and is monotonically increasing, which implies the relation that the BTE method predictions are not only quantitatively, but also qualitatively inconsistent with our MD simulation results. In 1987, Jeyadev and Conwell calculated polaron mobility in trans-polyacetylene [79] based on the BTE and deformation potential method. They added a velocity limit to the polaron

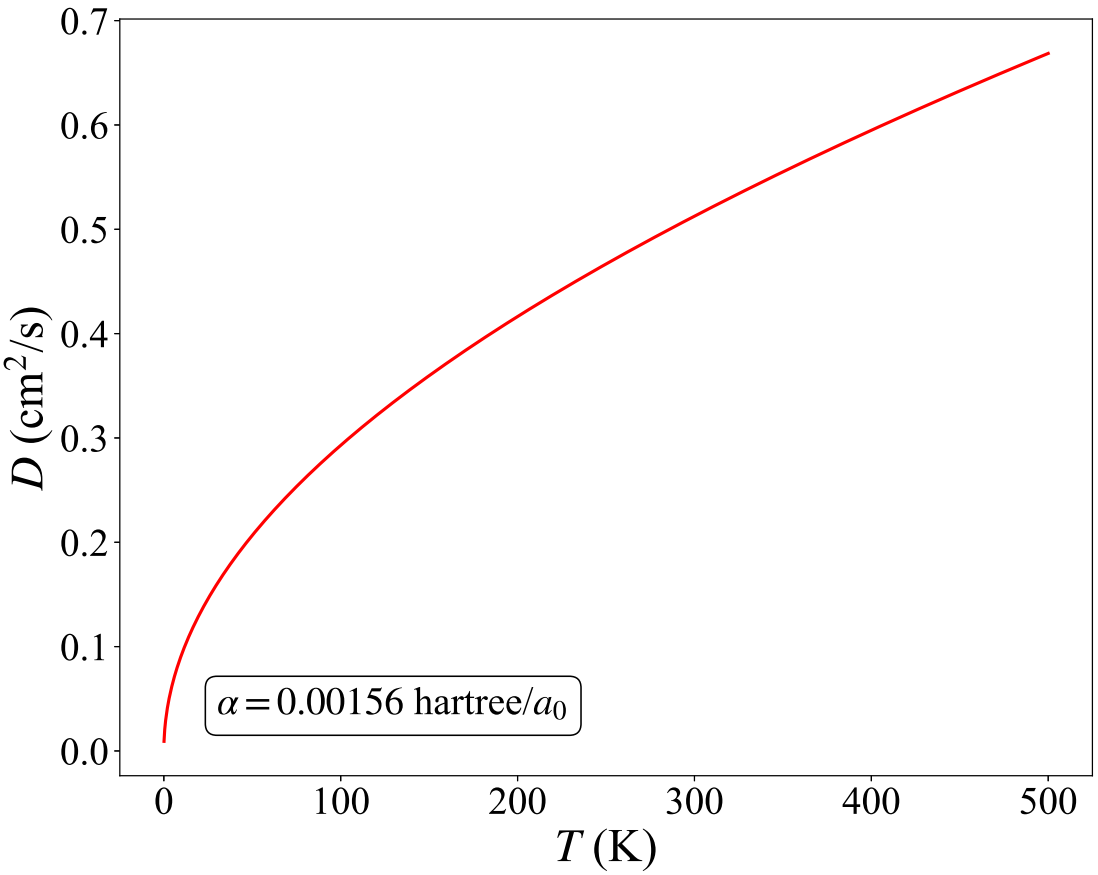

Figure 3.5: D-T relation predicted by Boltzmann transport theory under deformation potential theory for $\alpha = 0.00156$ hartree/a_0.

so that the diffusion constant starts to decrease when temperature is above certain value. When temperature is lower than that value, the diffusion constant still increases as temperature is increasing. Their results are qualitatively similar to our MD simulation, but quantitatively smaller. Moreover, their results are obtained using the original SSH parameter, with which we cannot observe a diffusive behavior in our simulation. Therefore, BTE method, even with a velocity limit, cannot explain our results. This inconsistency may originate from that Boltzmann transport theory predicts more scattering events than there really are in this 1-D non-dimerized SSH model.

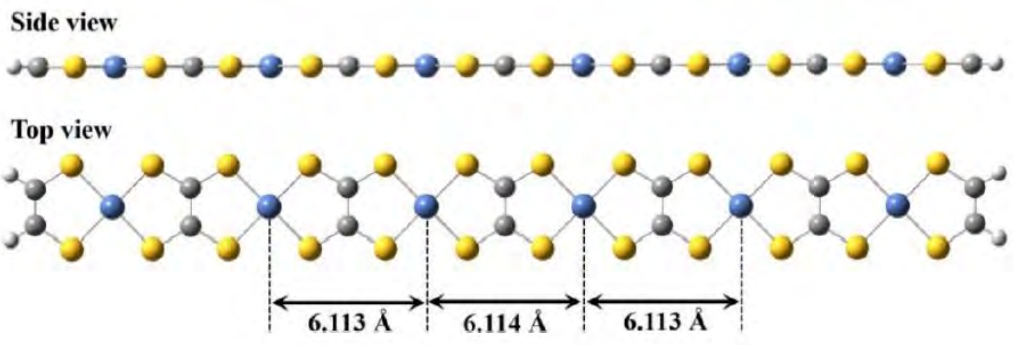

Figure 3.6: Structure of the poly(Ni-C_2S_4). The upper one is viewed from a side, and the lower one is from the top. Grey, yellow, blue, and white balls represent carbon, sulphur, nickel, and hydrogen atoms, respectively. Reprinted figure with permission from [71]. Copyright 2021 American Chemical Society.

3.3 Numerical Simulation for Poly(Ni-C_2S_4)

3.3.1 First-principles Calculations

The poly(Ni-C_2S_4) has a quasi 1-D structure with polymer backbones lie along the x axis as shown in Fig. 3.6. In each monomer, there are one nickel, two carbons, and four sulfurs, and they can move in three-dimensional space, which means there are 21 phonon modes. According to our collaborator, Tianqi Deng, who is one of the authors of the published work cited as [71], the B3LYP exchange correlation functional [80] in Gaussian 09 program [81] with LanL2DZ basis set [82] for Ni atom and 6-31G(d) basis set [83] for other atoms are employed to optimize the structure, and the lattice constant turns to be $a = 6.113$ Å.

We use H^i to represent the electron hopping integrals obtained form the first-principles calculations, where i is to locate relative positions between two monomers. The value of i ranges from -8 to 8 (8 is the chosen cutoff based on the first-principles

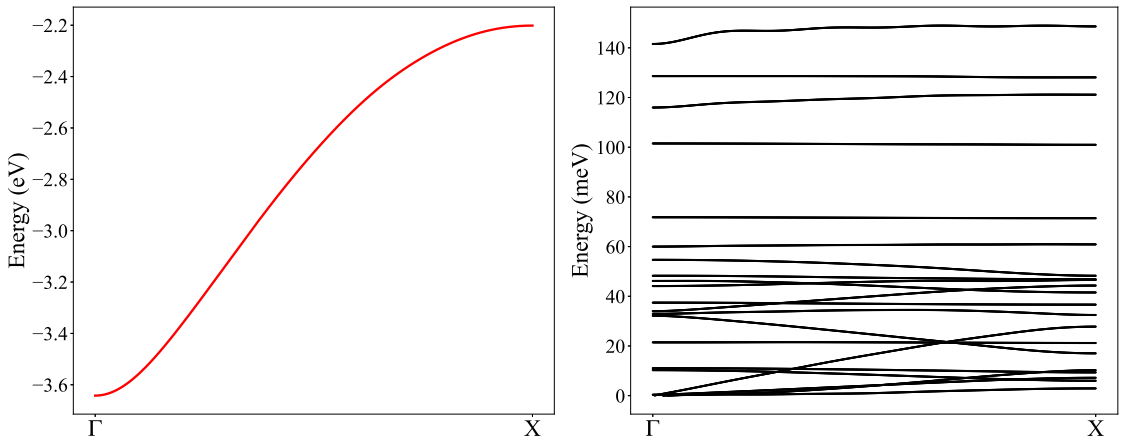

(a) (b)

Figure 3.7: (a) Electron band. (b) Phonon dispersion. Both plots are along the high-symmetry path $\Gamma \to X$, where $\Gamma = (0, 0, 0)$ and $X = (0.5, 0, 0)$.

calculations) indicating we not only consider onsite and nearest neighbors, but also further neighbors. The extracted spring constant matrix between any two monomers is labeled as $K^i_{ll'}$, where i still represents the relative positions with the range $[-8, 8]$, and l, $l' = 1, 2, 3, \cdots, 21$ refer to the normal modes. With these numerical results, we can easily calculate the corresponding electron band and phonon dispersion. Since we want to simulate single electron's motion, only the first conduction band of the poly(Ni-C_2S_4) as shown in Fig. 3.7(a) is considered. Twenty-one phonon branches are plotted in Fig. 3.7(b), from which we can determine the frequency range used in calculating the phonons' Green's functions.

The EPI in this polymer can be expressed by a tensor M^{kl}_{ij}. We use the index l to declare the phonon normal modes from 1 to 21, the index k to address the phonons in k-th supercell, and the indices i, j to locate the electron wavefunctions in i-th and j-th supercell interacting with the phonons in k-th supercell. Based on the results of the first-principles calculations, we truncate the EPI accordingly so that

$|i-j| <= 8$, and $\min(|k-i|, |k-j|) <= 8$. For simplicity, we can take an index transformation: $i \to i-j$, $j \to j-k$, $k \to (k-1) \times 21 + l$ so that the transformed i represents the relative position between two electron wavefunctions ranging from -8 to 8, j represents the relative position between one of the electron wavefunction and the phonons, which is in the range $[-16, 16]$, and k merges the location of phonons and their normal modes with a new range from 1 to $N \times 21$, where N is the number of supercells. The updated indices i, j should satisfy the restriction $|i-j| <= 8$.

3.3.2 MD Simulation Details, Results and Comparison

In our MD simulation, there is still only one electron, and we only allow the electron to hop between monomers. Therefore, compared with previous simulation for the SSH model, the only difference is the degrees of freedom of the phonons. Since the phonons' Green's function can be easily extended to three dimension using the same algorithms as before, it is not a big problem. Recall the Sancho's iterative method we introduced previously, the ingredients k_{00}, k_{01}, k_{10} for the phonons' Green's functions are block matrices in this case,

$$k_{00} = \begin{pmatrix} K^0 & K^1 & \cdots & K^8 \\ K^{-1} & K^0 & \cdots & K^7 \\ \vdots & \ddots & \ddots & \ddots \\ K^{-8} & K^{-7} & \cdots & K^0 \end{pmatrix}, \; k_{01} = \begin{pmatrix} 0 & 0 & \cdots & 0 \\ K^8 & 0 & \cdots & 0 \\ \vdots & \ddots & \ddots & \ddots \\ K^1 & K^2 & \cdots & 0 \end{pmatrix}, \; k_{10} = k_{01}^T. \tag{3.61}$$

The real issue is how to generate the noise in this case. The noise still satisfies the fluctuation-dissipation relation, except that the self energy $\Pi^r[\omega]$ is a block matrix

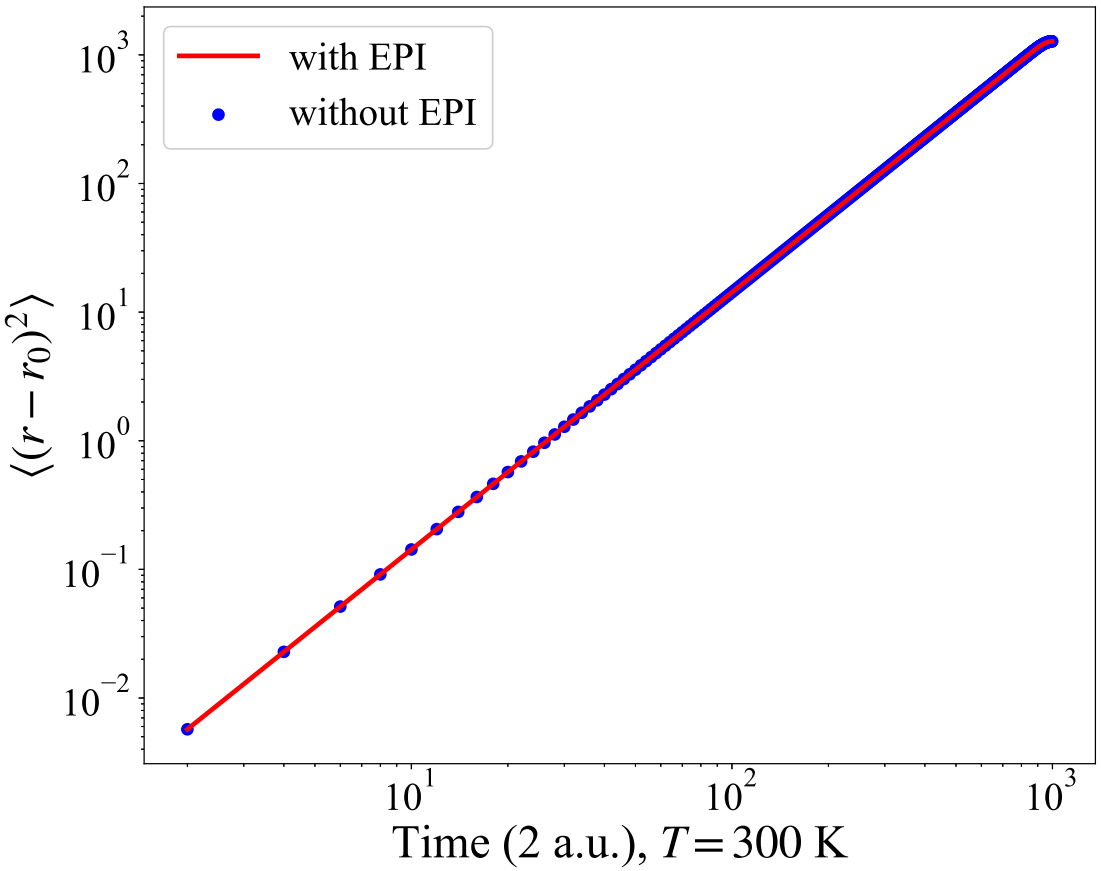

Figure 3.8: Ensemble averaged squared displacement versus time at $T = 300$ K for the poly(Ni-C_2S_4). The step length of the time is chosen to be 2 in atomic units, and the total simulation time is 2000 in atomic units (about 48.4 fs).

now,

$$\Pi^r[\omega] = \begin{pmatrix} k_{10} g_L^r[\omega] k_{01} & 0 & 0 \\ 0 & 0 & 0 \\ 0 & 0 & k_{01} g_R^r[\omega] k_{10} \end{pmatrix}_{(N\times 21)\times(N\times 21)} , \tag{3.62}$$

where we have assumed the leads-center couplings are only non-zero for corner block elements. The surface Greens' functions are also block matrices. To generate the noise, we can use the algorithm discussed by Fishman in his book [84] using the Cholesky decomposition. If a random vector $\boldsymbol{Z}$ has a mean vector $\boldsymbol{\mu}$ and a covariance

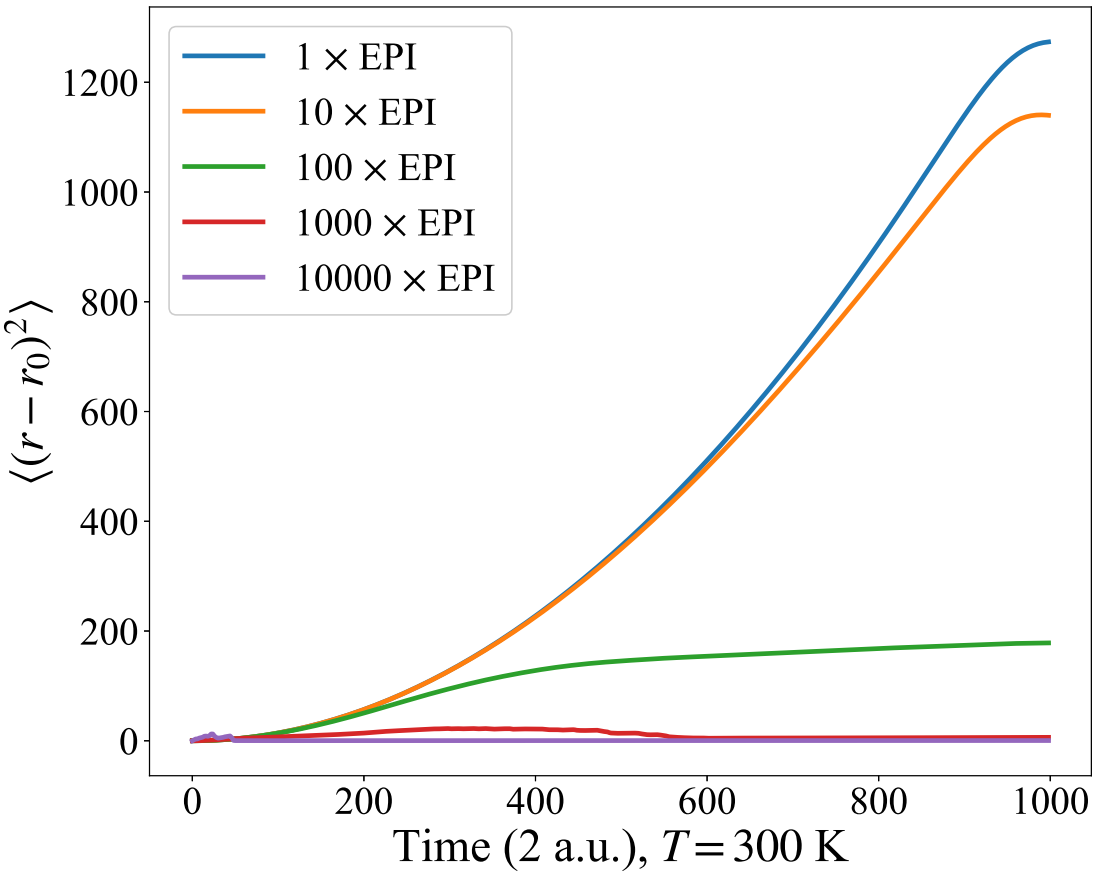

Figure 3.9: Ensemble averaged squared displacement against time at $T = 300$ K for different strength of the EPI with time step length 2 and total simulation time 2000 in atomic units.

matrix Σ which is positive definite, it can be generated by following equation:

$$\boldsymbol{Z} = c\boldsymbol{X} + \boldsymbol{\mu}, \tag{3.63}$$

where c is the lower triangular matrix of the Cholesky decomposition of Σ, *i.e.*, $cc^T = \Sigma$, and $\boldsymbol{X}$ is a vector obeying standard uncorrelated Gaussian distribution $\mathcal{N}(\mathbf{0}, I)$.

Due to the complexity of this three-dimensional case, we only put 99 monomers in the central part with total simulation time 2000 in atomic units (about 48.4 fs). We still let the electron locate at the middle site initially. The ensemble averaged

mean square displacement of the electron against time with and without EPI are illustrated in Fig. 3.8. It can be seen that the two cases are almost coincident. The slope in this log-scaled plot is about 1.99 meaning that the electron's motion is in the ballistic region. After reviewing the original data, we find that the EPI tensor is several orders of magnitude smaller than the electron hopping term. Therefore, we can conclude that in this polymer, the EPI is too weak to affect the electron's hopping, which implies there should be high conductivity. In the limit of low concentration of charge carriers we can reach, the BTE method predicts that the diffusion constant D is about 66 $\mathrm{cm^2 s^{-1}}$ [71], which is already very high. According to our simulation, D can reach 90 $\mathrm{cm^2 s^{-1}}$, although it does not converge due to the size limit. Moreover, if we manually enlarge the EPI, the electron's motion gets slowed down and can be localized when the EPI is strong enough as indicated in Fig. 3.9. The EPI effectively contributes a random onsite terms to the electron's Hamiltonian making it similar to the Anderson tight-binding model, which results in the Anderson localization [85]. However, the original EPI in the polymer is rather weak that the localization length is too large to reach in our simulation.

3.4 Summary

In summary, we have developed a MD method to explore single electron's transport behavior in 1-D among a phonon system with phonon leads at two ends. In our approach, although we have made some classical assumptions, the bath effect is treated quantum mechanically at least, and it has the advantage that it can deal with large system where fully quantum-mechanical treatment is not applicable.

Based on our results, the motion of single electron in the 1-D SSH model with parameters for trans-polyacetylene does not lie in the diffusive region, but in a super diffusive region. When we increase the coupling constant α, it becomes diffusive. However, even in the diffusive range, the diffusion constant is much larger than the prediction of the BTE method. Therefore, the BTE method is inapplicable to the 1-D SSH model. Furthermore, the simulation for poly(Ni-C_2S_4) tells us that the EPI in this polymer is so weak that we need to simulate a large size for a long time to observe a small effect on electron's motion, which is not acceptable. Nonetheless, at least we can conclude that for both the SSH model and poly(Ni-C_2S_4), our simulation gives higher diffusion constant than what the BTE method predicts.

Chapter 4

Phonon Hall effect

Phonon Hall effect, as a phonon analog to the quantum Hall effect of electrons, was not discovered until last decade. However, a hint of this effect can be traced back to a pioneer study by Mead and Truhlar in 1979 [86]. Consider a system with a Hamiltonian as follows:

$$\begin{aligned} H_{\text{total}} &= H_{\text{ph}}(\boldsymbol{R}) + H_{\text{el}}(\boldsymbol{r}) + H_{\text{EPI}}(\boldsymbol{r}, \boldsymbol{R}), \\ H_{\text{ph}} &= \sum_{n=1}^{3N} \frac{(-i\hbar\nabla_{\boldsymbol{R}_n})^2}{2M_n} + U(\boldsymbol{R}), \end{aligned} \tag{4.1}$$

where the three terms represent the phonons' Hamiltonian, electrons' Hamiltonian, and electron-phonon interaction, respectively. $\boldsymbol{R}$ locates the ions, and $\boldsymbol{r}$ locates the electrons. M_n is the mass of n-th ion, N is the total number of ions, and $U(\boldsymbol{R})$ is the total potential among them. If we apply the Born-Oppenheimer approximation to this system, the total wave function is

$$\Psi(\boldsymbol{r}, \boldsymbol{R}) = \psi(\boldsymbol{R})|\alpha_i(\boldsymbol{R})\rangle, \tag{4.2}$$

where ψ is the nuclear wave function, and $\alpha_i(\boldsymbol{R})$ is the i-th member of the set of orthonormal eigenstates of the electronic Hamiltonian satisfying

$$\begin{aligned}(H_{\rm el}+H_{\rm EPI})|\alpha_i(\boldsymbol{R})\rangle &= \varepsilon_i(\boldsymbol{R})|\alpha_i(\boldsymbol{R})\rangle,\\ \langle\alpha_i(\boldsymbol{R})|\alpha_{i'}(\boldsymbol{R})\rangle &= \delta_{ii'},\end{aligned} \tag{4.3}$$

where ε_i is the electronic energy. It can be seen that under the Born-Oppenheimer approximation, electrons' degrees of freedom are not considered in the total wave function. Therefore, the total wave function satisfies

$$\Big[\sum_{n=1}^{3N}\big(\frac{(-i\hbar\nabla_{\boldsymbol{R}_n})^2}{2M_n}\big)+U(\boldsymbol{R})+\varepsilon_i(\boldsymbol{R})\Big]\psi(\boldsymbol{R})|\alpha_i(\boldsymbol{R})\rangle = E\psi(\boldsymbol{R})|\alpha_i(\boldsymbol{R})\rangle, \tag{4.4}$$

where E is the total energy. The second-order derivative of the first term in the left hand site can be expanded to be

$$\begin{aligned}\nabla^2_{\boldsymbol{R}_n}\Big(\psi(\boldsymbol{R})|\alpha_i(\boldsymbol{R})\rangle\Big) &= \nabla_{\boldsymbol{R}_n}\cdot\Big[\Big(\nabla_{\boldsymbol{R}_n}\psi(\boldsymbol{R})\Big)|\alpha_i(\boldsymbol{R})\rangle+\psi(\boldsymbol{R})\nabla_{\boldsymbol{R}_n}|\alpha_i(\boldsymbol{R})\rangle\Big]\\ &= \Big(\nabla^2_{\boldsymbol{R}_n}\psi(\boldsymbol{R})\Big)|\alpha_i(\boldsymbol{R})\rangle+2\Big(\nabla_{\boldsymbol{R}_n}\psi(\boldsymbol{R})\Big)\nabla_{\boldsymbol{R}_n}|\alpha_i(\boldsymbol{R})\rangle\\ &\quad+\psi(\boldsymbol{R})\nabla^2_{\boldsymbol{R}_n}|\alpha_i(\boldsymbol{R})\rangle.\end{aligned} \tag{4.5}$$

Multiplied by $\langle\alpha_i(\boldsymbol{R})|$, the Eq. (4.4) becomes

$$\begin{aligned}\sum_{n=1}^{3N}\Big[\frac{(-i\hbar\nabla_{\boldsymbol{R}_n})^2}{2M_n}-\frac{\hbar^2}{M_n}\langle\alpha_i(\boldsymbol{R})|\nabla_{\boldsymbol{R}_n}|\alpha_i(\boldsymbol{R})\rangle\nabla_{\boldsymbol{R}_n}-\frac{\hbar^2}{2M_n}\langle\alpha_i(\boldsymbol{R})|\nabla^2_{\boldsymbol{R}_n}|\alpha_i(\boldsymbol{R})\rangle\Big]\psi(\boldsymbol{R})\\ +\Big(U(\boldsymbol{R})+\varepsilon_i(\boldsymbol{R})\Big)\psi(\boldsymbol{R})=E\psi(\boldsymbol{R}).\end{aligned} \tag{4.6}$$

For convenience, we define $\boldsymbol{A}_n(\boldsymbol{R}) \equiv i\hbar\langle\alpha_i(\boldsymbol{R})|\nabla_{\boldsymbol{R}_n}|\alpha_i(\boldsymbol{R})\rangle$, which currently is difficult to compute in first-principles calculations and needs further investigations. Moreover, if we insert the completeness $\sum_i|\alpha_i(\boldsymbol{R})\rangle\langle\alpha_i(\boldsymbol{R})|=I$ into the second-order derivative on $|\alpha_i(\boldsymbol{R})\rangle$, and use the Born-Oppenheimer approximation again so that

other electronic states do not couple to each other, *i.e.*, $\langle\alpha_i(\boldsymbol{R})|\nabla_{\boldsymbol{R}_n}|\alpha_{i'}(\boldsymbol{R})\rangle = \delta_{ii'}$, we obtain

$$\begin{aligned}\hbar^2\langle\alpha_i(\boldsymbol{R})|\nabla^2_{\boldsymbol{R}_n}|\alpha_i(\boldsymbol{R})\rangle &= \hbar^2\sum_{i'}\langle\alpha_i(\boldsymbol{R})|\nabla_{\boldsymbol{R}_n}|\alpha_{i'}(\boldsymbol{R})\rangle\langle\alpha_{i'}(\boldsymbol{R})|\nabla_{\boldsymbol{R}_n}|\alpha_i(\boldsymbol{R})\rangle \\ &= \hbar^2\langle\alpha_i(\boldsymbol{R})|\nabla_{\boldsymbol{R}_n}|\alpha_i(\boldsymbol{R})\rangle^2 \\ &= -\boldsymbol{A}_n^2\end{aligned} \tag{4.7}$$

Therefore, the Eq. (4.4) can be further simplified:

$$\Big[\sum_{n=1}^{3N}\frac{(\boldsymbol{P}_n-\boldsymbol{A}_n)^2}{2M_n}+V_{\text{eff}}(\boldsymbol{R})\Big]\psi(\boldsymbol{R}) \equiv H_{\text{eff}}\psi(\boldsymbol{R}) = E\psi(\boldsymbol{R}), \tag{4.8}$$

where we have used the definition $\boldsymbol{P}_n = -i\hbar\nabla_{\boldsymbol{R}_n}$, and define $V_{\text{eff}}(\boldsymbol{R}) \equiv U(\boldsymbol{R})+\varepsilon_i(\boldsymbol{R})$ as an effective potential term. The $\boldsymbol{A}_n(\boldsymbol{R})$ is just the Berry phase of the electronic structure in this system. Moreover, this effective Hamiltonian has the same form as the Hamiltonian under a magnetic field indicating that the Berry phase here plays a similar role as the vector potential of a magnetic field.

Although this derivation has been known for a long time, the effect of the Berry phase is usually ignored due to the difficulty to calculate it. Since it is similar to a magnetic field, applying an external magnetic field to the system should have the same effect, which is exactly what experiments did in recent years. More generally, it is natural to think that if there is any other kind of interaction contributing a Berry-phase-like term, we should observe the same effect.

4.1 Phonon Hall Effect under Non-zero Vector Potential

What is the most general form of a Hamiltonian for phonons that can result in a Hall effect? Let us consider a very general system described by $2N$ Hermitian variables y_j, $j = 1, 2, \cdots, 2N$, for a system of N degrees of freedom (2-D case). In column vector notation, we denote this by y, where x components come first, then followed by y components for each degree of freedom. We assume that the Hamiltonian takes a quadratic form of $\hat{H} = \frac{1}{2} y^T H y$, here we assume H is real and symmetric, superscript T is the matrix transpose. The operators y_j are completely characterized by their commutation relations, $[y_j, y_{j'}] = i\hbar J_{jj'}$. We assume that $J_{jj'}$ is a complex number. Since y is Hermitian, we can show that the matrix J is real and antisymmetric. The Heisenberg equation of motion is simply

$$\frac{dy}{dt} = JHy. \tag{4.9}$$

Two common choices of y appear in the literature, that of Zhang *et al.* use conjugate pairs of displacement coordinates u and momenta p, while Qin *et al.* use the displacements u and velocities $v = du/dt = p - Au$. Here in this paper, we follow Qin's convention. Then the matrix J takes the following form:

$$J = \begin{pmatrix} 0 & I \\ -I & -2A \end{pmatrix}, \quad \text{with} \quad y = \begin{pmatrix} u \\ v \end{pmatrix}, \tag{4.10}$$

here the matrix A is antisymmetric and it is related to the vector potential $\boldsymbol{A}(\boldsymbol{R})$ discussed in last subsection. The vector potential can come from the electronic Berry phases but can also be the effect of other interactions such as Raman-type

spin-phonon interaction, external magnetic fields [25], or spin-orbit interaction within electronic structure [2]. Through out this subsection, index j for bold symbol stands for atom sites, for unbold symbol, j also includes Cartesian components. In a periodic lattice system with a harmonic approximation, we can transform the system into the reciprocal space, and use a combined coordinate and velocity variable $y_{\boldsymbol{q}}$ so that $\hat{H} = \frac{1}{2}\sum_{\boldsymbol{q}} y_{\boldsymbol{q}}^\dagger H(\boldsymbol{q}) y_{\boldsymbol{q}}$. Here $\boldsymbol{q}$ is the wavevector sampling over the first Brillouin zone. Note that $y_{\boldsymbol{q}}$ is not a Hermitian operator; it is a vector of smaller dimension varying over twice the degrees of freedom per unit cell for each $\boldsymbol{q}$. Elements of the $H(\boldsymbol{q})$ matrix are determined by $y_{\boldsymbol{q}}$. The commutation relation in $\boldsymbol{q}$ space is [28]

$$[y_{j\boldsymbol{q}}, y_{j'\boldsymbol{q}'}^\dagger] = i\hbar J_{jj'}(\boldsymbol{q})\delta_{\boldsymbol{q}\boldsymbol{q}'}. \tag{4.11}$$

Next by assuming $y_{\boldsymbol{q}} = \psi_{\boldsymbol{q}} e^{-i\omega t}$, the corresponding eigensystem of the equation of motion will be

$$iJ(\boldsymbol{q})H(\boldsymbol{q})\psi_{\boldsymbol{q}} \equiv H_{\text{eff}}\psi_{\boldsymbol{q}} = \omega\psi_{\boldsymbol{q}}. \tag{4.12}$$

Since the effective Hamiltonian is non-Hermitian, the left eigenvector is not related by Hermitian conjugate to the right eigenvector. We can choose the left eigenvector as $\bar{\psi}_{\boldsymbol{q}} = \psi_{\boldsymbol{q}}^\dagger H(\boldsymbol{q})$. The normalization condition is then $\psi_{\boldsymbol{q}}^\dagger H(\boldsymbol{q})\psi_{\boldsymbol{q}} \equiv \bar{\psi}_{\boldsymbol{q}}\psi_{\boldsymbol{q}} = 1$. This eigen equation is general to any possible source of the non-zero vector potential. For example, we can choose $y_{\boldsymbol{q}} = (\boldsymbol{u}_{\boldsymbol{q}}, \boldsymbol{v}_{\boldsymbol{q}})^T$ where $\boldsymbol{v}_{\boldsymbol{q}} = \dot{\boldsymbol{u}}_{\boldsymbol{q}}, \boldsymbol{u}_{j\boldsymbol{q}} = \sqrt{M_j/N}\sum_l \boldsymbol{x}_{lj} e^{-i\boldsymbol{q}\cdot\boldsymbol{R}_l^0}$ with $\boldsymbol{R}_l^0$ being the real space lattice vector, $\boldsymbol{x}_{lj}$ being the deviation from equilibrium positions of atom j in cell l. N is the total number of unit cells. We write $\boldsymbol{u}_{\boldsymbol{q}}$ without the index j as a column vector consisting of the degrees in a unit cell.

4.1.1 Phonon Hall Conductivity

In last subsection, we have written the general form of a 2-D phonon system with a non-zero vector potential in its Hamiltonian, now we can study the heat transport in this system based on the traditional linear response theory [87] and a correction to it which is called *energy magnetization* [26].

4.1.1.1 General derivation

Consider a general Hamiltonian $H = \int d\boldsymbol{r}\varepsilon(\boldsymbol{r})$, where ε is the energy density. Applying an external gravitational field $\psi(\boldsymbol{r})$ [88] to this system, we obtain the new energy density $\varepsilon_\psi(\boldsymbol{r}) = \Big(1+\psi(\boldsymbol{r})\Big)\varepsilon(\boldsymbol{r})$. The continuity relation requires

$$\frac{\partial\varepsilon_\psi(\boldsymbol{r})}{\partial t} = \frac{1}{i\hbar}[\varepsilon_\psi(\boldsymbol{r}), H] = -\boldsymbol{\nabla}\cdot\boldsymbol{J}_\psi(\boldsymbol{r}), \tag{4.13}$$

where $\boldsymbol{J_\psi(r)}$ is the heat current. Then we assume there is a simple scaling law between the perturbed and unperturbed heat current that: $\boldsymbol{J}_\psi(\boldsymbol{r}) = \Big(1+\psi(\boldsymbol{r})\Big)^2\boldsymbol{J}(\boldsymbol{r})$. This assumption is consistent with the energy scaling. When in equilibrium, we can always define the heat current as the curl of a vector $\boldsymbol{M}$ describing a circulating current due to the property that the divergence of a curl is always zero,

$$\boldsymbol{J}^{\rm eq}_\psi(\boldsymbol{r}) \equiv \nabla\times\boldsymbol{M}_\psi(\boldsymbol{r}) = \Big(1+\psi(\boldsymbol{r})\Big)^2\boldsymbol{J}^{\rm eq}(\boldsymbol{r}) \equiv \Big(1+\psi(\boldsymbol{r})\Big)^2\boldsymbol{\nabla}\times\boldsymbol{M}(\boldsymbol{r}). \tag{4.14}$$

Therefore, $\boldsymbol{M}_\psi(\boldsymbol{r}) = \Big(1+\psi(\boldsymbol{r})\Big)^2\boldsymbol{M}(\boldsymbol{r}) + \boldsymbol{\nabla}\phi(\boldsymbol{r})$, where $\phi(\boldsymbol{r})$ is an arbitrary function. Of course, this circulating current can exist even not in equilibrium, which is usually ignored. In equilibrium, the density matrix is: $\rho_0 = \frac{1}{Z_0}e^{-\beta_0 H}$, where $\beta_0 = 1/k_BT_0$, T_0 is the corresponding temperature. When not in equilibrium, to be consistent

with the thermodynamics that

$$\rho_\psi = \frac{1}{Z_\psi}\exp\Big[-\int d\boldsymbol{r}\frac{\Big(1+\psi(\boldsymbol{r})\Big)\varepsilon(\boldsymbol{r})}{k_BT(\boldsymbol{r})}\Big], \tag{4.15}$$

we define $\beta(\boldsymbol{r}) \equiv \Big[k_B\Big(1+\psi(\boldsymbol{r})\Big)T(\boldsymbol{r})\Big]^{-1}$ with the conjugate force $\boldsymbol{X} = \boldsymbol{\nabla}\beta(\boldsymbol{r})$. The nonequilibrium density matrix can be approximately divided into two parts: $\rho_\psi = \rho^{\rm leq} + \delta\rho_\psi$. $\rho^{\rm leq}$ is the local equilibrium density matrix determined by the local temperature $T(\boldsymbol{r})$ [26],

$$\rho^{\rm leq} = \frac{1}{Z}\exp\Big[-\int d\boldsymbol{r}\frac{\varepsilon(\boldsymbol{r})}{k_BT(\boldsymbol{r})}\Big]. \tag{4.16}$$

The second term is the linear response correction to $\rho^{\rm leq}$ which is determined by $i\hbar\partial\rho_\psi/\partial t = -[H_\psi, \rho_\psi]$. With the help of the density matrix, we can calculate the expectation value of the heat current:

$$\boldsymbol{J}_\psi(\boldsymbol{r}) = {\rm Tr}[\rho^{\rm leq}\boldsymbol{J}_\psi(\boldsymbol{r})] + {\rm Tr}[\delta\rho_\psi\boldsymbol{J}_\psi(\boldsymbol{r})]. \tag{4.17}$$

With no doubt, the second term is the standard Kubo contribution $\boldsymbol{J}^{\rm Kubo}$. The extra contribution is due to the inhomogeneous temperature field. To handle it, we assume $1/T(\boldsymbol{r}) \approx 1/T_0 + \delta\Big(1/T(\boldsymbol{r})\Big)$, and define the perturbation as $x(\boldsymbol{r}) = -T_0\delta\Big(1/T(\boldsymbol{r})\Big)$. Using the linear response theory, we obtain

$$\boldsymbol{J}^{\rm leq} = {\rm Tr}[\rho^{\rm leq}\boldsymbol{J}_\psi(\boldsymbol{r})] \approx {\rm Tr}[\rho_0\boldsymbol{J}_\psi(\boldsymbol{r})] + \int d\boldsymbol{r}'\boldsymbol{\chi}(\boldsymbol{r},\boldsymbol{r}')x(\boldsymbol{r}'), \tag{4.18}$$

where $\boldsymbol{\chi}(\boldsymbol{r},\boldsymbol{r}') = \beta_0\langle\varepsilon(\boldsymbol{r}');\boldsymbol{J}(\boldsymbol{r})\rangle_0$. Let us calculate the divergence of this response function,

$$\begin{aligned}\boldsymbol{\nabla}\cdot\boldsymbol{\chi}(\boldsymbol{r},\boldsymbol{r}') &= -\beta_0\langle\varepsilon(\boldsymbol{r}');\dot{\varepsilon}(\boldsymbol{r})\rangle_0 \\ &= \frac{1}{i\hbar}\langle[\varepsilon(\boldsymbol{r}'),\varepsilon(\boldsymbol{r})]\rangle_0,\end{aligned} \tag{4.19}$$

where we have used the equations: $\boldsymbol{\nabla}\cdot\boldsymbol{J}(\boldsymbol{r}) = -\dot{\varepsilon}(\boldsymbol{r})$, and $-i\hbar\beta_0\langle A;\dot{B}\rangle_0 = \langle[A,B]\rangle_0$.

Define the response function in $\boldsymbol{q}$ space as follows:

$$\boldsymbol{\chi}_{\boldsymbol{q}}(\boldsymbol{r}) \equiv \int d\boldsymbol{r}'\boldsymbol{\chi}(\boldsymbol{r},\boldsymbol{r}')e^{-i\boldsymbol{q}\cdot(\boldsymbol{r}-\boldsymbol{r}')}. \tag{4.20}$$

Then the divergence of $\boldsymbol{\chi}_{\boldsymbol{q}}(\boldsymbol{r})$ is

$$\boldsymbol{\nabla}\cdot\boldsymbol{\chi}_{\boldsymbol{q}}(\boldsymbol{r}) = -i\boldsymbol{q}\cdot\boldsymbol{\chi}_{\boldsymbol{q}}(\boldsymbol{r}) + \frac{1}{i\hbar}\int d\boldsymbol{r}'\langle[\varepsilon(\boldsymbol{r}'),\varepsilon(\boldsymbol{r})]\rangle_0 e^{-i\boldsymbol{q}\cdot(\boldsymbol{r}-\boldsymbol{r}')} \tag{4.21}$$

If we set $1+\psi(\boldsymbol{r}) = e^{i\boldsymbol{q}\cdot\boldsymbol{r}}$, the right hand side becomes

$$\begin{aligned}\frac{1}{i\hbar}\int d\boldsymbol{r}'\langle[\varepsilon_\psi(\boldsymbol{r}'),\varepsilon_{psi}(\boldsymbol{r})]\rangle_0 e^{-2i\boldsymbol{q}\cdot\boldsymbol{r}} &= \boldsymbol{\nabla}\cdot\Big(e^{2i\boldsymbol{q}\cdot\boldsymbol{r}}\boldsymbol{J}(\boldsymbol{r})\Big)e^{-2i\boldsymbol{q}\cdot\boldsymbol{r}} \\ &= \langle\boldsymbol{\nabla}\cdot\boldsymbol{J}(\boldsymbol{r})\rangle_0 + 2i\boldsymbol{q}\cdot\langle\boldsymbol{J}(\boldsymbol{r})\rangle_0 \\ &= 2i\boldsymbol{q}\cdot\Big(\boldsymbol{\nabla}\times\boldsymbol{M}(\boldsymbol{r})\Big),\end{aligned} \tag{4.22}$$

where we have used $[H_\psi,\varepsilon_\psi(\boldsymbol{r})] = i\hbar\boldsymbol{\nabla}\cdot\boldsymbol{J}_\psi(\boldsymbol{r})$, $\boldsymbol{\nabla}\cdot\boldsymbol{J}^{\mathrm{eq}}(\boldsymbol{r}) = 0$, and $\boldsymbol{J}^{\mathrm{eq}}(\boldsymbol{r}) = \boldsymbol{\nabla}\times\boldsymbol{M}(\boldsymbol{r})$. Therefore, the response function $\boldsymbol{\chi}_{\boldsymbol{q}}(\boldsymbol{r})$ satisfies

$$\boldsymbol{\nabla}\cdot\boldsymbol{\chi}_{\boldsymbol{q}}(\boldsymbol{r}) + i\boldsymbol{q}\cdot\boldsymbol{\chi}_{\boldsymbol{q}}(\boldsymbol{r}) - 2i\boldsymbol{q}\cdot\Big(\boldsymbol{\nabla}\times\boldsymbol{M}(\boldsymbol{r})\Big) = 0. \tag{4.23}$$

This equation has a formal solution: $\boldsymbol{\chi}_{\boldsymbol{q}}(\boldsymbol{r}) = -2i\boldsymbol{q}\times\boldsymbol{M}(\boldsymbol{r}) + e^{-i\boldsymbol{q}\cdot\boldsymbol{r}}\boldsymbol{\nabla}\times\boldsymbol{\Lambda}_{\boldsymbol{q}}(\boldsymbol{r})$, where $\boldsymbol{\Lambda}_{\boldsymbol{q}}(\boldsymbol{r})$ is an arbitrary function.

In the Eq. (4.18), the linear response term can be related to $\boldsymbol{\Lambda}_{\boldsymbol{q}=0}(\boldsymbol{r})$,

$$\begin{aligned}\delta\boldsymbol{J}^{\mathrm{eq}}(\boldsymbol{r}) &\approx -\int d\boldsymbol{r}'\boldsymbol{\chi}(\boldsymbol{r},\boldsymbol{r}')T_0\delta(1/T_0) \\ &= -\boldsymbol{\chi}_{\boldsymbol{q}=0}(\boldsymbol{r})T_0\delta(1/T_0) \\ &= -\boldsymbol{\nabla}\times\Big[\boldsymbol{\Lambda}_{\boldsymbol{q}=0}(\boldsymbol{r})T_0\delta(1/T_0)\Big].\end{aligned} \tag{4.24}$$

Meanwhile, this deviation can be defined as $\delta\boldsymbol{J}^{\mathrm{eq}}(\boldsymbol{r}) \equiv \boldsymbol{\nabla}\times\delta\boldsymbol{M}(\boldsymbol{r})$. Therefore, comparing these two equations, we obtain

$$\boldsymbol{\Lambda}_{\boldsymbol{q}=0}(\boldsymbol{r}) = -\frac{\delta\boldsymbol{M}}{T_0\delta(1/T_0)} = T_0\frac{\partial\boldsymbol{M}(\boldsymbol{r})}{\partial T_0}. \tag{4.25}$$

To pick out the $\boldsymbol{\Lambda}_{\boldsymbol{q}=0}(\boldsymbol{r})$ from $\boldsymbol{\chi}_{\boldsymbol{q}}(\boldsymbol{r})$, with the help of the cross product rule $\boldsymbol{\nabla}\times(\boldsymbol{A}\times\boldsymbol{B})=\boldsymbol{A}(\boldsymbol{\nabla}\cdot\boldsymbol{B})-\boldsymbol{B}(\boldsymbol{\nabla}\cdot\boldsymbol{A})+(\boldsymbol{B}\cdot\boldsymbol{\nabla})\boldsymbol{A}-(\boldsymbol{A}\cdot\boldsymbol{\nabla})\boldsymbol{B}$ and $\boldsymbol{\nabla}\times(\phi\boldsymbol{A})=(\boldsymbol{\nabla}\phi)\times\boldsymbol{A}+\phi\boldsymbol{\nabla}\times\boldsymbol{A}$ for any scalar ϕ and vector $\boldsymbol{A},\boldsymbol{B}$, we apply $\boldsymbol{\nabla}_{\boldsymbol{q}}\times$ to $\boldsymbol{\chi}_{\boldsymbol{q}}(\boldsymbol{r})$:

$$\begin{aligned}\boldsymbol{\nabla}\times\boldsymbol{\chi}_{\boldsymbol{q}}(\boldsymbol{r}) &= \boldsymbol{\nabla}_{\boldsymbol{q}}\times\Big\{-i\boldsymbol{q}\times\Big[2\boldsymbol{M}(\boldsymbol{r})-e^{-i\boldsymbol{q}\cdot\boldsymbol{r}}\boldsymbol{\Lambda}_{\boldsymbol{q}}(\boldsymbol{r})\Big]\Big\}+\boldsymbol{\nabla}_{\boldsymbol{q}}\times\boldsymbol{\nabla}\times\Big[e^{-i\boldsymbol{q}\cdot\boldsymbol{r}}\boldsymbol{\Lambda}_{\boldsymbol{q}}(\boldsymbol{r})\Big]\\ &= (-i\boldsymbol{q})\Big\{\boldsymbol{\nabla}_{\boldsymbol{q}}\cdot\Big[2\boldsymbol{M}(\boldsymbol{r})-e^{-i\boldsymbol{q}\cdot\boldsymbol{r}}\boldsymbol{\Lambda}_{\boldsymbol{q}}(\boldsymbol{r})\Big]\Big\}+\Big[2\boldsymbol{M}(\boldsymbol{r})-e^{-i\boldsymbol{q}\cdot\boldsymbol{r}}\boldsymbol{\Lambda}_{\boldsymbol{q}}(\boldsymbol{r})\Big]\boldsymbol{\nabla}_{\boldsymbol{q}}\cdot(i\boldsymbol{q})\\ &\quad-\Big\{\Big[2\boldsymbol{M}(\boldsymbol{r})-e^{-i\boldsymbol{q}\cdot\boldsymbol{r}}\boldsymbol{\Lambda}_{\boldsymbol{q}}(\boldsymbol{r})\Big]\cdot\boldsymbol{\Lambda}_{\boldsymbol{q}}\Big\}(-i\boldsymbol{q})+i\boldsymbol{q}\cdot\boldsymbol{\nabla}_{\boldsymbol{q}}\Big[2\boldsymbol{M}(\boldsymbol{r})-e^{-i\boldsymbol{q}\cdot\boldsymbol{r}}\boldsymbol{\Lambda}_{\boldsymbol{q}}(\boldsymbol{r})\Big]\\ &\quad+\boldsymbol{\nabla}_{\boldsymbol{q}}\times\boldsymbol{\nabla}\times\Big[e^{-i\boldsymbol{q}\cdot\boldsymbol{r}}\boldsymbol{\Lambda}_{\boldsymbol{q}}(\boldsymbol{r})\Big].\end{aligned}\tag{4.26}$$

Since $\boldsymbol{A}(\boldsymbol{\nabla}_{\boldsymbol{q}}\cdot\boldsymbol{q})=3\boldsymbol{A}$ and $(\boldsymbol{A}\cdot\boldsymbol{\nabla}_{\boldsymbol{q}})\boldsymbol{q}=\boldsymbol{A}$, if we take $\boldsymbol{q}\to 0$, we obtain

$$\boldsymbol{\nabla}_{\boldsymbol{q}}\times\boldsymbol{\chi}_{\boldsymbol{q}}(\boldsymbol{r})|_{\boldsymbol{q}\to 0}=4i\boldsymbol{M}(\boldsymbol{r})-2i\boldsymbol{\Lambda}_{\boldsymbol{q}=0}(\boldsymbol{r})+\boldsymbol{\nabla}_{\boldsymbol{q}}\times\boldsymbol{\nabla}\times\Big[e^{-i\boldsymbol{q}\cdot\boldsymbol{r}}\boldsymbol{\Lambda}_{\boldsymbol{q}}(\boldsymbol{r})\Big]\Big|_{\boldsymbol{q}\to 0}.\tag{4.27}$$

By defining $\boldsymbol{U}(\boldsymbol{r})\equiv\frac{i}{2}\boldsymbol{\nabla}_{\boldsymbol{q}}\times\Big[e^{-i\boldsymbol{q}\cdot\boldsymbol{r}}\boldsymbol{\Lambda}_{\boldsymbol{q}}(\boldsymbol{r})\Big]\Big|_{\boldsymbol{q}\to 0}$, it becomes

$$\frac{i}{2}\boldsymbol{\nabla}_{\boldsymbol{q}}\times\boldsymbol{\chi}_{\boldsymbol{q}}(\boldsymbol{r})|_{\boldsymbol{q}\to 0}=-2\boldsymbol{M}(\boldsymbol{r})+\boldsymbol{\Lambda}_{\boldsymbol{q}=0}-\boldsymbol{\nabla}\times\boldsymbol{U}(\boldsymbol{r}).\tag{4.28}$$

Finally, to obtain the global circulating current $\boldsymbol{M}\equiv\int d\boldsymbol{r}\boldsymbol{M}(\boldsymbol{r})$, we integrate over $\boldsymbol{r}$ on both sides so that

$$\begin{aligned}2\boldsymbol{M}-T_0\frac{\partial\boldsymbol{M}}{\partial T_0} &= \frac{1}{2i}\boldsymbol{\nabla}_{\boldsymbol{q}}\times\boldsymbol{\chi}_{\boldsymbol{q}}|_{\boldsymbol{q}\to 0}\\ &= \frac{\beta_0}{2i}\boldsymbol{\nabla}_{\boldsymbol{q}}\times\langle\varepsilon_{-\boldsymbol{q}};\boldsymbol{J}_{\boldsymbol{q}}\rangle_0|_{\boldsymbol{q}\to 0},\end{aligned}\tag{4.29}$$

where we have assumed that $\int d\boldsymbol{r}\boldsymbol{\nabla}\times\boldsymbol{U}(\boldsymbol{r})=0$ for it is an integral of a total derivative of a well behaved function. $\varepsilon_{-\boldsymbol{q}},\boldsymbol{J}_{\boldsymbol{q}}$ are the Fourier transform of $\varepsilon(\boldsymbol{r}),\boldsymbol{J}(\boldsymbol{r})$, respectively.

Let us go back to the Eq. (4.18), with the inverse Fourier transformation of $\boldsymbol{\chi}(\boldsymbol{r},\boldsymbol{r}')$,

$$\boldsymbol{\chi}(\boldsymbol{r},\boldsymbol{r}')=\int\frac{d\boldsymbol{q}}{(2\pi)^3}\Big[-2i\boldsymbol{q}\times\boldsymbol{M}(\boldsymbol{r})+e^{-i\boldsymbol{q}\cdot\boldsymbol{r}}\boldsymbol{\nabla}\boldsymbol{\Lambda}_{\boldsymbol{q}}(\boldsymbol{r})\Big]e^{i\boldsymbol{q}\cdot(\boldsymbol{r}-\boldsymbol{r}')}, \tag{4.30}$$

the local equilibrium current can be rewritten as follows:

$$\begin{aligned}\boldsymbol{J}^{\mathrm{leq}}&\approx\boldsymbol{J}^{\mathrm{eq}}(\boldsymbol{r})+\int d\boldsymbol{r}'\int\frac{d\boldsymbol{q}}{(2\pi)^3}\Big\{-2[\boldsymbol{\nabla}(e^{i\boldsymbol{q}\cdot\boldsymbol{r}})]\times\boldsymbol{M}(\boldsymbol{r})+\boldsymbol{\Lambda}_{\boldsymbol{q}}(\boldsymbol{r})\Big\}x(\boldsymbol{r}')e^{-i\boldsymbol{q}\cdot\boldsymbol{r}'}\\&=\boldsymbol{J}^{\mathrm{eq}}(\boldsymbol{r})+2\boldsymbol{M}(\boldsymbol{r})\times\boldsymbol{\nabla}x(\boldsymbol{r})+\boldsymbol{\nabla}\times\int d\boldsymbol{r}'\boldsymbol{\Lambda}(\boldsymbol{r},\boldsymbol{r}')x(\boldsymbol{r}'),\end{aligned} \tag{4.31}$$

where we have used

$$\int d\boldsymbol{r}'\int\frac{d\boldsymbol{q}}{(2\pi)^3}e^{i\boldsymbol{q}\cdot(\boldsymbol{r}-\boldsymbol{r}')}x(\boldsymbol{r}')=\int d\boldsymbol{r}'\delta(\boldsymbol{r}-\boldsymbol{r}')x(\boldsymbol{r}')=x(\boldsymbol{r}), \tag{4.32}$$

and defined $\boldsymbol{\Lambda}(\boldsymbol{r},\boldsymbol{r}')\equiv\int\frac{d\boldsymbol{q}}{(2\pi)^3}\boldsymbol{\Lambda}_{\boldsymbol{q}}(\boldsymbol{r})e^{-i\boldsymbol{q}\cdot\boldsymbol{r}'}$. Recall that $x(\boldsymbol{r})=-T_0\delta\Big(1/T(\boldsymbol{r})\Big)$, and $\delta\Big(1/T(\boldsymbol{r})\Big)=\Big(1/T(\boldsymbol{r})-1/T_0\Big)$. Therefore, $\boldsymbol{\nabla}x(\boldsymbol{r})=-T_0\boldsymbol{\nabla}(1/T)$. Moreover, $\boldsymbol{J}^{\mathrm{eq}}=\Big(1+\psi(\boldsymbol{r})\Big)^2\boldsymbol{\nabla}\times\boldsymbol{M}(\boldsymbol{r})$. Combining all these formulas, the local equilibrium current is

$$\boldsymbol{J}^{\mathrm{leq}}\approx\Big(1+\psi(\boldsymbol{r})\Big)^2\boldsymbol{\nabla}\times\boldsymbol{M}(\boldsymbol{r})-2\boldsymbol{M}(\boldsymbol{r})\times T_0\boldsymbol{\nabla}\Big(\frac{1}{T(\boldsymbol{r})}\Big). \tag{4.33}$$

Furthermore, the derivative of the inverse of local temperature can be related to the external filed ψ and predefined $\beta(\boldsymbol{r})$:

$$\begin{aligned}\boldsymbol{\nabla}\Big(\frac{1}{T(\boldsymbol{r})}\Big)&=\boldsymbol{\nabla}\Big[k_B\beta(\boldsymbol{r})\Big(1+\psi(\boldsymbol{r})\Big)\Big]\\&=\frac{1}{\beta(\boldsymbol{r})T(\boldsymbol{r})}\boldsymbol{X}(\boldsymbol{r})+\frac{1}{\Big(1+\psi(\boldsymbol{r})\Big)T(\boldsymbol{r})}\boldsymbol{\nabla}\psi(\boldsymbol{r})\\&=\Big(T_0\delta\Big(\frac{1}{T(\boldsymbol{r})}\Big)+1\Big)\Big[\frac{1}{\beta(\boldsymbol{r})}\boldsymbol{X}(\boldsymbol{r})+\frac{1}{\Big(1+\psi(\boldsymbol{r})\Big)}\boldsymbol{\nabla}\psi(\boldsymbol{r})\Big].\end{aligned} \tag{4.34}$$

Substituting this formula into $\boldsymbol{J}^{\mathrm{eq}}(\boldsymbol{r})$, we obtain

$$\begin{aligned}\boldsymbol{J}^{\mathrm{leq}} &\approx \Big(1+\psi(\boldsymbol{r})\Big)^2\boldsymbol{\nabla}\times\boldsymbol{M}(\boldsymbol{r})+2\boldsymbol{\nabla}\psi(\boldsymbol{r})\times\boldsymbol{M}(\boldsymbol{r})-\frac{2}{\beta(\boldsymbol{r})}\boldsymbol{M}(\boldsymbol{r})\times\boldsymbol{X}(\boldsymbol{r})+\boldsymbol{\nabla}\times\delta\boldsymbol{M}(\boldsymbol{r})\\ &=\boldsymbol{\nabla}\times\Big[\Big(1+\psi(\boldsymbol{r})\Big)^2\boldsymbol{M}(\boldsymbol{r})\Big]-\frac{2}{\beta(\boldsymbol{r})}\boldsymbol{M}(\boldsymbol{r})\times\boldsymbol{X}(\boldsymbol{r})+\boldsymbol{\nabla}\times\delta\boldsymbol{M}(\boldsymbol{r})\\ &\equiv\boldsymbol{\nabla}\times\boldsymbol{M}_{\psi}(\boldsymbol{r})-\frac{2}{\beta(\boldsymbol{r})}\boldsymbol{M}(\boldsymbol{r})\times\boldsymbol{X}(\boldsymbol{r}),\end{aligned} \tag{4.35}$$

where we keep only the linear order of $\psi(\boldsymbol{r})$ and $\delta(1/T(\boldsymbol{r}))$, and define $\boldsymbol{M}_{\psi}(\boldsymbol{r})\equiv\Big(1+\psi(\boldsymbol{r})\Big)^2\boldsymbol{M}(\boldsymbol{r})+\delta\boldsymbol{M}(\boldsymbol{r}),\delta\boldsymbol{M}(\boldsymbol{r})\equiv\int d\boldsymbol{r}'\boldsymbol{\Lambda}(\boldsymbol{r},\boldsymbol{r}')x(\boldsymbol{r}')$.

Going through the derivation, the Eq. (4.17) can be rewritten as

$$\boldsymbol{J}_{\psi}(\boldsymbol{r})=\boldsymbol{J}^{\mathrm{Kubo}}(\boldsymbol{r})+\boldsymbol{\nabla}\times\boldsymbol{M}_{\psi}(\boldsymbol{r})-\frac{2}{\beta(\boldsymbol{r})}\boldsymbol{M}(\boldsymbol{r})\times\boldsymbol{X}(\boldsymbol{r}). \tag{4.36}$$

However, this expression does not satisfy the fundamental Onsager relation and Einstein relation in nonequilibrium thermodynamics which require the heat current should be proportional to the conjugate force, $\boldsymbol{X}(\boldsymbol{r})$, in our case. Therefore, we define the transport heat current as follows:

$$\boldsymbol{J}^{\mathrm{tr}}(\boldsymbol{r})\equiv\boldsymbol{J}_{\psi}(\boldsymbol{r})-\boldsymbol{\nabla}\times\boldsymbol{M}_{\psi}(\boldsymbol{r}). \tag{4.37}$$

Integrating over $\boldsymbol{r}$, we obtain the global transport heat current,

$$\begin{aligned}\boldsymbol{J}^{\mathrm{tr}}&\equiv\frac{1}{V}\int d\boldsymbol{r}\boldsymbol{J}^{\mathrm{tr}}(\boldsymbol{r})\\ &=\frac{1}{V}\int d\boldsymbol{r}\Big[\boldsymbol{J}^{\mathrm{Kubo}}(\boldsymbol{r})-\frac{1}{\beta(\boldsymbol{r})}\boldsymbol{M}(\boldsymbol{r})\times\boldsymbol{X}(\boldsymbol{r})\Big].\end{aligned} \tag{4.38}$$

In linear response theory, to calculate the transport coefficient, we choose the "rapid" case [88], *i.e.*, the external fields vary rapidly so that the energy density almost stays the same. In this situation, the temperature field can also be regarded as a constant. Moreover, if we set $\psi(\boldsymbol{r})=\psi_{\boldsymbol{q}}e^{i\boldsymbol{q}\cdot\boldsymbol{r}}$, then $\boldsymbol{\nabla}\psi(\boldsymbol{r})=i\boldsymbol{q}e^{i\boldsymbol{q}\cdot\boldsymbol{r}}\psi_{\boldsymbol{q}}$. In the "rapid"

case, $\boldsymbol{q} \to 0$, therefore, $\boldsymbol{\nabla}\psi(\boldsymbol{r})$ will be irrelevant to $\boldsymbol{r}$. Based on the discussion above, we can extract $\boldsymbol{X}$ out of the integral. With the Kubo formula [88], the Kubo contribution is [26]

$$\begin{aligned} &\frac{1}{V}\int d\boldsymbol{r}\boldsymbol{J}^{\mathrm{Kubo}}(\boldsymbol{r}) \equiv \overleftrightarrow{L}\,\boldsymbol{X}, \\ &\overleftrightarrow{L}_{\alpha\gamma} = \frac{1}{V}\lim_{s\to 0}\lim_{\boldsymbol{q}\to 0}\int_0^\infty dt e^{-st}\langle J_{\gamma,-\boldsymbol{q}}; J_{\alpha,\boldsymbol{q}}(t)\rangle_0. \end{aligned} \tag{4.39}$$

Therefore, the total transport heat current becomes

$$\boldsymbol{J}^{\mathrm{tr}} = \overleftrightarrow{L}\,\boldsymbol{X} - \frac{2}{V\beta_0}\boldsymbol{M}\times\boldsymbol{X}. \tag{4.40}$$

By definition, $\boldsymbol{J}^{\mathrm{tr}} \equiv \kappa^{\mathrm{tr}}\boldsymbol{\nabla}T$. When we measure the thermal conductivity κ in a 2-D system, we set $\psi = 0$ so that $\boldsymbol{X} = -\boldsymbol{\nabla}T/k_B T_0^2$. Comparing the two sides, we obtain

$$\kappa^{\mathrm{tr}}_{xy} = \frac{\overleftrightarrow{L}_{xy}}{k_B T_0^2} + \frac{2M_z}{VT_0}. \tag{4.41}$$

This result was obtained by Qin *et al.* in 2011 [26].

4.1.1.2 Application to Lattice System

Previously, we have introduced a general 2-D phonon system with non-zero vector potential. The transport phonon Hall conductivity in the system contains two parts: one is the traditional Kubo contribution and the other is from the circulating energy magnetization $\boldsymbol{M}$. Compared with a typical phonon system without vector potential, it is the vector potential that causes the energy magnetization. To obtain the phonon Hall conductivity in practical calculation, we apply the general formula to that 2-D phonon system.

In the lattice system, we use $\boldsymbol{R}_{lj} = (\boldsymbol{R}_l, \boldsymbol{r}_j)$ to represent the positions of nuclei, where $\boldsymbol{R}_l = l_1\boldsymbol{a}_1 + l_2\boldsymbol{a}_2$ labels the l-th cell with integer pair (l_1, l_2), $\boldsymbol{r}_j$ labels the

j-th ion within the cell. The energy of l-th cell is

$$\begin{aligned}\varepsilon_l &= \frac{1}{2}\boldsymbol{v}_l^2 + \frac{1}{2}\sum_{l'}\boldsymbol{u}_l K_{ll'}\boldsymbol{u}_{l'} \\ &\equiv \frac{1}{4}\sum_{l'} y_l^T H_{ll'} y_{l'} + \text{h.c.}\end{aligned} \tag{4.42}$$

Here we define $\boldsymbol{u}_{lj} \equiv \sqrt{m_j}\boldsymbol{x}_{lj}$ as the reduced displacement. K is the force constant matrix with dimension $2N$, and $\boldsymbol{v}_l = \boldsymbol{p}_l - (\boldsymbol{A}\boldsymbol{u})_l$ is the velocity under vector potential $\boldsymbol{A}(\boldsymbol{R})$. $y_l \equiv (\boldsymbol{u}_l, \boldsymbol{v}_l)^T$ combines the displacement and velocity so that $H = \text{diag}\{K, I\}$, I is identity matrix. Energy density can be defined as follows:

$$\begin{aligned}\varepsilon(\boldsymbol{r}) &\equiv \sum_l \delta(\boldsymbol{r} - \boldsymbol{R}_l)\varepsilon_l \\ \int d\boldsymbol{r}\varepsilon(\boldsymbol{r}) &= \hat{H}.\end{aligned} \tag{4.43}$$

Continuity requires

$$\frac{\partial\varepsilon(\boldsymbol{r})}{\partial t} + \boldsymbol{\nabla}\cdot\boldsymbol{j}(\boldsymbol{r},t) = 0,\ \boldsymbol{j}(\boldsymbol{r},t) = \boldsymbol{j}^{\text{Kubo}}(\boldsymbol{r},t) + \boldsymbol{\nabla}\times\boldsymbol{M}(\boldsymbol{r},t). \tag{4.44}$$

Transferring into continuous Fourier space by $\varepsilon_{\boldsymbol{k}} = \int \varepsilon(\boldsymbol{r})e^{-i\boldsymbol{k}\cdot\boldsymbol{r}}d\boldsymbol{r}$, $\boldsymbol{j}_{\boldsymbol{k}} = \int \boldsymbol{j}(\boldsymbol{r})e^{-i\boldsymbol{k}\cdot\boldsymbol{r}}d\boldsymbol{r}$, and taking limit $\boldsymbol{k}\to 0$, we have

$$\begin{aligned}\boldsymbol{k}\cdot\boldsymbol{j}_{\boldsymbol{k}} &= i\dot{\varepsilon}_{\boldsymbol{k}} \\ &= \frac{1}{\hbar}\Big[\varepsilon_{\boldsymbol{k}}, H\Big] \\ &= \frac{1}{\hbar}\Big[\sum_l \varepsilon_l e^{-i\boldsymbol{k}\cdot\boldsymbol{R}_l}, H\Big] \\ &\approx \frac{1}{\hbar}\Big[\sum_l \varepsilon_l - i\boldsymbol{k}\cdot\sum_l \varepsilon_l\boldsymbol{R}_l, \sum_{l'}\varepsilon_{l'}\Big] \\ &= \frac{1}{i\hbar}\sum_{ll'}\boldsymbol{k}\cdot\boldsymbol{R}_l\Big[\varepsilon_l, \varepsilon_{l'}\Big] \\ &= \frac{1}{2i\hbar}\sum_{ll'}\boldsymbol{k}\cdot(\boldsymbol{R}_l - \boldsymbol{R}_{l'})\Big[\varepsilon_l, \varepsilon_{l'}\Big].\end{aligned} \tag{4.45}$$

Since $\lim_{\boldsymbol{k}\to 0}\boldsymbol{j}_{\boldsymbol{k}} = \int \boldsymbol{j}_{\boldsymbol{r}} d\boldsymbol{r} \equiv \boldsymbol{J}_{\text{heat}}$ with $\boldsymbol{J}_{\text{heat}}$ as the total heat current, we can eliminate the $\boldsymbol{k}$ on the both sides to obtain the total heat current $\boldsymbol{J}_{\text{heat}}$. Expanding the commutator using the Eq. (4.42), we obtain

$$\begin{aligned}\frac{1}{2i\hbar}\sum_{ll'}(\boldsymbol{R}_l-\boldsymbol{R}_{l'})[\varepsilon_l,\varepsilon_{l'}] &= \frac{1}{2i\hbar}\sum_{ll'}(\boldsymbol{R}_l-\boldsymbol{R}_{l'}) \\ &\quad\times\Big[\frac{1}{4}\sum_m y_l^T H_{lm} y_m + \text{h.c.}, \frac{1}{4}\sum_{m'} y_{l'}^T H_{l'm'} y_{m'} + \text{h.c.}\Big] \\ &= \frac{1}{32i\hbar}\cdot\sum_{ll'}\sum_{mm'}(\boldsymbol{R}_l-\boldsymbol{R}_{l'})\Big\{y_{m'}^T H_{m'l'}[y_l, y_{l'}^T] H_{lm} y_m \\ &\quad + y_{l'}^T H_{l'm'}[y_l, y_{m'}^T] H_{lm} y_m + y_l^T H_{lm}[y_m, y_{l'}^T] H_{l'm'} y_{l'} \\ &\quad + y_l^T H_{lm}[y_m, y_{m'}^T] H_{m'l'} y_{l'}\Big\} + \textbf{other three terms}.\end{aligned} \tag{4.46}$$

Similar to previous definition, $[y_l, y_{l'}^T] \equiv i\hbar J_{ll'}, J = -J^T$. Moreover, we define $(\boldsymbol{AB})'_{ll'} \equiv (\boldsymbol{R}_l - \boldsymbol{R}_{l'})(AB)_{ll'}$. With the definitions, the commutators can be further simplified:

$$\begin{aligned}\frac{1}{2i\hbar}\sum_{ll'}(\boldsymbol{R}_l-\boldsymbol{R}_{l'})[\varepsilon_l,\varepsilon_{l'}] = \frac{1}{32}\sum_{ll'}\sum_{mm'}\Big[&y_{m'}^T H_{m'l'}\boldsymbol{J}'_{l'l} H_{lm} y_m + y_{l'}^T(\boldsymbol{HJ})'_{l'l} H_{lm} y_m \\ &+ y_l^T(\boldsymbol{HJ})'_{ll'} H_{l'm'} y_{m'} + y_l^T(\boldsymbol{HJH})'_{ll'} y_{l'}\Big] \\ &+ \textbf{other three terms}.\end{aligned} \tag{4.47}$$

In the same way, it is easy to find that $\sum_{ll'}(\boldsymbol{R}_l-\boldsymbol{R}_{l'})\Big[\sum_m y_l^T H_{lm} y_m, (\sum_{m'} y_{l'}^T H_{l'm'} y_{m'})^\dagger\Big] = \sum_{ll'}(\boldsymbol{R}_l-\boldsymbol{R}_{l'})\Big[\sum_m y_l^T H_{lm} y_m, \sum_{m'} y_{l'}^T H_{l'm'} y_{m'}\Big]$, and the rest two terms are the conjugate of these two terms. Therefore, the heat current is

$$\begin{aligned}\boldsymbol{J}_{\text{heat}} = \frac{1}{16}\sum_{ll'}\sum_{mm'}\Big[&y_{m'}^T H_{m'l'}\boldsymbol{J}'_{l'l} H_{lm} y_m + y_{l'}^T(\boldsymbol{HJ})'_{l'l} H_{lm} y_m \\ &+ y_l^T(\boldsymbol{HJ})'_{ll'} H_{l'm'} y_{m'} + y_l^T(\boldsymbol{HJH})'_{ll'} y_{l'} + \text{h.c.}\Big].\end{aligned} \tag{4.48}$$

Furthermore, it is natural to define the local current operator $\boldsymbol{j}_l$ as

$$\begin{aligned}\boldsymbol{j}_l = \frac{1}{16}\sum_{l'}\sum_{mm'}\Big[&y^T_{m'}H_{m'l'}\boldsymbol{J}'_{l'l}H_{lm}y_m + y^T_{l'}(\boldsymbol{HJ})'_{l'l}H_{lm}y_m \\ &+ y^T_l(\boldsymbol{HJ})'_{ll'}H_{l'm'}y_{m'} + y^T_l(\boldsymbol{HJH})'_{ll'}y_{l'} + \text{h.c.}\Big].\end{aligned} \tag{4.49}$$

For convenience in subsequent derivation, we define $H_{\text{eff}} \equiv iJH$, $(\boldsymbol{H}_{\text{eff}})_{ll'} \equiv i(\boldsymbol{JH})'_{ll'}$, which has the property that $(\boldsymbol{H}^T_{\text{eff}})_{ll'} = i(\boldsymbol{HJ})'_{ll'}$.

Let us firstly work out the Kubo term. Switching to reciprocal space, we define the second quantization as follows:

$$\begin{aligned}&y_l \equiv \sum_k \sqrt{\frac{\hbar|\omega_k|}{N}}\psi_k e^{i\boldsymbol{k}\cdot\boldsymbol{R}_l}a_k,\ k \equiv (\boldsymbol{k},\sigma),\\ &[a_k, a^\dagger_{k'}] = \text{sgn}(\sigma)\delta_{kk'},\\ &a^\dagger_k = a_{-k},\ \omega_k = -\omega_{-k},\end{aligned} \tag{4.50}$$

where $\bar{\psi}_k \equiv \psi^\dagger H_{\boldsymbol{k}}$, ω_k is the eigenvalue of the system which has positive and negative branches labelled by σ. This choice differs from the standard second quantization in solid state textbooks where the ω is in the denominator. With this choice, the Hamiltonian can be written as

$$\begin{aligned}\hat{H} &= \frac{1}{4}\sum_{ll'}\Big(\sum_k\sqrt{\frac{\hbar|\omega_k|}{N}}\psi^\dagger_k e^{-i\boldsymbol{k}\cdot\boldsymbol{R}_l}a^\dagger_k\Big)H_{ll'}\Big(\sum_{k'}\sqrt{\frac{\hbar|\omega_{k'}|}{N}}\psi_{k'}e^{i\boldsymbol{k'}\cdot\boldsymbol{R}_{l'}}a_{k'}\Big) + \text{h.c.}\\ &= \frac{\hbar}{4N}\sum_{ll'}\sum_{kk'}\sqrt{|\omega_k||\omega_{k'}|}\psi^\dagger_k e^{-i\boldsymbol{R}_{l'}\cdot(\boldsymbol{k}-\boldsymbol{k'})}H_{ll'}e^{-i\boldsymbol{k}\cdot(\boldsymbol{R}_l-\boldsymbol{R}_{l'})}\psi_{k'}a^\dagger_k a_{k'} + \text{h.c.}\\ &= \frac{1}{4}\sum_{kk'}\hbar\sqrt{|\omega_k||\omega_{k'}|}\psi^\dagger_k H_k\psi_{k'}\delta_{\boldsymbol{kk'}}a^\dagger_k a_{k'} + \text{h.c.}\\ &= \frac{1}{2}\sum_k\hbar|\omega_k|a^\dagger_k a_k.\end{aligned} \tag{4.51}$$

Here we have employed the identity $\sum_{l'} e^{-i\boldsymbol{R}_{l'}\cdot(\boldsymbol{k}-\boldsymbol{k'})} = N\delta_{\boldsymbol{kk'}}$ and $\psi^\dagger_k H_k\psi_{k'} = \bar{\psi}_k\psi_{k'} = \delta_{kk'}$ from the eigensystem in the Eq. (4.12). The Hermitian conjugate of the first

term is just the same itself. Note that this representation includes both positive and negative ω_k. If we only consider the positive branches, it is just the typical form of Harmonic oscillators with second quantization: $\hat{H} = \sum_k \hbar\omega_k(a_k^\dagger a_k + \frac{1}{2})$.

In the reciprocal space, the local heat current becomes

$$\begin{aligned}\boldsymbol{j}_{\boldsymbol{q}} = \sum_l \boldsymbol{j}_l e^{-i\boldsymbol{q}\cdot\boldsymbol{R}_l} = \frac{\hbar}{16N}\sum_{ll'}\sum_{mm'}\sum_{kk'}\sqrt{|\omega_k||\omega_{k'}|}a_k^\dagger a_{k'}\psi_k^\dagger \\ \times\Big[H_{m'l'}\boldsymbol{J}'_{l'l}H_{lm}e^{-i\boldsymbol{k}\cdot\boldsymbol{R}_{m'}+i\boldsymbol{k}'\cdot\boldsymbol{R}_m-i\boldsymbol{q}\cdot\boldsymbol{R}_l} + (\boldsymbol{HJ})'_{l'l}H_{lm}e^{-i\boldsymbol{k}\cdot\boldsymbol{R}_{l'}+i\boldsymbol{k}'\cdot\boldsymbol{R}_m-i\boldsymbol{q}\cdot\boldsymbol{R}_l} \\ + (\boldsymbol{HJ})'_{ll'}H_{l'm'}e^{-i\boldsymbol{k}\cdot\boldsymbol{R}_l+i\boldsymbol{k}'\cdot\boldsymbol{R}_{m'}-i\boldsymbol{q}\cdot\boldsymbol{R}_l} + (\boldsymbol{HJH})'_{ll'}e^{-i\boldsymbol{k}\cdot\boldsymbol{R}_l+i\boldsymbol{k}'\cdot\boldsymbol{R}_{l'}-i\boldsymbol{q}\cdot\boldsymbol{R}_l}\Big]\psi_{k'} \\ + (\text{h.c.}, \boldsymbol{q}\to-\boldsymbol{q}).\end{aligned} \tag{4.52}$$

With the help of the discrete Fourier transform and its identity relation, we can further simplify the expression:

$$\begin{aligned}\boldsymbol{j}_{\boldsymbol{q}} = \frac{\hbar}{16}\sum_{kk'}\sqrt{|\omega_k||\omega_{k'}|}a_k^\dagger a_{k'}\psi_k^\dagger\Big[H_{\boldsymbol{k}}\tilde{\boldsymbol{J}}_{\boldsymbol{k}}H_{\boldsymbol{k}'} + \tilde{\boldsymbol{V}}_{\boldsymbol{k}}^\dagger H_{\boldsymbol{k}'} + \tilde{\boldsymbol{V}}_{\boldsymbol{k}'}^\dagger H_{\boldsymbol{k}'} + (\widetilde{\boldsymbol{HJH}})_{\boldsymbol{k}'} \\ H_{\boldsymbol{k}}\tilde{\boldsymbol{J}}_{\boldsymbol{k}'}H_{\boldsymbol{k}'} + H_{\boldsymbol{k}}\tilde{\boldsymbol{V}}_{\boldsymbol{k}'} + H_{\boldsymbol{k}}\tilde{\boldsymbol{V}}_{\boldsymbol{k}} + (\widetilde{\boldsymbol{HJH}})_{\boldsymbol{k}}\Big]\psi_{k'}\delta_{\boldsymbol{k}',\boldsymbol{k}+\boldsymbol{q}},\end{aligned} \tag{4.53}$$

where $\tilde{\boldsymbol{J}}_{\boldsymbol{k}} \equiv i\boldsymbol{\nabla}_{\boldsymbol{k}}J_{\boldsymbol{k}}$, $\tilde{\boldsymbol{V}}_{\boldsymbol{k}}^\dagger \equiv \boldsymbol{\nabla}_{\boldsymbol{k}}(H_{\text{eff}}^\dagger)_{\boldsymbol{k}}$, $(\widetilde{\boldsymbol{HJH}})_{\boldsymbol{k}'} \equiv i\boldsymbol{\nabla}_{\boldsymbol{k}}(HJH)_{\boldsymbol{k}'}$. Substituting the matrix form of J and H defined before, the final formula for the local heat current is

$$\boldsymbol{j}_{\boldsymbol{q}} = \frac{\hbar}{8}\sum_{kk'}\sqrt{|\omega_k||\omega_{k'}|}a_k^\dagger a_{k'}\psi_k^\dagger(\tilde{\boldsymbol{V}}_{\boldsymbol{k}} + \tilde{\boldsymbol{V}}_{\boldsymbol{k}'} + \tilde{\boldsymbol{V}}_{\boldsymbol{k}}^\dagger + \tilde{\boldsymbol{V}}_{\boldsymbol{k}'}^\dagger)\psi_{k'}\delta_{\boldsymbol{k}',\boldsymbol{k}+\boldsymbol{q}}. \tag{4.54}$$

Compared with the formula in an old paper by Hardy for the current [89], the position of eigenfrequencies in our formula is different since we choose a different basis and quantization.

In the Kubo term, two heat currents are in simple multiplication, therefore it is

safe to take $\boldsymbol{q} \to 0$ initially:

$$\begin{aligned}\boldsymbol{j}_{\boldsymbol{q}} &= \frac{\hbar}{4}\sum_{kk'}\sqrt{|\omega_k||\omega_{k'}|}a_k^\dagger a_{k'}\psi_k^\dagger(\tilde{\boldsymbol{V}}_{\boldsymbol{k}}+\tilde{\boldsymbol{V}}_{\boldsymbol{k}}^\dagger)\psi_{k'}\delta_{\boldsymbol{k}',\boldsymbol{k}} \\ &= \frac{\hbar}{4}\sum_{kk'}\sqrt{|\omega_k||\omega_{k'}|}\bar{\psi}_k\tilde{\boldsymbol{V}}_{\boldsymbol{k}}\psi_{k'}\delta_{\boldsymbol{k}\boldsymbol{k}'}(a_k^\dagger a_{k'}+a_{k'}a_k^\dagger).\end{aligned} \tag{4.55}$$

Here we have used the following properties of this system:

$$\begin{aligned}&\psi_k^\dagger\tilde{\boldsymbol{V}}_{\boldsymbol{k}}^\dagger\psi_{k'} = (\psi_{k'}^\dagger\tilde{\boldsymbol{V}}_{\boldsymbol{k}}\psi_k)^\dagger = (\psi_{k'}^\dagger\tilde{\boldsymbol{V}}_{\boldsymbol{k}}\psi_k)^*, \\ &\psi_k^* = \psi_{-k},\ \omega_k^* = \omega_k = -\omega_{-k}, \\ &\tilde{\boldsymbol{V}}_{\boldsymbol{k}}^* = \tilde{\boldsymbol{V}}_{-\boldsymbol{k}},\ H_{\boldsymbol{k}}^* = H_{-\boldsymbol{k}}, \\ &a_k^\dagger = a_{-k}, \\ &H_{\boldsymbol{k}}\tilde{\boldsymbol{V}}_{\boldsymbol{k}} = \tilde{\boldsymbol{V}}_{\boldsymbol{k}}.\end{aligned} \tag{4.56}$$

We calculate the Kubo term in the phonon Hall conductivity using the Eq. (4.39):

$$\begin{aligned}\kappa_{xy}^{\text{Kubo}} &= \frac{1}{VT}\lim_{s\to0}\lim_{\boldsymbol{q}\to0}\int_0^\beta d\lambda\int_0^\infty dt e^{-st}\langle j_{-\boldsymbol{q}}^y(-i\hbar\lambda)j_{\boldsymbol{q}}^x(t)\rangle_0 \\ &= \frac{\hbar^2}{16VT}\lim_{s\to0}\int_0^\beta d\lambda\int_0^\infty dt e^{-st}\sum_{kk'}\sum_{pp'}\sqrt{|\omega_k||\omega_{k'}||\omega_p||\omega_{p'}|}\bar{\psi}_k\tilde{V}_{\boldsymbol{k}}^y\psi_{k'}\bar{\psi}_p\tilde{V}_{\boldsymbol{p}}^x\psi_{p'} \\ &\times\delta_{\boldsymbol{k}\boldsymbol{k}'}\delta_{\boldsymbol{p}\boldsymbol{p}'}[\langle a_k^\dagger(-i\hbar\lambda)a_{k'}(-i\hbar\lambda)a_p^\dagger(t)a_{p'}(t)\rangle_0 \\ &+\langle a_k^\dagger(-i\hbar\lambda)a_{k'}(-i\hbar\lambda)a_{p'}(t)a_p^\dagger(t)\rangle_0] + \text{h.c.} \\ &= \frac{\hbar^2}{16VT}\sum_{kk'}\sum_{pp'}\sqrt{|\omega_k||\omega_{k'}||\omega_p||\omega_{p'}|}\bar{\psi}_k\tilde{V}_{\boldsymbol{k}}^y\psi_{k'}\bar{\psi}_p\tilde{V}_{\boldsymbol{p}}^x\psi_{p'} \\ &\times\delta_{\boldsymbol{k}\boldsymbol{k}'}\delta_{\boldsymbol{p}\boldsymbol{p}'}[\langle a_k^\dagger a_{k'}a_p^\dagger a_{p'}\rangle_0+\langle a_k^\dagger a_{k'}a_{p'}a_p^\dagger\rangle_0] \\ &\times\lim_{s\to0}\int_0^\beta d\lambda\int_0^\infty dt e^{\hbar(\omega_k-\omega_{k'})\lambda+i(\omega_p-\omega_{p'})t-st} + \text{h.c.} \\ &= \frac{i\hbar}{16VT}\sum_{kk'}\sum_{pp'}\frac{e^{\hbar\beta(\omega_k-\omega_{k'})}-1}{(\omega_k-\omega_{k'})(\omega_p-\omega_{p'})}\sqrt{|\omega_k||\omega_{k'}||\omega_p||\omega_{p'}|}\bar{\psi}_k\tilde{V}_{\boldsymbol{k}}^y\psi_{k'}\bar{\psi}_p\tilde{V}_{\boldsymbol{p}}^x\psi_{p'} \\ &\times\delta_{\boldsymbol{k}\boldsymbol{k}'}\delta_{\boldsymbol{p}\boldsymbol{p}'}[\langle a_k^\dagger a_{k'}a_p^\dagger a_{p'}\rangle_0+\langle a_k^\dagger a_{k'}a_{p'}a_p^\dagger\rangle_0] + \text{h.c.},\end{aligned} \tag{4.57}$$

where $a_k(-i\hbar\lambda) = a_k e^{-\hbar\omega_k\lambda}$, $a_p(t) = a_p e^{-i\omega_p t}$. Wick theorem says

$$\langle a_k^\dagger a_{k'} a_p^\dagger a_{p'}\rangle_0 = \langle a_k^\dagger a_{k'}\rangle_0\langle a_p^\dagger a_{p'}\rangle_0 + \langle a_k^\dagger a_{p'}\rangle_0\langle a_{k'} a_p^\dagger\rangle_0 + \langle a_k^\dagger a_p^\dagger\rangle_0\langle a_{k'} a_{p'}\rangle_0. \tag{4.58}$$

The first term separates the $j^x_{\boldsymbol{q}}$ and $j^y_{-\boldsymbol{q}}$ exactly, which should be 0 for in equilibrium there is no transport heat current. Therefore, we only focus on the last two terms. Since $\langle a_k^\dagger a_{k'}\rangle = n_k \mathrm{sgn}(k)\delta_{kk'}$, $n_k = 1/[e^{\beta\hbar\omega_k} - 1]$, we have

$$\langle a_k^\dagger a_{k'} a_p^\dagger a_{p'}\rangle_0 = \langle a_k^\dagger a_{k'} a_{p'} a_p^\dagger\rangle_0 = \mathrm{sgn}(k)\mathrm{sgn}(k')n_k(1+n_{k'})(\delta_{kp'}\delta_{k'p} + \delta_{k,-p}\delta_{k'}, -p'), \tag{4.59}$$

where $\mathrm{sgn}(k) = \mathrm{sgn}(\sigma)$, the branch labelling. Substituting into the Kubo formula, it becomes

$$\begin{aligned}
\kappa_{xy}^{\mathrm{Kubo}} &= \frac{i\hbar}{16VT}\sum_{kk'}\sum_{pp'}\frac{e^{\hbar\beta(\omega_k-\omega_{k'})}-1}{(\omega_k-\omega_{k'})(\omega_p-\omega_{p'})}\times\Big[2n_k(1+n_{k'})\Big]\Big[\mathrm{sgn}(k)\mathrm{sgn}(k') \\
&\quad\times\sqrt{|\omega_k||\omega_{k'}||\omega_p||\omega_{p'}|}(\delta_{kp'}\delta_{k'p}+\delta_{k,-p}\delta_{k',-p'})\bar\psi_k\tilde V^y_{\boldsymbol{k}}\psi_{k'}\bar\psi_p\tilde V^x_{\boldsymbol{p}}\psi_{p'}\delta_{\boldsymbol{kk'}}\delta_{\boldsymbol{pp'}}\Big] + \text{h.c.} \\
&= \frac{i\hbar}{8VT}\sum_{kk'}\frac{n_k-n_{k'}}{(\omega_k-\omega_{k'})^2}\omega_k\omega_{k'}\delta_{\boldsymbol{kk'}}[\bar\psi_k\tilde V^y_{\boldsymbol{k}}\psi_{k'}\bar\psi_{k'}\tilde V^x_{\boldsymbol{k'}}\psi_k + \bar\psi_k\tilde V^y_{\boldsymbol{k}}\psi_{k'}\bar\psi_{-k}\tilde V^x_{-\boldsymbol{k}}\psi_{-k'}] + \text{h.c.} \\
&= \frac{i\hbar}{8VT}\sum_{kk'}\frac{n_k-n_{k'}}{(\omega_k-\omega_{k'})^2}\omega_k\omega_{k'}\delta_{\boldsymbol{kk'}}\bar\psi_k\tilde V^y_{\boldsymbol{k}}\psi_{k'}[\bar\psi_{k'}\tilde V^x_{\boldsymbol{k'}}\psi_k + \psi^\dagger_{k'}\tilde V^{\dagger x}_{\boldsymbol{k}}\bar\psi^\dagger_k] + \text{h.c.}.
\end{aligned} \tag{4.60}$$

The sign part together with the square root is always positive so we can ignore it. To further simplify the formula, we take one of the terms as an example to show the

procedure:

$$\begin{aligned}
&\frac{i\hbar}{8VT}\sum_{kk'}\frac{n_k}{(\omega_k-\omega_{k'})^2}\omega_k\omega_{k'}\delta_{\boldsymbol{kk'}}\bar{\psi}_k\tilde{V}^y_{\boldsymbol{k}}\psi_{k'}\bar{\psi}_{k'}\tilde{V}^x_{\boldsymbol{k'}}\psi_k \\
&=\frac{i\hbar}{8VT}\sum_{\boldsymbol{k},i,j}\frac{n_{\boldsymbol{k}i}}{(\omega_{\boldsymbol{k}i}-\omega_{\boldsymbol{k}j})^2}\omega_{\boldsymbol{k}i}\omega_{\boldsymbol{k}j}\bar{\psi}_{\boldsymbol{k}i}\tilde{V}^y_{\boldsymbol{k}}\psi_{\boldsymbol{k}j}\bar{\psi}_{\boldsymbol{k}j}\tilde{V}^x_{\boldsymbol{k}}\psi_{\boldsymbol{k}i} \\
&=\frac{i\hbar}{8VT}\sum_{\boldsymbol{k},i,j}\frac{n_{\boldsymbol{k}i}}{(\omega_{\boldsymbol{k}i}-\omega_{\boldsymbol{k}j})^2}\omega_{\boldsymbol{k}i}\omega_{\boldsymbol{k}j}\bar{\psi}_{\boldsymbol{k}i}\frac{\partial H_{\text{eff}}}{\partial k_y}\psi_{\boldsymbol{k}j}\bar{\psi}_{\boldsymbol{k}j}\frac{\partial H_{\text{eff}}}{\partial k_x}\psi_{\boldsymbol{k}i} \\
&=\frac{-i\hbar}{8VT}\sum_{\boldsymbol{k},i,j}n_{\boldsymbol{k}i}\omega_{\boldsymbol{k}i}\omega_{\boldsymbol{k}j}\bar{\psi}_{\boldsymbol{k}i}\frac{\partial\psi_{\boldsymbol{k}j}}{\partial k_y}\bar{\psi}_{\boldsymbol{k}j}\frac{\partial\psi_{\boldsymbol{k}i}}{\partial k_x} \\
&=\frac{i\hbar}{8VT}\sum_{\boldsymbol{k},i}n_{\boldsymbol{k}i}\omega_{\boldsymbol{k}i}\Big(\sum_j\frac{\partial\bar{\psi}_{\boldsymbol{k}i}}{\partial k_y}\omega_{\boldsymbol{k}j}\psi_{\boldsymbol{k}j}\bar{\psi}_{\boldsymbol{k}j}\frac{\partial\psi_{\boldsymbol{k}i}}{\partial k_x}\Big) \\
&=\frac{i\hbar}{8VT}\sum_{\boldsymbol{k},i}\omega_{\boldsymbol{k}i}n_{\boldsymbol{k}i}\frac{\partial\bar{\psi}_{\boldsymbol{k}i}}{\partial k_y}H_{\text{eff}}\frac{\partial\psi_{\boldsymbol{k}i}}{\partial k_x}.
\end{aligned} \tag{4.61}$$

For simplicity, we ignore the subscript of the matrices. From the third line to the fourth line, we have used the property of the eigensystem that

$$\bar{\psi}_{\boldsymbol{k}i}\frac{\partial H_{\text{eff}}}{\partial k_y}\psi_{\boldsymbol{k}j}=(\omega_{\boldsymbol{k}j}-\omega_{\boldsymbol{k}i})\bar{\psi}_{\boldsymbol{k}i}\frac{\partial\psi_{\boldsymbol{k}j}}{\partial k_y}+\frac{\partial\omega_{\boldsymbol{k}i}}{\partial k_y}\delta_{ij}. \tag{4.62}$$

Intraband terms are ignored for they only contribute symmetric partial derivatives $\frac{\partial\omega_{\boldsymbol{k}i}}{\partial k_y}\frac{\partial\omega_{\boldsymbol{k}i}}{\partial k_x}$ which will be cancelled by their Hermitian conjugate. In the last two lines, $\bar{\psi}_{\boldsymbol{k}i}\psi_{\boldsymbol{k}j}=\delta_{ij}$ and $H_{\text{eff}}=\sum_j\omega_{\boldsymbol{k}j}\psi_{\boldsymbol{k}j}\bar{\psi}_{\boldsymbol{k}j}$ are employed. Following the same procedure, we obtain all eight terms:

$$\begin{aligned}
\kappa^{\text{Kubo}}_{xy}=\frac{i\hbar}{8VT}\sum_{\boldsymbol{k},i}\omega_{\boldsymbol{k}i}n_{\boldsymbol{k}i}\Big[&\frac{\partial\bar{\psi}_{\boldsymbol{k}i}}{\partial k_y}H_{\text{eff}}\frac{\partial\psi_{\boldsymbol{k}i}}{\partial k_x}+\frac{\partial\psi^\dagger_{\boldsymbol{k}i}}{\partial k_y}H^\dagger_{\text{eff}}\frac{\partial\bar{\psi}^\dagger_{\boldsymbol{k}i}}{\partial k_x} \\
&+\frac{\partial\bar{\psi}_{\boldsymbol{k}i}}{\partial k_y}H_{\text{eff}}H^{-1}\frac{\partial\bar{\psi}_{\boldsymbol{k}i}}{\partial k_x}^\dagger+\frac{\partial\psi^\dagger_{\boldsymbol{k}i}}{\partial k_y}H^\dagger_{\text{eff}}H\frac{\partial\psi_{\boldsymbol{k}i}}{\partial k_x}-(k_x\leftrightarrow k_y)\Big].
\end{aligned} \tag{4.63}$$

Since $\bar{\psi} = \psi^\dagger H$, $H^\dagger = H$, the last two terms can be further simplified:

$$\begin{aligned}
&\frac{\partial \bar{\psi}_{\boldsymbol{k}i}}{\partial k_y} H_{\text{eff}} H^{-1} \frac{\partial \bar{\psi}_{\boldsymbol{k}i}}{\partial k_x}^\dagger + \frac{\partial \psi^\dagger_{\boldsymbol{k}i}}{\partial k_y} H^\dagger_{\text{eff}} H \frac{\partial \psi_{\boldsymbol{k}i}}{\partial k_x} \\
&= \frac{\partial \bar{\psi}_{\boldsymbol{k}i}}{\partial k_y} H_{\text{eff}} \frac{\partial \psi_{\boldsymbol{k}i}}{\partial k_x} + \frac{\partial \psi^\dagger_{\boldsymbol{k}i}}{\partial k_y} H^\dagger_{\text{eff}} \frac{\partial \bar{\psi}^\dagger_{\boldsymbol{k}i}}{\partial k_x} \\
&- \frac{\partial \bar{\psi}_{\boldsymbol{k}i}}{\partial k_y} H_{\text{eff}} \frac{\partial H^{-1}}{\partial k_x} \bar{\psi}^\dagger_{\boldsymbol{k}i} - \frac{\partial \psi^\dagger_{\boldsymbol{k}i}}{\partial k_y} H^\dagger_{\text{eff}} \frac{\partial H}{\partial k_x} \psi_{\boldsymbol{k}i} \\
&= \frac{\partial \bar{\psi}_{\boldsymbol{k}i}}{\partial k_y} H_{\text{eff}} \frac{\partial \psi_{\boldsymbol{k}i}}{\partial k_x} + \frac{\partial \psi^\dagger_{\boldsymbol{k}i}}{\partial k_y} H^\dagger_{\text{eff}} \frac{\partial \bar{\psi}^\dagger_{\boldsymbol{k}i}}{\partial k_x} \\
&- \frac{\partial \psi^\dagger_{\boldsymbol{k}i}}{\partial k_y} H^\dagger_{\text{eff}} \frac{\partial H}{\partial k_x} \psi_{\boldsymbol{k}i} - \psi_{\boldsymbol{k}i} \frac{\partial H}{\partial k_y} H_{\text{eff}} \frac{\partial H^{-1}}{\partial k_x} \bar{\psi}^\dagger_{\boldsymbol{k}i} + \frac{\partial \psi^\dagger_{\boldsymbol{k}i}}{\partial k_y} H H_{\text{eff}} H^{-1} \frac{\partial H}{\partial k_x} \psi_{\boldsymbol{k}i} \\
&= \frac{\partial \bar{\psi}_{\boldsymbol{k}i}}{\partial k_y} H_{\text{eff}} \frac{\partial \psi_{\boldsymbol{k}i}}{\partial k_x} + \frac{\partial \psi^\dagger_{\boldsymbol{k}i}}{\partial k_y} H^\dagger_{\text{eff}} \frac{\partial \bar{\psi}^\dagger_{\boldsymbol{k}i}}{\partial k_x}.
\end{aligned} \tag{4.64}$$

In the last line, we used the properties: $H H_{\text{eff}} H^{-1} = iHJHH^{-1} = iHJ = H^\dagger_{\text{eff}}$, and

$$\frac{\partial H}{\partial k_y} H_{\text{eff}} \frac{\partial H^{-1}}{\partial k_x} = \begin{pmatrix} \frac{\partial K}{\partial k_y} & 0 \\ 0 & 0 \end{pmatrix} \begin{pmatrix} 0 & iI \\ -iK & -i2A \end{pmatrix} \begin{pmatrix} \frac{\partial K^{-1}}{\partial k_x} & 0 \\ 0 & 0 \end{pmatrix} = 0 \cdot I. \tag{4.65}$$

Therefore, the final formula for the Kubo term is

$$\begin{aligned}
\kappa^{\text{Kubo}}_{xy} &= \frac{i\hbar}{4VT} \sum_{\boldsymbol{k},i} \omega_{\boldsymbol{k}i} n_{\boldsymbol{k}i} \Big[\frac{\partial \bar{\psi}_{\boldsymbol{k}i}}{\partial k_y} H_{\text{eff}} \frac{\partial \psi_{\boldsymbol{k}i}}{\partial k_x} + \frac{\partial \psi^\dagger_{\boldsymbol{k}i}}{\partial k_y} H^\dagger_{\text{eff}} \frac{\partial \bar{\psi}^\dagger_{\boldsymbol{k}i}}{\partial k_x} - (k_x \leftrightarrow k_y) \Big] \\
&= \frac{\hbar}{2VT} \sum_{\boldsymbol{k},i} \omega_{\boldsymbol{k}i} n_{\boldsymbol{k}i} \text{Im} \Big[\frac{\partial \bar{\psi}_{\boldsymbol{k}i}}{\partial k_x} H_{\text{eff}} \frac{\partial \psi_{\boldsymbol{k}i}}{\partial k_y} - \frac{\partial \bar{\psi}_{\boldsymbol{k}i}}{\partial k_y} H_{\text{eff}} \frac{\partial \psi_{\boldsymbol{k}i}}{\partial k_x} \Big].
\end{aligned} \tag{4.66}$$

This formula sums over both the positive and negative branches of the eigensystem.

Next we will show that this Kubo term is cancelled by the inter-band contribution of the energy magnetization. We calculate the energy magnetization term in z direction according to the Eq. (4.29):

$$\begin{aligned}
2M_z - T\frac{\partial M_z}{\partial T} \equiv \tilde{M}_z &= \frac{\beta}{2i} \boldsymbol{\nabla}_{\boldsymbol{q}} \times \langle \varepsilon_{-\boldsymbol{q}}; \boldsymbol{j}_{\boldsymbol{q}} \rangle_0 |_{z, \boldsymbol{q}\to 0} \\
&= \frac{i}{2} \frac{\partial}{\partial q_y} \int_0^\beta d\lambda \langle \varepsilon_{-\boldsymbol{q}} (-i\hbar\lambda) j^x_{\boldsymbol{q}} \rangle_0 \Big|_{\boldsymbol{q}\to 0} - (x \leftrightarrow y).
\end{aligned} \tag{4.67}$$

There is a derivative with respect to $\boldsymbol{q}$ in this formula, therefore we must explicitly work out the Kubo correlator up to the first order of the $\boldsymbol{q}$. The energy density operator in the reciprocal space can be quantized as follows:

$$\begin{aligned}\varepsilon_{-\boldsymbol{q}} &= \sum_l \varepsilon_l e^{i\boldsymbol{q}\cdot\boldsymbol{R}_l} \\ &= \frac{\hbar}{4N}\sum_{ll'}\sum_{kk'} e^{i\boldsymbol{q}\cdot\boldsymbol{R}_l}\sqrt{|\omega_k||\omega_{k'}|}(\psi_k^\dagger e^{-i\boldsymbol{k}\cdot\boldsymbol{R}_l} H_{ll'}\psi_{k'} e^{i\boldsymbol{k}'\cdot\boldsymbol{R}_{l'}} a_k^\dagger a_{k'} + \text{h.c.}) \\ &= \frac{\hbar}{4}\sum_{kk'}\sqrt{|\omega_k||\omega_{k'}|}\Big[\psi_k^\dagger(H_{\boldsymbol{k}} + H_{\boldsymbol{k}'})\psi_{k'} a_k^\dagger a_{k'}\delta_{\boldsymbol{k}',\boldsymbol{k}-\boldsymbol{q}}\Big].\end{aligned} \tag{4.68}$$

Firstly, we integrate over variable λ as before so that

$$\begin{aligned}\tilde{M}_z = \frac{i\hbar}{64}\frac{\partial}{\partial q_y}\sum_{kk'}\sum_{pp'}\frac{e^{\beta\hbar(\omega_k-\omega_{k'})}-1}{(\omega_k-\omega_{k'})}\sqrt{|\omega_k||\omega_{k'}||\omega_p||\omega_{p'}|} \\ \times \psi_k^\dagger(H_{\boldsymbol{k}} + H_{\boldsymbol{k}'})\psi_{k'}\psi_p^\dagger(\tilde{V}_{\boldsymbol{p}}^x + \tilde{V}_{\boldsymbol{p}'}^x + \tilde{V}_{\boldsymbol{p}}^{\dagger x} + \tilde{V}_{\boldsymbol{p}'}^{\dagger x})\psi_{p'} \\ \times \langle a_k^\dagger a_{k'} a_p^\dagger a_{p'}\rangle_0 \delta_{\boldsymbol{k}',\boldsymbol{k}-\boldsymbol{q}}\delta_{\boldsymbol{p}',\boldsymbol{p}+\boldsymbol{q}}\Big|_{\boldsymbol{q}\to 0} - (x\leftrightarrow y).\end{aligned} \tag{4.69}$$

Again, we utilize the Wick theorem and the fact $\langle\varepsilon_{-\boldsymbol{q}}\rangle_0 = 0$, $\langle\boldsymbol{j}_{\boldsymbol{q}}\rangle_0 = 0$ when $\boldsymbol{q}\neq 0$ to obtain

$$\begin{aligned}\langle a_k^\dagger a_{k'} a_p^\dagger a_{p'}\rangle_0 &= \langle a_k^\dagger a_{p'}\rangle_0\langle a_{k'} a_p^\dagger\rangle_0 + \langle a_k^\dagger a_p^\dagger\rangle_0\langle a_{k'} a_{p'}\rangle_0 \\ &= \text{sgn}(k)\text{sgn}(k')n_k(n_{k'}+1)[\delta_{kp'}\delta_{k'p} + \delta_{k,-p}\delta_{k',-p'}].\end{aligned} \tag{4.70}$$

Therefore, previous $\tilde{M}_z$ becomes

$$\begin{aligned}\tilde{M}_z = \frac{i\hbar}{32}\frac{\partial}{\partial q_y}\sum_{kk'}\omega_k\omega_{k'}\frac{n_{k'}-n_k}{\omega_k-\omega_{k'}}\psi_k^\dagger(H_{\boldsymbol{k}} + H_{\boldsymbol{k}'})\psi_{k'} \\ \times \psi_{k'}^\dagger(\tilde{V}_{\boldsymbol{k}}^x + \tilde{V}_{\boldsymbol{k}'}^x + \tilde{V}_{\boldsymbol{k}}^{\dagger x} + \tilde{V}_{\boldsymbol{k}'}^{\dagger x})\psi_k\delta_{\boldsymbol{k}',\boldsymbol{k}-\boldsymbol{q}}\Big|_{\boldsymbol{q}\to 0} - (x\leftrightarrow y),\end{aligned} \tag{4.71}$$

where we have used the properties in Eq. (4.56). It seems rather messy if we take the partial derivative term by term, however, many terms will not contribute due to the $x\leftrightarrow y$ symmetry.

Let us apply the Taylor expansion to ω up to the first order so that $\omega_{\boldsymbol{k}-\boldsymbol{q}\sigma'} \approx \omega_k - (\partial\omega_k/\partial\boldsymbol{k})\cdot\boldsymbol{q}$. When the partial derivative works on $\omega_{k'}$ in the formula for $\tilde{M}_z$, $\partial\omega_{k'}/\partial q_y = -\partial\omega_k/\partial k_y$ and the rest terms will just take $\boldsymbol{q}\to 0$ to maintain the linear order of $\boldsymbol{q}$. $\partial n_{k'}/\partial q_y$ is the same due to the chain rule. Since $\psi_k^\dagger H_k\psi_{k'} = \bar{\psi}_k\psi_{k'} = \delta_{kk'}$, there will be only intra terms. Moreover, due to the property of the system described by Eq. (4.62), we have $\psi_k^\dagger\tilde{V}_{\boldsymbol{k}}^x\psi_k = \bar{\psi}_k\tilde{V}_{\boldsymbol{k}}^x\psi_k = \partial\omega_k/\partial k_x$. As a result, we obtain a factor being $\frac{\partial\omega_k}{\partial k_y}\frac{\partial\omega_k}{\partial k_x}$ which will be canceled by $x\leftrightarrow y$ operation. Therefore, non-zero terms in $\tilde{M}_z$ is

$$\begin{aligned}\tilde{M}_z = \frac{i\hbar}{32}\sum_{kk'}\omega_k\omega_{k'}\frac{n_{k'}-n_k}{\omega_k-\omega_{k'}}\frac{\partial}{\partial q_y}\Big[\psi_k^\dagger(H_{\boldsymbol{k}}+H_{\boldsymbol{k}'})\psi_{k'} \\ \times\psi_{k'}^\dagger(\tilde{V}_{\boldsymbol{k}}^x+\tilde{V}_{\boldsymbol{k}'}^x+\tilde{V}_{\boldsymbol{k}}^{\dagger x}+\tilde{V}_{\boldsymbol{k}'}^{\dagger x})\psi_k\Big]\Big|_{\boldsymbol{q}\to 0} - (x\leftrightarrow y).\end{aligned} \tag{4.72}$$

Firstly, we calculate the inter-band term that $k=(\boldsymbol{k},\sigma)\neq(\boldsymbol{k},\sigma')=k'$ in the formula. In this case, the partial derivative can only act on the term $\psi_k^\dagger(H_{\boldsymbol{k}}+H_{\boldsymbol{k}'})\psi_{k'}$ otherwise there will be a $\delta_{kk'}$ contradicting with our assumption.

$$\begin{aligned}\tilde{M}_z^{\text{inter}} &= -\frac{i\hbar}{16}\sum_{kk'}\omega_k\omega_{k'}\frac{n_{k'}-n_k}{\omega_k-\omega_{k'}}[\bar{\psi}_k\frac{\partial\psi_{k'}}{\partial k_y}+\psi_k^\dagger\frac{\partial\bar{\psi}_{k'}^\dagger}{\partial k_y}]\psi_{k'}(\tilde{V}_{\boldsymbol{k}}^x+\tilde{V}_{\boldsymbol{k}}^{\dagger x})\psi_k-(x\leftrightarrow y)\\
&= -\frac{i\hbar}{16}\sum_{kk'}\omega_k\omega_{k'}\frac{n_{k'}-n_k}{\omega_k-\omega_{k'}}\Big[\bar{\psi}_k\frac{\partial\psi_{k'}}{\partial k_y}-\Big(\bar{\psi}_{k'}\frac{\partial\psi_k}{\partial k_y}\Big)^\dagger\Big]\psi_{k'}(\tilde{V}_{\boldsymbol{k}}^x+\tilde{V}_{\boldsymbol{k}}^{\dagger x})\psi_k-(x\leftrightarrow y)\\
&= \frac{i\hbar}{16}\sum_{kk'}\omega_k\omega_{k'}\frac{n_{k'}-n_k}{(\omega_k-\omega_{k'})^2}\psi_k^\dagger(\tilde{V}_{\boldsymbol{k}}^y+\tilde{V}_{\boldsymbol{k}}^{\dagger y})\psi_{k'}\psi_{k'}^\dagger(\tilde{V}_{\boldsymbol{k}}^x+\tilde{V}_{\boldsymbol{k}}^{\dagger x})\psi_k-(x\leftrightarrow y)\\
&= -\mathrm{Re}\Big[\frac{i\hbar}{8}\sum_{kk'}\omega_k\omega_{k'}\frac{n_k-n_{k'}}{(\omega_k-\omega_{k'})^2}\psi_k^\dagger(\tilde{V}_{\boldsymbol{k}}^y+\tilde{V}_{\boldsymbol{k}}^{\dagger y})\psi_{k'}\psi_{k'}^\dagger(\tilde{V}_{\boldsymbol{k}}^x+\tilde{V}_{\boldsymbol{k}}^{\dagger x})\psi_k\Big].\end{aligned} \tag{4.73}$$

where properties in the Eq. (4.56) are employed again. The last line is valid for the $x\leftrightarrow y$ operation is equivalent to take the Hermitian conjugate. Recall the Eq.

(4.60), we can rewritten it as follows:

$$\begin{aligned}\kappa_{xy}^{\text{Kubo}} &= \frac{i\hbar}{8VT}\sum_{kk'}\frac{n_k-n_{k'}}{(\omega_k-\omega_{k'})^2}\omega_k\omega_{k'}\delta_{\boldsymbol{kk'}}\bar{\psi}_k\tilde{V}_{\boldsymbol{k}}^y\psi_{k'}[\bar{\psi}_{k'}\tilde{V}_{\boldsymbol{k'}}^x\psi_k+\psi_{k'}^\dagger\tilde{V}_{\boldsymbol{k}}^{\dagger x}\bar{\psi}_k^\dagger]+\text{h.c.}\\ &= \frac{i\hbar}{8VT}\sum_{kk'}\frac{n_k-n_{k'}}{(\omega_k-\omega_{k'})^2}\omega_k\omega_{k'}\psi_k^\dagger\tilde{V}_{\boldsymbol{k}}\psi_{k'}(\psi_{k'}^\dagger\tilde{V}_{\boldsymbol{k}}^x\psi_k+\psi_{k'}^\dagger\tilde{V}_{\boldsymbol{k}}^{\dagger x}\psi_k)+\text{h.c.}\\ &= \frac{i\hbar}{8VT}\sum_{kk'}\frac{n_k-n_{k'}}{(\omega_k-\omega_{k'})^2}\omega_k\omega_{k'}\psi_k^\dagger(\tilde{V}_{\boldsymbol{k}}^y+\tilde{V}_{\boldsymbol{k}}^{\dagger y})\psi_{k'}\psi_{k'}^\dagger(\tilde{V}_{\boldsymbol{k}}^x+\tilde{V}_{\boldsymbol{k}}^{\dagger x})\psi_k.\end{aligned}\tag{4.74}$$

From the first line to the second line, we use the properties $H_{\boldsymbol{k}}\tilde{\boldsymbol{V}}_{\boldsymbol{k}}=\tilde{\boldsymbol{V}}_{\boldsymbol{k}}$, and $\tilde{\boldsymbol{V}}_{\boldsymbol{k}}^\dagger H_{\boldsymbol{k}}^\dagger=\tilde{\boldsymbol{V}}_{\boldsymbol{k}}^\dagger$. The third line is obtained by taking the Hermitian conjugate and switch $k\leftrightarrow k'$ (note the factor $n_k-n_{k'}$ will change sign after this switch). It is easy to verify this expression is real, which is consistent with the fact that $\kappa_{xy}^{\text{Kubo}}$ is a physical observable. Compared with the inter-band term $\tilde{M}_z^{\text{inter}}$, we have

$$\begin{aligned}\tilde{M}_z^{\text{inter}} &= -VT\kappa_{xy}^{\text{Kubo}}\\ &= -\frac{\hbar}{2}\sum_{\boldsymbol{k},i}\omega_{\boldsymbol{k}i}n_{\boldsymbol{k}i}\text{Im}\Big[\frac{\partial\bar{\psi}_{\boldsymbol{k}i}}{\partial k_x}H_{\text{eff}}\frac{\partial\psi_{\boldsymbol{k}i}}{\partial k_y}-\frac{\partial\bar{\psi}_{\boldsymbol{k}i}}{\partial k_y}H_{\text{eff}}\frac{\partial\psi_{\boldsymbol{k}i}}{\partial k_x}\Big].\end{aligned}\tag{4.75}$$

For $k=k'$, the partial derivative can not act on the $\tilde{V}_{\boldsymbol{k'}}^x$ because it will result in a symmetric second order derivative cancelled by the $x\leftrightarrow y$ operation. Thus the intra-band term is

$$\begin{aligned}\tilde{M}_z^{\text{intra}} &= \frac{i\hbar}{16}\sum_k\omega_k^2\frac{n_{k'}-n_k}{\omega_k-\omega_{k'}}\Big|_{\boldsymbol{q}\to 0}\Big\{-\Big[\bar{\psi}_k\frac{\partial\psi_k}{\partial k_y}+\psi_k^\dagger\frac{\partial\bar{\psi}_k^\dagger}{\partial k_y}\Big]\psi_k^\dagger(\tilde{V}_{\boldsymbol{k}}^x+\tilde{V}_{\boldsymbol{k}}^{\dagger x})\psi_k\\ &\quad -2\Big[\frac{\partial\bar{\psi}_k}{\partial k_y}\tilde{V}_{\boldsymbol{k}}^x\psi_k+\frac{\partial\psi_k^\dagger}{\partial k_y}\tilde{V}_{\boldsymbol{k}}^{\dagger x}\bar{\psi}_k^\dagger\Big]\Big\}-(x\leftrightarrow y)\\ &= \frac{i\hbar}{8}\sum_k\omega_k^2\frac{\partial n_k}{\partial\omega}\Big[\bar{\psi}_k\frac{\partial\psi_k}{\partial k_y}\frac{\partial\omega_k}{\partial k_x}+\psi_k^\dagger\frac{\partial\bar{\psi}_k^\dagger}{\partial k_y}\frac{\partial\omega_k}{\partial k_x}+\frac{\partial\bar{\psi}_k}{\partial k_y}\tilde{V}_{\boldsymbol{k}}^x\psi_k+\frac{\partial\psi_k^\dagger}{\partial k_y}\tilde{V}_{\boldsymbol{k}}^{\dagger x}\bar{\psi}_k^\dagger\Big]-(x\leftrightarrow y).\end{aligned}\tag{4.76}$$

Since $\bar{\psi}_k H_{\text{eff}}=\omega_k\bar{\psi}_k$, applying the partial derivative $\partial/\partial k_x$ to both sides, we obtain

$$\frac{\partial\bar{\psi}_k}{\partial k_x}H_{\text{eff}}+\bar{\psi}_k\frac{\partial H_{\text{eff}}}{\partial k_x}=\frac{\partial\omega_k}{\partial k_x}\bar{\psi}_k+\omega_k\frac{\partial\bar{\psi}_k}{\partial k_x}.\tag{4.77}$$

Subsequently, we multiply $\partial\psi_k/\partial k_y$ to the right on both sides so that

$$\bar{\psi}_k \frac{\partial \psi_k}{\partial k_y}\frac{\partial \omega_k}{\partial k_x} = \frac{\partial \bar{\psi}_k}{\partial k_x}(H_{\text{eff}} - \omega_k)\frac{\partial \psi_k}{\partial k_y} + \bar{\psi}_k \frac{\partial H_{\text{eff}}}{\partial k_x}\frac{\partial \psi_k}{\partial k_y}. \tag{4.78}$$

Similarly, if we apply this procedure to $\psi_k^\dagger H_{\text{eff}}^\dagger = \omega_k \psi_k^\dagger$, we obtain another term in $\tilde{M}_z^{\text{intra}}$,

$$\psi_k^\dagger \frac{\partial \bar{\psi}_k^\dagger}{\partial k_y}\frac{\partial \omega_k}{\partial k_x} = \frac{\partial \psi_k^\dagger}{\partial k_x}(H_{\text{eff}}^\dagger - \omega_k)\frac{\partial \bar{\psi}_k^\dagger}{\partial k_y} + \psi_k^\dagger \frac{\partial H_{\text{eff}}^\dagger}{\partial k_x}\frac{\partial \bar{\psi}_k^\dagger}{\partial k_y}. \tag{4.79}$$

Therefore, the $\tilde{M}_z^{\text{intra}}$ becomes

$$\begin{aligned}\tilde{M}_z^{\text{intra}} = \frac{i\hbar}{8}\sum_k \omega_k^2 \frac{\partial n_k}{\partial \omega}\Big[&\frac{\partial \bar{\psi}_k}{\partial k_x}(H_{\text{eff}} - \omega_k)\frac{\partial \psi_k}{\partial k_y} + \frac{\partial \psi_k^\dagger}{\partial k_x}(H_{\text{eff}}^\dagger - \omega_k)\frac{\partial \bar{\psi}_k^\dagger}{\partial k_y} \\ &+ \bar{\psi}_k \frac{\partial H_{\text{eff}}}{\partial k_x}\frac{\partial \psi_k}{\partial k_y} + \psi_k^\dagger \frac{\partial H_{\text{eff}}^\dagger}{\partial k_x}\frac{\partial \bar{\psi}_k^\dagger}{\partial k_y} + \frac{\partial \bar{\psi}_k}{\partial k_y}\frac{\partial H_{\text{eff}}}{\partial k_x}\psi_k + \frac{\partial \psi_k^\dagger}{\partial k_y}\frac{\partial H_{\text{eff}}^\dagger}{\partial k_x}\bar{\psi}_k^\dagger\Big] - (x \leftrightarrow y).\end{aligned} \tag{4.80}$$

Obviously, the sum of the last four terms are real, so they have no contribution. Therefore, the intra-band contribution is

$$\begin{aligned}\tilde{M}_z^{\text{intra}} &= -\frac{\hbar}{4}\sum_{\boldsymbol{k},i}\omega_{\boldsymbol{k}i}^2 \frac{\partial n_{\boldsymbol{k}i}}{\partial \omega}\text{Im}\Big[\frac{\partial \bar{\psi}_{\boldsymbol{k}i}}{\partial k_x}(H_{\text{eff}} - \omega_{\boldsymbol{k}i})\frac{\partial \psi_{\boldsymbol{k}i}}{\partial k_y} - \frac{\partial \bar{\psi}_{\boldsymbol{k}i}}{\partial k_y}(H_{\text{eff}} - \omega_{\boldsymbol{k}i})\frac{\partial \psi_{\boldsymbol{k}i}}{\partial k_x}\Big] \\ &= -\frac{\hbar}{4}\sum_{\boldsymbol{k},i}\omega_{\boldsymbol{k}i}^2 \frac{\partial n_{\boldsymbol{k}i}}{\partial \omega}\Big\{\text{Im}\Big[\frac{\partial \bar{\psi}_{\boldsymbol{k}i}}{\partial k_x}H_{\text{eff}}\frac{\partial \psi_{\boldsymbol{k}i}}{\partial k_y} - \frac{\partial \bar{\psi}_{\boldsymbol{k}i}}{\partial k_y}H_{\text{eff}}\frac{\partial \psi_{\boldsymbol{k}i}}{\partial k_x}\Big] + \omega_{\boldsymbol{k}i}\Omega_{\boldsymbol{k}i}^z\Big\},\end{aligned} \tag{4.81}$$

where $\boldsymbol{\Omega}_{\boldsymbol{k}i} \equiv -\text{Im}\Big[\frac{\partial \bar{\psi}_{\boldsymbol{k}i}}{\partial \boldsymbol{k}} \times \frac{\partial \bar{\psi}_{\boldsymbol{k}i}}{\partial \boldsymbol{k}}\Big]$ is the Berry curvature of the eigensystem.

Finally, we integrate over temperature T to obtain the M_z. For convenience, we define

$$\mathcal{M}_{\boldsymbol{k}i} \equiv \text{Im}\Big[\frac{\partial \bar{\psi}_{\boldsymbol{k}i}}{\partial \boldsymbol{k}} \times H_{\text{eff}}\frac{\partial \psi_{\boldsymbol{k}i}}{\partial \boldsymbol{k}}\Big], \tag{4.82}$$

and rewrite the Eq. (4.67) with $\beta = 1/k_B T$ as follows:

$$\begin{aligned} 2M_z - T\frac{\partial M_z}{\partial T} = \tilde{M}^z \implies & 2M_z + \beta\frac{\partial M_z}{\partial \beta} = \tilde{M}^z \\ \implies & 2\beta M_z + \beta^2\frac{\partial M_z}{\partial \beta} = \beta\tilde{M}^z \\ \implies & \frac{\partial \beta^2 M_z}{\partial \beta} = \beta\tilde{M}^z. \end{aligned} \tag{4.83}$$

After integrating over the β, we obtain

$$\begin{aligned} M_z &= \frac{1}{\beta^2}\int_0^\beta \lambda\tilde{M}_z d\lambda. \\ &= \frac{1}{\beta^2}\int_0^\beta \lambda\Big\{ -\frac{\hbar}{4}\sum_{\boldsymbol{k}i}\omega_{\boldsymbol{k}i}\Big[\mathcal{M}^z_{\boldsymbol{k}i}(2n_{\boldsymbol{k}i}(\lambda) + \omega_{\boldsymbol{k}i}\frac{\partial n_{\boldsymbol{k}i}(\lambda)}{\partial\omega}) + \omega^2_{\boldsymbol{k}i}\Omega^z_{\boldsymbol{k}i}\frac{\partial n_{\boldsymbol{k}i}(\lambda)}{\partial\omega}\Big]\Big\} d\lambda. \end{aligned} \tag{4.84}$$

Only $n_{\boldsymbol{k}i}(\lambda)$ and $\frac{\partial n_{\boldsymbol{k}i}(\lambda)}{\partial\omega} = \frac{\lambda}{\omega_{\boldsymbol{k}i}}\frac{dn_{\boldsymbol{k}i}(\lambda)}{d\lambda}$ contains λ. The integral containing the partial derivative can be worked out as follows:

$$\begin{aligned} \int_0^\beta \lambda\frac{\partial n_{\boldsymbol{k}i}(\lambda)}{\partial\omega}d\lambda &= \int_0^\beta \frac{\lambda^2}{\omega_{\boldsymbol{k}i}}\frac{dn_{\boldsymbol{k}i}(\lambda)}{d\lambda}d\lambda \\ &= \frac{1}{\omega_{\boldsymbol{k}i}}\Big[\lambda^2 n_{\boldsymbol{k}i}(\lambda)\Big|_0^\beta - \int_0^\beta 2\lambda n_{\boldsymbol{k}i}(\lambda)d\lambda\Big] \\ &= \frac{\beta^2 n_{\boldsymbol{k}i}}{\omega_{\boldsymbol{k}i}} - \frac{1}{\omega_{\boldsymbol{k}i}}\int_0^\beta 2\lambda n_{\boldsymbol{k}i}(\lambda)d\lambda. \end{aligned} \tag{4.85}$$

Substituting the result into the Eq. (4.84), we obtain

$$M_z = -\frac{\hbar}{4}\sum_{\boldsymbol{k}i}\omega_{\boldsymbol{k}i}\mathcal{M}^z_{\boldsymbol{k}i}n_{\boldsymbol{k}i} - \frac{\hbar}{4}\sum_{\boldsymbol{k}i}\omega^2_{\boldsymbol{k}i}\Omega^z_{\boldsymbol{k}i}n_{\boldsymbol{k}i} + \frac{\hbar}{2\beta^2}\sum_{\boldsymbol{k}i}\omega^2_{\boldsymbol{k}i}\Omega^z_{\boldsymbol{k}i}\int_0^\beta \lambda n_{\boldsymbol{k}i}(\lambda)d\lambda. \tag{4.86}$$

Therefore, the total phonon Hall conductivity is

$$\kappa^{\mathrm{tr}}_{xy} = -\frac{\hbar}{2VT}\sum_{\boldsymbol{k}i}\omega^2_{\boldsymbol{k}i}\Omega^z_{\boldsymbol{k}i}n_{\boldsymbol{k}i} + \frac{\hbar}{VT\beta^2}\sum_{\boldsymbol{k}i}\omega^2_{\boldsymbol{k}i}\Omega^z_{\boldsymbol{k}i}\int_0^\beta \lambda n_{\boldsymbol{k}i}(\lambda)d\lambda. \tag{4.87}$$

To make the formula more compact, we define a new quantity $\tilde{\sigma}_{xy}(\epsilon)$,

$$\tilde{\sigma}_{xy}(\epsilon) \equiv \frac{d\sigma_{xy}(\epsilon)}{d\epsilon} = -\frac{1}{V\hbar}\sum_{\boldsymbol{k}i}\Omega^z_{\boldsymbol{k}i}\delta(\epsilon - \hbar\omega_{\boldsymbol{k}i}). \tag{4.88}$$

With the $\tilde{\sigma}_{xy}$, the phonon Hall conductivity can be rewritten as

$$\begin{aligned}\kappa_{xy}^{\mathrm{tr}} &= \frac{1}{2T}\int_{-\infty}^{\infty} d\epsilon\tilde{\sigma}(\epsilon)\Big[\epsilon^2 n(\epsilon) - 2\int^{\epsilon} xn(x)dx\Big] \\ &= \frac{1}{2T}\sigma_{xy}(\epsilon)\Big[\epsilon^2 n(\epsilon) - 2\int^{\epsilon} xn(x)dx\Big]\Big|_{-\infty}^{\infty} - \frac{1}{2T}\int_{-\infty}^{\infty} d\epsilon\epsilon^2\sigma_{xy}(\epsilon)\frac{n(\epsilon)}{d\epsilon},\end{aligned} \tag{4.89}$$

where $x \equiv \epsilon\lambda/\beta$. Since $\sigma_{xy}(\epsilon) = \int_{-\infty}^{\epsilon} dx\tilde{\sigma}_{xy}(x)$, $\sigma_{xy}(-\infty) = 0$. $\sigma_{xy}(\infty)$ is also 0 due to the symmetry of $\psi_{\boldsymbol{k}i}$. Therefore, the final formula is

$$\kappa_{xy}^{\mathrm{tr}} = -\frac{1}{2T}\int_{-\infty}^{\infty} d\epsilon\epsilon^2\sigma_{xy}(\epsilon)\frac{n(\epsilon)}{d\epsilon}. \tag{4.90}$$

Although the derivation is rather long and tricky, we have rigorously confirmed Qin's result [2].

To sum up, once we have obtained the eigenvalues and associated eigenvectors of the effective Hamiltonian, we can calculate its Berry curvature and phonon Hall conductivity using the following formulas:

$$\boldsymbol{\Omega}_{\boldsymbol{q}i} = -\mathrm{Im}\Big[\frac{\partial\bar{\psi}_{\boldsymbol{q}i}}{\partial\boldsymbol{q}} \times \frac{\partial\psi_{\boldsymbol{q}i}}{\partial\boldsymbol{q}}\Big], \tag{4.91}$$

and

$$\kappa_{xy} = -\frac{1}{2T}\int_{-\infty}^{\infty} d\epsilon\epsilon^2\sigma_{xy}(\epsilon)\frac{dn(\epsilon)}{d\epsilon}, \tag{4.92}$$

where

$$\sigma_{xy}(\epsilon) = -\frac{1}{V\hbar}\sum_{\hbar\omega_{\boldsymbol{q}i}\leq\epsilon}\Omega_{\boldsymbol{q}i}^{z}, \tag{4.93}$$

$n(\epsilon) = 1/(e^{\epsilon/(k_B T)} - 1)$ is the Bose function at temperature T, and k_B the Boltzmann constant. For clarity, here we replace the $\boldsymbol{k}$ with $\boldsymbol{q}$ as the phonon wave vector in subsequent sections. In the above summation over mode $\boldsymbol{q}i$, all modes with both positive and negative frequencies, are included. Since we are dealing with a

two-dimensional sheet, the volume V is an ill-defined concept. We use $V = L^2 a$, the area times the thickness, choosing a somewhat arbitrarily to match the units of W/(mK) of the usual three-dimensional thermal conductivity. When estimating the phonon Hall conductivity κ_{xy} in a graphene-like lattice, we assume the thickness of the sample is the same as the bond length $a = 1.42$ Å of graphene.

4.1.2 An Optimization: the Theta Function

Although equation (4.92) is enough to calculate the phonon Hall conductivity, it is usually difficult to implement the integral over the energy accurately for the Berry curvatures at some $\boldsymbol{q}$ have large values. However, it is possible to avoid this difficulty if we integrate out the intergral by hand:

$$\begin{aligned} \kappa_{xy} &= \frac{1}{2TV\hbar} \sum_{\boldsymbol{q},i} \Omega^z_{\boldsymbol{q}i} \int_{-\infty}^{\infty} d\epsilon \epsilon^2 \theta(\epsilon - \hbar\omega_{\boldsymbol{q}i}) \frac{dn}{d\epsilon} \\ &\equiv \frac{k_B^2 T}{2V\hbar} \sum_{\boldsymbol{q},i} \Omega^z_{\boldsymbol{q}i} \Theta(\beta\hbar\omega_{\boldsymbol{q}i}), \end{aligned} \tag{4.94}$$

where θ is the step function, $\beta = 1/k_B T$, and

$$\Theta(x) = \int_x^{\infty} y^2 dn, \tag{4.95}$$

with the substitution $\beta\epsilon \to y$. By integration by parts, we will obtain

$$\Theta(x) = \frac{x^2}{e^x - 1} + \int_x^{\infty} \frac{2ydy}{e^y - 1}. \tag{4.96}$$

When $x = 0$, the first term is a indeterminate value, but the original integral in this case has a definite value $\pi^2/3$. When $x \neq 0$, we make another substitution $y \to -\ln u$ so that

$$\Theta(x) = \frac{x^2}{e^x - 1} - 2\int_{0^+}^{e^{-x}} \frac{\ln u}{1 - u} du. \tag{4.97}$$

Again we use integration by parts,

$$\begin{aligned}\Theta(x) &= \frac{x^2}{e^x-1} + 2\ln u\, d\ln(|1-u|)\Big|_{0^+}^{e^{-x}} - 2\int_{0^+}^{e^{-x}} \frac{\ln|1-u|}{u}du \\ &= \frac{x^2}{e^x-1} - 2x\ln(|1-e^{-x}|) - 2\int_{0^+}^{e^{-x}} \frac{\ln|1-u|}{u}du.\end{aligned} \tag{4.98}$$

The last term is related to the Spence's function or the dilogarithm function,

$$-\int_{0^+}^{x} \frac{\ln|1-u|}{u}du = \begin{cases} \mathrm{Li}_2(x), & x \le 1, \\ \pi^2/3 - \ln^2(x)/2 - \mathrm{Li}_2(1/x), & x > 1. \end{cases} \tag{4.99}$$

Since $\mathrm{Li}_2(x) + \mathrm{L}i_2(1/x) = \pi^2/6 - \ln^2(-x)/2$, we can combine two cases so that finally we obtain

$$\Theta(x) = \begin{cases} \frac{x^2}{e^x-1} - 2x\ln(|e^x-1|) + 2\mathrm{Re}[\mathrm{Li}_2(e^{-x})], & x \neq 0. \\ \pi^2/3, & x = 0. \end{cases} \tag{4.100}$$

Here we always take the real part of the $\mathrm{Li}_2(e^{-x})$ for when $e^{-x} > 1$, it is a complex value while $\Theta(x)$ is real. Although the Li_2 still contains an integral, there are developed reliable packages to calculate accurately in many langauages such as fortran, C++ and Mathematica. With this integrated equation, the accuracy can be greatly boosted, therefore I call it an optimization.

4.2 Current-induced Non-zero Vector Potential

Lü *et al.* [18] theoretically studied the effect of electric current on a molecular bridge connecting two metallic electrodes. They found a new mechanism, which involves Berry phase, that can lead to a breakdown of the bridge by a "run away" mode. Their discovery inspired us to ask if we introduce electric current into a

lattice system, *e.g.*, the honeycomb lattice, is there a phonon Hall effect? The "run away" mode means the amplitude of oscillation including those perpendicular to the molecular bridge will grow in time, therefore if we extend it to a 2D lattice, this "run away" mode induced by electric current may result in a phonon Hall current. Figure 4.1 provides a possible setup on a honeycomb lattice for this current-induced phonon Hall effect.

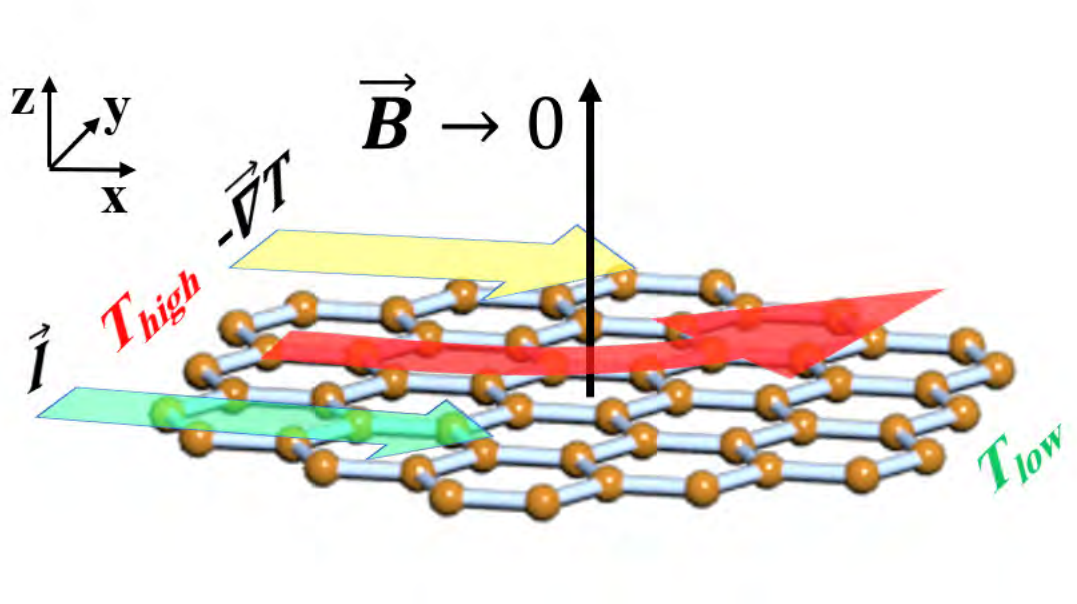

Figure 4.1: The schematic setup to detect current-induced phonon Hall effect. Electric current and temperature gradient are needed which are parallel to each other. A very small magnetic field, which is about 10^{-5} tesla, is to perturb the system and distinguish the direction of the phonon Hall current.

For convenience, we use the renormalized coordinate $\boldsymbol{u}_{lj} \equiv \sqrt{M_j}\boldsymbol{x}_{lj}$ to denote the nucleus displacement in real space. Electrons in a metal or a semi-conductor carrying electric current can interact with the lattice phonons through the electron-phonon interaction (EPI). In the NEGF formalism, EPI effect is included as a self-energy

term in the phonon retarded Green's function [1],

$$\mathrm{D}(\omega, \boldsymbol{q}) = \left[\omega^2 I - \tilde{K}_{\boldsymbol{q}} - \Pi(\omega{=}0) - \Pi^{\mathrm{NA}}_{\boldsymbol{q}}(\omega)\right]^{-1}, \tag{4.101}$$

where I is the identity matrix in site space of a unit cell, $\tilde{K}_{\boldsymbol{q}}$ is the dynamic matrix. $\Pi(\omega{=}0)$ is the second term in the equation below. We subtract it off so that the leading contribution is proportional to the frequency ω in the so-called non-adiabatic self-energy due to electrons:

$$\begin{aligned}\Pi^{\mathrm{NA}}_{\boldsymbol{q}jj'}(\omega) = \frac{1}{N}\sum_{mn}\sum_{\boldsymbol{k}} g^*_{mnj}(\boldsymbol{k},\boldsymbol{q}) g_{mnj'}(\boldsymbol{k},\boldsymbol{q}) \\ \times\left[\frac{f_{m\boldsymbol{k}+\boldsymbol{q}} - f_{n\boldsymbol{k}}}{\varepsilon_{m\boldsymbol{k}+\boldsymbol{q}} - \varepsilon_{n\boldsymbol{k}} - \hbar\omega - i\eta} - \frac{f_{m\boldsymbol{k}+\boldsymbol{q}} - f_{n\boldsymbol{k}}}{\varepsilon_{m\boldsymbol{k}+\boldsymbol{q}} - \varepsilon_{n\boldsymbol{k}}}\right],\end{aligned} \tag{4.102}$$

where f is the Fermi function, g is the converted EPI matrix falling in electron mode space and phonon reciprocal space, $\boldsymbol{k}$ and $\boldsymbol{q}$ are wave vectors of electrons and phonons respectively, $\varepsilon_{n\boldsymbol{k}}$ is the electron dispersion relation, the subscripts m and n indicate the electron bands, and the subscripts j and j' denote the atomic labels in a unit cell including both atom sites and Cartesian directions. The summation is over the first Brillouin zone of the electrons. A small positive η attributes the electrons with a finite life time. The self energy can be computed from a first-principle package.

Alternatively, the movement of the ions can also be described semi-classically by an equation of motion taking into account the effect of the electrons. For a general electron-phonon system, there is a generalized Langevin equation describing the atoms' movement [90]:

$$\ddot{\boldsymbol{u}} = -K\boldsymbol{u} - \int^t \Pi^r_{\mathrm{epi}}(t-t')\boldsymbol{u}(t')dt' + \xi. \tag{4.103}$$

Here we do not consider the bath contribution and set the noise term ξ to zero, for our system is infinitely large. We can define $d\Gamma(t)/dt \equiv \Pi^r_{\text{epi}}(t)$ and integrate by parts so that the equation of motion becomes:

$$\ddot{\boldsymbol{u}} = -K\boldsymbol{u} - \int^t \Gamma(t-t')\dot{\boldsymbol{u}}(t')dt'. \tag{4.104}$$

Next we apply a Markov approximation to $\Gamma(t-t')$ so that $\Gamma(t-t') \approx 4A(t')\delta(t-t')$ (factor 4 is for consistency). The final expression of the equation of motion will be

$$\ddot{\boldsymbol{u}} = -K\boldsymbol{u} - 2A\dot{\boldsymbol{u}}, \tag{4.105}$$

where K is the spring constant matrix in real space corresponding to the dynamic matrix $\tilde{K}_{\boldsymbol{q}}$ in reciprocal space, and A can be regarded as the matrix representation of the vector potential induced by EPI which is antisymmetric. Therefore, the phonon Green's function is:

$$\mathrm{D}(\omega, \boldsymbol{q}) = \left[\omega^2 I - \tilde{K}_{\boldsymbol{q}} + 2i\omega\tilde{A}_{\boldsymbol{q}}\right]^{-1}. \tag{4.106}$$

Comparing the two expressions, if we ignore the higher order terms of ω in $\Pi^{\mathrm{NA}}(\omega)$, and note that $\tilde{A}_{\boldsymbol{q}}$ is anti-Hermitian (the anti-Hermitian part of $\Pi^{\mathrm{NA}}(\omega)$ is the source of dissipative Joule heating, which we will ignore.), we can conclude that:

$$\tilde{A}_{\boldsymbol{q}} = \lim_{\omega\to 0} \frac{\Pi^{\mathrm{NA}}(\omega) + (\Pi^{\mathrm{NA}})^\dagger(\omega)}{-4i\omega}. \tag{4.107}$$

The Markov approximation adopted here is well justified as the electrons move on a much faster time scale than that of the nuclear degrees of freedom. In terms of the energy scale, an electron has typical energy of order eV, while phonon $\hbar\omega$ is of the order 100 meV or less. So keeping the leading ω dependence only on self-energy is a

good approximation. We can trace back to an effective Hamiltonian for phonons with the electrons taken into account through a non-dissipative term as

$$\hat{H} = \frac{1}{2}(p - Au)^2 + \frac{1}{2}u^T K u, \tag{4.108}$$

and the corresponding eigen equation is

$$\begin{aligned} \omega\psi_{\boldsymbol{q}} &= i \begin{pmatrix} 0 & I \\ -I & -2\tilde{A}_{\boldsymbol{q}} \end{pmatrix} \begin{pmatrix} \tilde{K}_{\boldsymbol{q}} & 0 \\ 0 & I \end{pmatrix} \psi_{\boldsymbol{q}} \\ &= \begin{pmatrix} 0 & iI \\ -i\tilde{K}_{\boldsymbol{q}} & -i2\tilde{A}_{\boldsymbol{q}} \end{pmatrix} \psi_{\boldsymbol{q}}. \end{aligned} \tag{4.109}$$

Here we choose $y_{\boldsymbol{q}} = (\boldsymbol{u}_{\boldsymbol{q}}, \boldsymbol{v}_{\boldsymbol{q}})^T$, and $\boldsymbol{v}_{\boldsymbol{q}} = \boldsymbol{p}_{\boldsymbol{q}} - \tilde{A}(\boldsymbol{q})\boldsymbol{u}_{\boldsymbol{q}}$ as before.

4.3 Model Implementation on a Graphene-like Lattice

4.3.1 Hamiltonian and Self-energy

Graphene has been widely studied and it has remarkably high electron mobility, therefore we choose a graphene-like lattice to implement our settings. We use a standard spinless tight-binding model for the electrons:

$$\hat{H}_e = -t \sum_{l\delta} \left[c^\dagger_{A,l} c_{B,l+\delta} + c^\dagger_{B,l} c_{A,l+\delta} \right], \tag{4.110}$$

where $t = 2.8\,\mathrm{eV}$ is the hopping parameter. A and B indicate the two sublattices, and l runs over the Bravais lattice sites and δ runs over the displacements of the three nearest neighbors of a given site. Zhang *et al.*[25] have proposed a simple phonon model for a graphene-like lattice in which the coupling matrix is diagonal

when the bond orientation is in the x direction between two atoms,

$$K_x = \begin{pmatrix} K_L & 0 \\ 0 & K_T \end{pmatrix}, \tag{4.111}$$

where $K_L = 0.144$ eV/(uÅ^2) is the longitudinal spring constant and $K_T = K_L/4$ is the transverse spring constant. In our coordinates, unit cell lattice vectors are $\boldsymbol{a_1} = (3a/2, \sqrt{3}a/2)$ and $\boldsymbol{a_2} = (3a/2, -\sqrt{3}a/2)$. The explicit coupling matrices among three nearest pair can be obtained by a rotation matrix U which are $K_{01} = U(\pi/3)K_xU(-\pi/3)$, $K_{02} = U(-\pi/3)K_xU(\pi/3)$ and $K_{03} = U(\pi)K_xU(-\pi)$ respectively. Based on these matrices, we can construct five coupling matrices between unit cells,

$$K_0 = \begin{pmatrix} K_{01}+K_{02}+K_{03} & -K_{03} \\ -K_{03} & K_{01}+K_{02}+K_{03} \end{pmatrix}, \tag{4.112}$$

$$K_1 = \begin{pmatrix} 0 & 0 \\ -K_{02} & 0 \end{pmatrix}, K_2 = \begin{pmatrix} 0 & 0 \\ -K_{01} & 0 \end{pmatrix}, \tag{4.113}$$

$$K_3 = \begin{pmatrix} 0 & -K_{02} \\ 0 & 0 \end{pmatrix}, K_4 = \begin{pmatrix} 0 & -K_{01} \\ 0 & 0 \end{pmatrix}. \tag{4.114}$$

Then the dynamic matrix is

$$\begin{aligned} \tilde{K}_{\boldsymbol{q}} &= \sum_{l'} K_{ll'} e^{i(\boldsymbol{R}^0_{l'} - \boldsymbol{R}^0_l)\cdot \boldsymbol{q}} \\ &= K_0 + K_1 e^{i(3q_xa/2 - \sqrt{3}q_ya/2)} + K_2 e^{i(3q_xa/2 + \sqrt{3}q_ya/2)} \\ &+ K_3 e^{-i(3q_xa/2 - \sqrt{3}q_ya/2)} + K_4 e^{-i(3q_xa/2 + \sqrt{3}q_ya/2)}. \end{aligned} \tag{4.115}$$

In this model, we have ignored the z mode and consider only the in-plane motion. The reason is that the motion in the direction perpendicular to the plane couples

quadratically to the electron degrees of freedom, and this is a higher order effect to the electron-phonon interaction. The electron bands and phonon dispersion of this lattice model are illustrated in Fig. 4.2. In Fig. 4.2(b), we compare the phonon dispersion of our model with the DFT results of the graphene. It can be seen our model is a rough model simulating the real graphene.

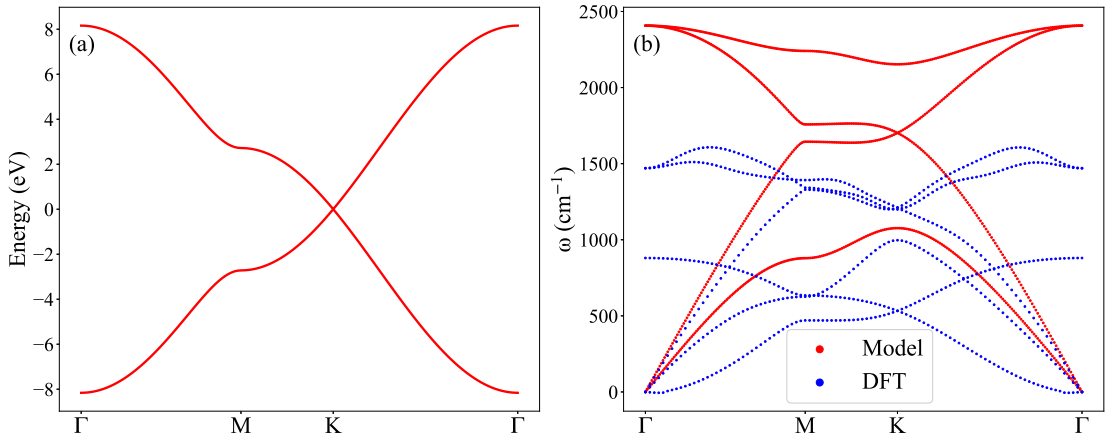

Figure 4.2: (a) Electron bands. (b) Phonon dispersion of the model compared with the phonon dispersion of graphene calculated by DFT.

For the electron-phonon interaction, we take a SSH-like model, as used in a previous work by Jiang and Wang [91],

$$\begin{aligned}\hat{H}_{\text{epi}} = J_1 \sum_{l\delta} \left[c^{\dagger}_{A,l} c_{B,l+\delta} + c^{\dagger}_{B,l+\delta} c_{A,l} \right] \\ \times \left[(\boldsymbol{u}_{B,l+\delta} - \boldsymbol{u}_{A,l}) \cdot \hat{\boldsymbol{e}}_{l,\delta} \right],\end{aligned} \tag{4.116}$$

where $J_1 = -6.0\,\text{eV/Å}$ and $\hat{\boldsymbol{e}}_{l,\delta}$ is the direction between two nearest atoms. The g matrix is given by

$$g_{mnj}(\boldsymbol{k}, \boldsymbol{q}) = \sum_{m'n'} S^{\dagger}_{mm'}(\boldsymbol{k} + \boldsymbol{q}) \Xi^{j}_{m'n'}(\boldsymbol{k}, \boldsymbol{q}) S_{n'n}(\boldsymbol{k}), \tag{4.117}$$

where $j = \{\mathrm{Ax}, \mathrm{Ay}, \mathrm{Bx}, \mathrm{By}\}$, $g_{mnj}(\boldsymbol{k}, \boldsymbol{q})^* = g_{nmj}(\boldsymbol{k}+\boldsymbol{q}, -\boldsymbol{q})$ due to hermicity of the Hamiltonian,

$$S(\boldsymbol{k}) = \frac{1}{\sqrt{2}} \begin{pmatrix} 1 & e^{i\phi(\boldsymbol{k})} \\ -e^{-i\phi(\boldsymbol{k})} & 1 \end{pmatrix}, \tag{4.118}$$

with $e^{i\phi(\boldsymbol{k})} = f(\boldsymbol{k})/|f(\boldsymbol{k})|$, $f(\boldsymbol{k}) = e^{-ik_x a} + e^{i(k_x a/2 + \sqrt{3}k_y a/2)} + e^{i(k_x a/2 - \sqrt{3}k_y a/2)}$, and $\Xi^j_{m'n'}(\boldsymbol{k}, \boldsymbol{q})$ is the reciprocal EPI matrix corresponding to $\hat{H}_{\mathrm{epi}}$. The non-zero reciprocal EPI matrix elements are

$$\begin{aligned}
\Xi^{\mathrm{Ax}}_{\mathrm{AB}}(\boldsymbol{k}, \boldsymbol{q}) &= -J_1[e^{ik_x a/2}\cos(\sqrt{3}k_y a/2) - e^{-ik_x a}], \\
\Xi^{\mathrm{Ay}}_{\mathrm{AB}}(\boldsymbol{k}, \boldsymbol{q}) &= -J_1\sqrt{3}ie^{ik_x a/2}\sin(\sqrt{3}k_y a/2), \\
\Xi^{\mathrm{Bx}}_{\mathrm{AB}}(\boldsymbol{k}, \boldsymbol{q}) &= J_1[e^{i(k_x+q_x)a/2}\cos(\sqrt{3}(k_y+q_y)a/2) - e^{-i(k_x+q_x)a}], \\
\Xi^{\mathrm{By}}_{\mathrm{AB}}(\boldsymbol{k}, \boldsymbol{q}) &= J_1\sqrt{3}ie^{i(k_x+q_x)a/2}\sin(\sqrt{3}(k_y+q_y)a/2), \\
\Xi^{j}_{\mathrm{BA}}(\boldsymbol{k}, \boldsymbol{q}) &= \left(\Xi^{j}_{\mathrm{AB}}(\boldsymbol{k}+\boldsymbol{q}, -\boldsymbol{q})\right)^*, j = \{\mathrm{Ax}, \mathrm{Ay}, \mathrm{Bx}, \mathrm{By}\}.
\end{aligned} \tag{4.119}$$

In this work, we focus on the EPI for $\boldsymbol{k}$ points near the Dirac points of the electrons and $\boldsymbol{q}$ near the Γ point of the phonons, for we find that they are dominant in determining the final phonon Hall conductivity. It seems that we have prepared all the ingredients to calculate $\tilde{A}_{\boldsymbol{q}}$. However, there is a problem that when we apply an electric current to this graphene-like two-dimensional surface, assuming the drift velocity v_1 of current is along the x direction, it is in a nonequilibrium state, therefore we cannot just substitute the Fermi function into the formula. To solve this problem, we use a single-mode relaxation approximation [62] so that:

$$f = f^0 - \frac{\partial f^0}{\partial \varepsilon}\Phi \approx f^0(\varepsilon - \Phi), \tag{4.120}$$

where $f^0 = [e^{(\varepsilon-\mu)/k_BT} + 1]^{-1}$ with μ being the chemical potential of electron, and $\Phi \equiv \Phi_{n\boldsymbol{k}}$ is mode dependent:

$$\Phi_{n\boldsymbol{k}} = -eE\tau_{nk}\frac{\partial\varepsilon_{n\boldsymbol{k}}}{\partial\hbar k_x}, \tag{4.121}$$

where E is the applied electric field, τ_{nk} is the relaxation time which is only related to the magnitude of the wave vector. In practice, since we don't know the relaxation time, we combine it with the electric field and replace them with the drift velocity v_1, for graphene-like lattice [92]:

$$\Phi_{n\boldsymbol{k}} = v_1\,\mathrm{Re}\Big[z^*\frac{\partial z}{\partial k_x}\Big]/(\hbar v_F^2), \tag{4.122}$$

where $v_F = 3at/(2\hbar)$ is the Fermi velocity, $a = 1.42$ Å is the distance between atoms, and $z = -tf(\boldsymbol{k})$. By requiring this correction to the Fermi function, the self-energy can be numerically calculated, and thereafter, the $\tilde{A}_{\boldsymbol{q}}$ matrix.

4.3.2 Geometric Way for Berry curvature

Usually there are two ways of calculating the Berry curvature, one is the explicit way,

$$\Omega_i = -\mathrm{Im}\sum_{i'\neq i}\frac{\bar{\psi}_i\frac{\partial H_{\mathrm{eff}}}{\partial q_x}\psi_{i'}\bar{\psi}_{i'}\frac{\partial H_{\mathrm{eff}}}{\partial q_y}\psi_i - (q_x \leftrightarrow q_y)}{(\omega_i - \omega_{i'})^2}. \tag{4.123}$$

However, to calculate the partial derivative of H_{eff}, we need numerical differentiation which will cost a large amount of computation to be precise enough. Therefore, we choose another way, a geometric way by dividing the Brillouin zone into plaquettes each consisting of four points on a square with area ΔS and calculating the Berry phase around them [63, 16]:

$$\phi = -\mathrm{Im}\ln(\bar{\psi}_1\psi_2\bar{\psi}_2\psi_3\bar{\psi}_3\psi_4\bar{\psi}_4\psi_1), \tag{4.124}$$

Compared with the Hermitian case, we have replaced the Hermitian conjugate of the eigenvector by the left eigenvector. If investigated further, we find that this replacement is not correct for $\bar{\psi}_1\psi_2 \neq (\bar{\psi}_2\psi_1)^*$. This break of the equality, a fundamental property of the inner product in Hilbert space, will invalidate Stokes' theorem so that we cannot obtain Berry curvature through Berry phase. To overcome this, we define a new version of inner product:

$$\langle\bar{\psi}_1\psi_2\rangle \equiv \frac{\bar{\psi}_1\psi_2 + (\bar{\psi}_2\psi_1)^*}{2}. \tag{4.125}$$

With this definition, property of inner product in Hilbert space and validity of Stokes' theorem are restored. Then the Berry curvature is calculated by

$$\Omega = \lim_{\Delta S\to 0} \frac{-\mathrm{Im}\ln\Big(\langle\bar{\psi}_1\psi_2\rangle\langle\bar{\psi}_2\psi_3\rangle\langle\bar{\psi}_3\psi_4\rangle\langle\bar{\psi}_4\psi_1\rangle\Big)}{\Delta S}. \tag{4.126}$$

4.3.3 Uniqueness of the Berry Curvature

As we have discussed in the previous section, the choice of $y_{\boldsymbol{q}}$ is not unique – at least three different choices exist in the literature. Zhang *et al.* choose $y_{\boldsymbol{q}} = (u_{\boldsymbol{q}}, p_{\boldsymbol{q}})$, Qin *et al.* choose $y_{\boldsymbol{q}} = (u_{\boldsymbol{q}}, v_{\boldsymbol{q}})$, Liu *et al.* choose $y_{\boldsymbol{q}} = (\tilde{K}_{\boldsymbol{q}}^{-\frac{1}{2}} u_{\boldsymbol{q}}, v_{\boldsymbol{q}})$ [25, 2, 93]. The difference between Zhang's and Qin's choices is like the difference between Lagrangian mechanics and Hamiltonian mechanics, therefore they are more or less equivalent. The special choice of Liu results in a Hermitian effective Hamiltonian, which implies immediately the eigenfrequencies are all real. When the vector potential term can be separated from the usual potential energy term as in our case, these three bases are related by similarity transformations explicitly. However, this kind of variable transformations is not gauge invariant. Therefore, generally, if $\tilde{A}_{\boldsymbol{q}}$ is not

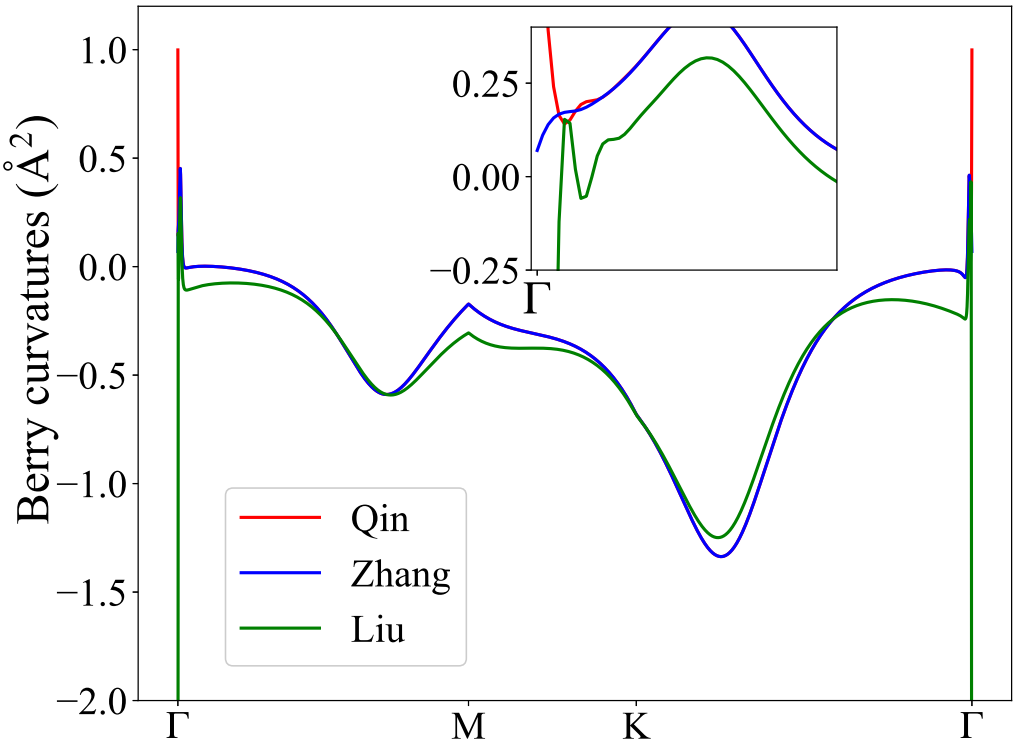

Figure 4.3: The Berry curvatures along the high-symmetry path under three different bases [25, 2, 93]. Although they do not differ so much from each other, they are indeed different. The inset shows the details of the Berry curvatures near the Γ point.

a constant matrix, they will result in different Berry curvatures. The question then arises as which one should be used to compute the phonon Hall conductivity? To illustrate and confirm that there is indeed a difference, we choose a smooth $\tilde{A}_{\boldsymbol{q}} = (\Lambda + i|\Lambda|) * (\boldsymbol{b} \cdot \boldsymbol{q} + c)$ matrix, where Λ is a constant 4×4 antisymmetric matrix, $|\Lambda|$ takes the absolute value of each element in Λ, $\boldsymbol{b}$ is a constant vector parameter, and c is another constant parameter. In principle, these three bases should result in different Berry curvatures, but in practice, the differences are small, especially between Zhang's and Qin's choices, therefore we choose such a highly

anisotropic case. We plot the corresponding Berry curvatures of the three bases along a high-symmetry path of the graphene-like lattice in Fig. 4.3. The parameter set is chosen to be: $\boldsymbol{b} \cdot \boldsymbol{q} = (1000\,\text{Å}, 1\,\text{Å}) \cdot \boldsymbol{q}, c = 0.1$ rad/ps, and Λ is a constant antisymmetric matrix with upper triangular elements, lower triangular elements and diagonal elements being 1.0, -1.0, and 0 rad/ps respectively. We see that there are sharp peaks at the Γ point. However, the signs of the peaks are opposite for Liu *et al.* definition to that of Zhang and Qin *et al.*. Away from the Γ point, the values tend to be close among the three. In conclusion, since only Qin *et al.* derived the correct formula for the phonon Hall conductivity with their definition of the Berry curvature, which considers an energy magnetization contribution to Hall conductivity [2] while Zhang *et al.* did not, we prefer to follow Qin's definition. It is natural that if we use other choices, we will obtain different formulas for phonon Hall conductivity.

4.3.4 Numerical Results and Discussions

In order to have a well-defined topological structure, we need to perturb our system to open tiny gaps at Γ and K points, as the Berry curvature becomes ill-defined when the bands are degenerate. This goal is achieved by adding a small onsite potential term to the phonon dynamic matrix and a nearly zero magnetic field which goes into the Hamiltonian through Raman-type spin-phonon interaction [25]. The effect of the magnetic field is described by a constant antisymmetric matrix A_h:

$$A_h = \begin{pmatrix} B_h & 0 \\ 0 & B_h \end{pmatrix}, B_h = \begin{pmatrix} 0 & h \\ -h & 0 \end{pmatrix}, \tag{4.127}$$

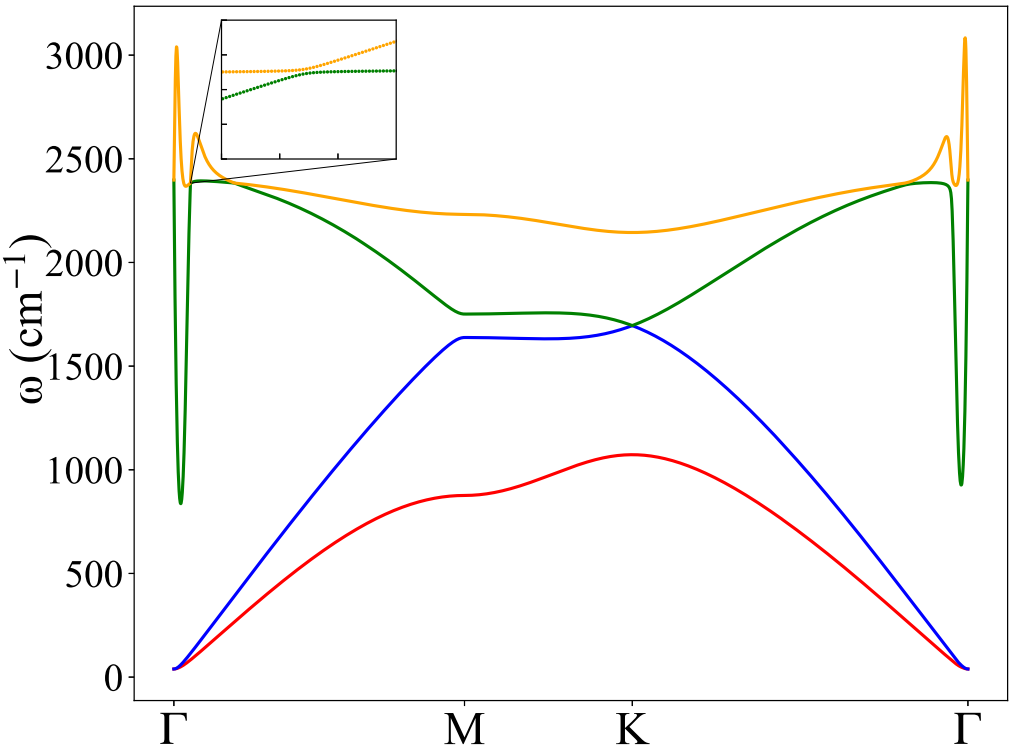

Figure 4.4: The dispersion relation of positive branches along high-symmetry path $\Gamma - M - K - \Gamma$ with $v_1 = 1.0 \times 10^4$ m/s, $T = 300\,\mathrm{K}$, $\mu = 0.1\,\mathrm{eV}$. A small onsite potential $V_{\mathrm{onsite}} = 1.0 \times 10^{-3} K_L$ and a nearly 0 magnetic field measured by effective parameter $h = 1.0 \times 10^{-9}$ rad/ps are employed to perturb the system. The inset shows one of the anti-crossing points. Note that the out-of-plane ZA mode is not considered here.

where h is an effective parameter representing magnetic field with units rad/ps (1 rad/ps $\approx$ 33.3 cm^{-1}). Adding this matrix to our previous $\tilde{A}_{\boldsymbol{q}}$ will introduce magnetic field into our system. When we calculate $\tilde{A}_{\boldsymbol{q}}$, a 400×400 $\boldsymbol{k}$ grids is used and the parameter η is set to be about 0.2 eV. We note that as a function of a constant magnetic field h, the Berry curvatures and the Chern numbers are odd functions of h and experience a discontinuity at $h = 0$, thus ill-defined at $h = 0$. Our results presented below thus should be considered as the limit when $h \to 0^+$

and $V_{\text{onsite}} \to 0^+$. This is physical since we can always apply a small magnetic field and put the system on a substrate, thereby acquiring an onsite interaction. There is one more important thing to note that inside the formula of $\tilde{A}_{\boldsymbol{q}}$, since we only focus on $\boldsymbol{q}$ points near Γ point, there is a hidden δ function behavior when temperature is low. This δ function originates from the difference of the intra-band Fermi functions in the numerator of $\tilde{A}_{\boldsymbol{q}}$ if we take a Taylor expansion of $\boldsymbol{q}$ near Γ point at low temperature. To handle this δ function numerically, we should compute in a very dense $\boldsymbol{k}$ grids which requires a lot of computation power. However, we can also broaden this δ function by tuning the electron parameter $\beta = 1/k_B T$. Through computation, we find that the differences of EPI at low temperature range, e.g., below 300 K or even below 500 K, are very small, therefore, when we calculate $\tilde{A}_{\boldsymbol{q}}$ at low temperature, we can make an approximation to fix the broadening parameter to be the value at higher temperature like 300 K or 500 K.

Figure 4.4 shows the positive part of the dispersion relation of our current-induced system, from which we can see that the two acoustic branches are very close to the pure phonon system without the drift current, while the two optical branches get modified drastically. This behavior is easy to understand if we review the EPI form of our model. The strength of EPI in our model is proportional to the relative displacement of atoms, therefore the optical modes, in which atoms move relatively, are equipped with stronger EPI than acoustic ones. It deserves notice that there are several anti-crossing points in the dispersion relations. These points will possess much larger Berry curvatures, therefore they are dominant in determining the topological properties of the system. Points in acoustic branches near Γ point

and anti-crossing points near K points also have large Berry curvatures. However, these pairs of Berry curvatures should cancel each other for they are similar to pure phonon system where there are no PHE.

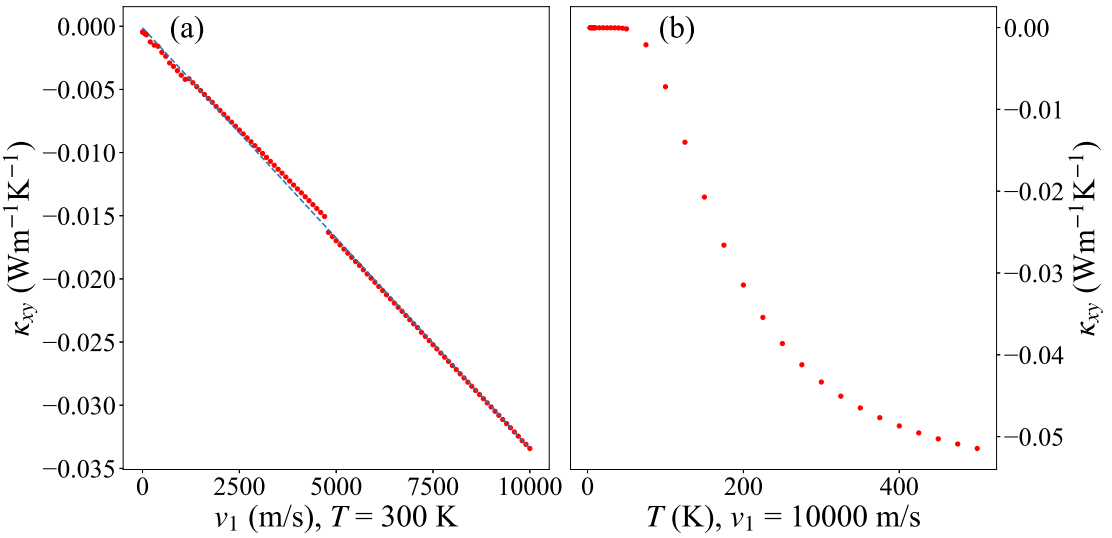

Figure 4.5: (a) Phonon Hall conductivity κ_{xy} versus drift velocity v_1 at a temperature $T = 300\,\mathrm{K}$. The broadening parameter is $\beta = 1/(k_B \times 300\mathrm{K})$. (b) Phonon Hall conductivity κ_{xy} versus temperature at $v_1 = 10000\,\mathrm{m/s}$. The broadening parameter is set to be $\beta = 1/(k_B \times 500\mathrm{K})$. These two plots share the same set of parameters of temperature, chemical potential, onsite potential and nearly 0 magnetic field as Fig. 4.4.

Figure 4.5(a) demonstrates the relationship between κ_{xy} and the drift velocity v_1. κ_{xy} is roughly linear dependent on v_1 for our picked velocity sequence. When v_1 is gradually close to the Fermi velocity of this graphene-like lattice system, our theory and approximation on EPI will gradually break down. The Chern numbers of positive branches are $C^1 = 1, C^2 = C^3 = 0, C^4 = -1$, respectively. In our range of the drift velocity, there is no jump among Chern numbers as the Fig. 4.6 shows, which seems kind of trivial. Since the topological structure of the system

does not change, the discontinuities should come from numerical errors. Figure 4.5(b) shows temperature dependence of κ_{xy}. When the temperature is very small, PHE tends to disappear, and in our temperature range, the absolute value of the phonon Hall conductivity gradually increases as temperature is increasing, but we can not conclude what the exact relationship between κ_{xy} and temperature is. In our calculation, numerical errors mainly come from the calculation of $\tilde{A}(\boldsymbol{q})$ and cubic interpolation to obtain its values with denser grids, which is 2000×2000.

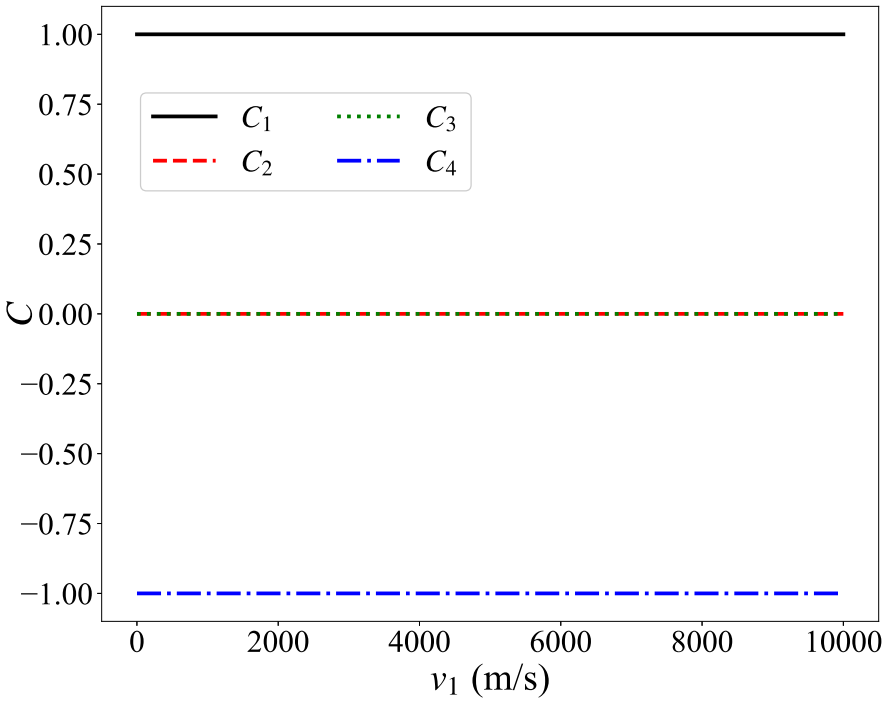

Figure 4.6: Chern numbers of four positive branches κ_{xy} against the drift velocity v_1. Larger indices are associated with higher frequencies.

The order of magnitude of our current-induced κ_{xy} is one order smaller than the case with the magnetic field parameter h being several rad/ps. It is instructive to compare the magnitude of the Hall conductivity to the universal conductance quantum which is $G_0 = T(\pi k_B)^2/(3h)$, when converted into the same units of

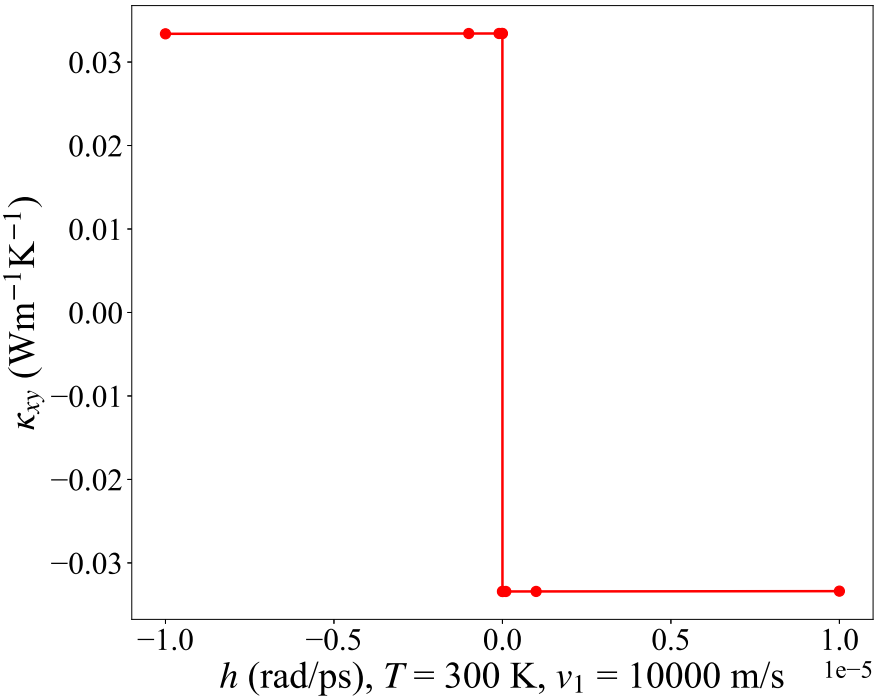

Figure 4.7: Phonon Hall conductivity κ_{xy} versus magnetic field parameter h. We can see κ_{xy} changes sign as h changes sign and there is a discontinuity when h crosses 0.

conductivity, G_0/a, at 300 K, we find it is about 2 W/(mK). Our result is about 1/100-th of the conductance quantum. Since κ_{xy} with our model is only about one order smaller than a pure magnetic field experimental results [19], it should be still observable experimentally in principle.

Figure 4.7 shows this sign jump of the phonon Hall conductivity. The role small magnetic field played in our system is to perturb our system at Γ point to induce circular polarisation like the "run away" mode in the work by Lü *et al.*, for the current-induced $\tilde{A}(\boldsymbol{q})$ is 0 there due to the translational symmetry. Therefore, the magnetic field determines the sign of the phonon Hall conductivity. Away from Γ point, current-induced $\tilde{A}(\boldsymbol{q})$ starts to affect the system so that there is a discontinuity of κ_{xy}. Previously, we said we ignore the Joule heating effect. However, in practice,

Joule heating always exists without special flowing direction. Therefore, it will not prevent us from observing PHE. We simply prepare a sample with temperature gradient in a direction, let electric current flow parallel to this temperature gradient, and apply small magnetic field twice with opposite direction, then measure the temperature differences in the direction transverse to the current flow. The Joule heating effect does not change sign while the Hall effect changes sign. From this, we can deduce the pure Hall contribution.

4.4 Summary

In summary, we have confirmed Tao Qin's theory through thorough derivation, and presented an optimization to calculate the phonon Hall conductivity more accurately. Moreover, we proposed a mechanism of the PHE induced by the electric current. Compared with other mechanisms of the PHE, no significant magnetic field is needed in our system. The Chern numbers of some phonon branches are not 0, but the total Chern number of all the branches is still 0. The property of our system is that for a suitable range of the drift velocities, the phonon Hall conductivity has a linear relation on the drift velocity which is proportional to the applied current. Our mechanism is also consistent with the thermodynamics that when temperature goes to 0, the PHE disappears. The magnitude of the phonon Hall conductivity grows nonlinearly when temperature is increasing, but the exact relation cannot be determined quantitatively.

Chapter 5

PHE with First-principles Calculations

Compared with the theoretical studies which are still hovering around the phenomenon-based models, all the recent experiments are performed on complex materials. The large phonon Hall conductivity and its strange behaviour in STO are challenging current microscopic theory [21, 31]. Therefore, it is difficult to understand them with simplified models, more accurate and persuasive first-principles calculations are needed.

Usually, harmonic assumption is made in first-principles calculations for phonon properties like phonon dispersion. However, in some highly anharmonic materials, harmonic terms alone will produce imaginary phonon frequencies, and it cannot explain those phenomena such as the thermal expansion, temperature-dependent phonon dispersion, and some phase transitions. Therefore, beyond harmonicity is a natural requirement to explore the PHE in complex materials like STO, and it was argued in a similar perovskite, BTO, that the anharmonic soft phonon modes will result in a large dielectric constant [46] which could act as a magnifier of the PHE [30]. Based on this understanding, anharmonicity should play an important role in

the PHE in real materials. In recent years, many packages based on first-principles calculations have been developed to calculate anharmonic properties in solids such as SCAILD, ALAMODE, and TDEP [94, 43, 95]. With the help of these packages, it is feasible for us to study the PHE in real materials, which could deepen our understandings in this area.

5.1 Anharmonic Self-consistent Phonon Calculation for Soft Phonon Modes

There are currently three approaches to handle the anharmonicity: many-body perturbation theory [96, 97], *ab initio* molecular dynamics (AIMD) [98, 95], and self-consistent phonon (SCPH) theory [99, 94, 100, 43]. Perturbation theory is only valid for weak anharmonicity, while AIMD is a nonperturbative approach. However, since AIMD is based on the time-dependent Schrödinger equation for all particles approximately [101], it cannot include zero-point vibration which is significant at low temperature. SCPH provides another choice to address anharmonicity nonperturbatively considering the quantum effect. Therefore, in this study, we focus on the SCPH approach, and borrow the ALAMODE package developed by Tadano and Tsuneyuki [43]. In this section, we briefly introduce the SCPH theory.

A general Hamiltonian with the third- and the fourth-order Taylor expansion of the potential can be described as follows:

$$\begin{aligned}\hat{H} = &\frac{1}{2}\sum_i p_i^2 + \frac{1}{2}u^T K u \\ &+ \frac{1}{3}\sum_{ijk}\Gamma_{ijk}u_i u_j u_k + \frac{1}{4}\sum_{ijkl}T_{ijkl}u_i u_j u_k u_l,\end{aligned} \tag{5.1}$$

where $u_i \equiv \sqrt{M_i}x_i$, M_i and x_i are mass and displacement of the i-th degree of freedom, respectively. Although the third-order term has important contribution for most anharmonic behaviors like thermal expansion and phonon lifetime, the fourth-order term is also important, especially for the soft phonon modes. Moreover, the fourth-order is simpler than the third if we apply a mean-field approximation by replacing u^4 with $\langle u^2\rangle u^2$. With this approximation, the problem goes back to a quadratic problem with the effective force constant being determined self-consistently. Therefore, in this thesis, we only focus on the fourth-order correction. By an equation of motion method [102], the non-equilibrium Green's function (NEGF) satisfies

$$\begin{aligned} G(1,2) &= G_0(1,2) \\ &\quad + \int d1'd2'd3d4 G_0(1,1')T(1',2',3,4)G(2',3,4,2), \end{aligned} \tag{5.2}$$

where $G(1,2) = -\frac{i}{\hbar}\langle \hat{T}u(1)u(2)\rangle$, $G(1,2,3,4) = -\frac{i}{\hbar}\langle \hat{T}u(1)u(2)u(3)u(4)\rangle$, $\hat{T}$ is the contour order operator, $G_0(1,2)$ is the non-interacting version of $G(1,2)$, and numbers represent the combination of (jt). To close this equation, we need to apply a mean-field approximation:

$$\begin{aligned} G(1,2,3,4) \approx i\hbar\Big[&G(1,2)G(3,4) + G(1,3)G(2,4) \\ &+ G(1,4)G(2,3)\Big]. \end{aligned} \tag{5.3}$$

Then we can work out the effective force constant matrix,

$$K^e = K + \Sigma, \tag{5.4}$$

where we define

$$\Sigma_{ij} = 3\sum_{kl} T_{ijkl}\langle u_k u_l\rangle. \tag{5.5}$$

The ingredient we need in the PHE is the dynamic matrix, and therefore we need to transform the equation into mode space, which is

$$\begin{aligned} D_{nn'}(\boldsymbol{q}) &= \omega_n(\boldsymbol{q})^2\delta_{nn'} \\ &\quad + 3\sum_{mm'\boldsymbol{q'}} T_{nn'mm'}(\boldsymbol{q},\boldsymbol{q'})\langle Q_m(\boldsymbol{q'})Q_{m'}(\boldsymbol{q'})^*\rangle, \end{aligned} \tag{5.6}$$

where Q represents normal modes, n and m are indices for normal modes, $\boldsymbol{q}$ and $\boldsymbol{q'}$ are lattice momentum, and ω_n is the eigenfrequency of the harmonic system. This equation should be solved self-consistently. In 2015, Tadano and Shinji have already discussed details within their ALAMODE package [43]. Therefore, we utilize their package to calculate the dynamic matrix for real materials.

5.2 Phonon Hall Effect Theory

Recall the general description of the PHE theory discussed in Chapter 4, the phonon dynamics can be described by the following eigen equation:

$$\omega_{\boldsymbol{q}i}\psi_{\boldsymbol{q}i} = \begin{pmatrix} 0 & iI \\ -iD_{\boldsymbol{q}} & -i2A_{\boldsymbol{q}} \end{pmatrix}\psi_{\boldsymbol{q}i} \equiv \tilde{H}_{\boldsymbol{q}}\psi_{\boldsymbol{q}i}. \tag{5.7}$$

Solving this eigensystem, we obtain the Berry curvatures and phonon Hall conductivity:

$$\boldsymbol{\Omega}_{\boldsymbol{q}i} = -\mathrm{Im}\Big[\frac{\partial\bar{\psi}_{\boldsymbol{q}i}}{\partial\boldsymbol{q}} \times \frac{\partial\psi_{\boldsymbol{q}i}}{\partial\boldsymbol{q}}\Big], \tag{5.8}$$

and

$$\kappa_{xy} = -\frac{1}{2T}\int_{-\infty}^{\infty} d\epsilon\, \epsilon^2\sigma_{xy}(\epsilon)\frac{dn(\epsilon)}{d\epsilon}, \tag{5.9}$$

where

$$\bar{\psi} = \psi^{\dagger} \begin{pmatrix} D_{\boldsymbol{q}} & 0 \\ 0 & I \end{pmatrix}, \qquad \sigma_{xy}(\epsilon) = -\frac{1}{V\hbar} \sum_{\hbar\omega_{\boldsymbol{q}i} \leq \epsilon} \Omega^{z}_{\boldsymbol{q}i}, \tag{5.10}$$

$n(\epsilon) = 1/(e^{\epsilon/(k_B T)} - 1)$ is the Bose function at temperature T, ϵ represents the energy, V is the volume in real space, and k_B is the Boltzmann constant. The summation includes both positive and negative frequencies. The most common source of the $A_{\boldsymbol{q}}$ is the external magnetic field which has been applied in many experiments measuring the PHE. To describe this process, SPI was introduced.

5.2.1 Lorentz Force Effect with Born Effective Charge

After the first observation of the PHE in 2005, several researchers have tried to explain the experiments theoretically [23, 24, 25], and all of them focused on the Raman-type SPI. Under an external magnetic field, the SPI in an ionic crystal lattice has the form of [25]

$$H_I = \sum_{\alpha} \boldsymbol{h}_{\alpha} \cdot (\boldsymbol{u}_{\alpha} \times \boldsymbol{p}_{\alpha}) \tag{5.11}$$

where $\boldsymbol{h}_{\alpha} = -\frac{q_{\alpha}}{2M_{\alpha}} \boldsymbol{B}$ if it is purely due to Lorentz force, m_{α} and q_{α} are the ionic mass and charge at site α, $\boldsymbol{u}_{\alpha}$ and $\boldsymbol{p}_{\alpha}$ are the vectors of displacement and momentum of the α-th lattice site, respectively. If one assumes the magnetic field is along z-axis, the SPI can be written as

$$H_I = u^T A p, \tag{5.12}$$

where A is an antisymmetric block diagonal matrix in real space with the diagonal block being $\begin{pmatrix} 0 & h_\alpha \\ -h_\alpha & 0 \end{pmatrix}$. However, using q_α as the charge of the ion is not very accurate in real materials, and in fact, ionic materials do not have free charges. Instead, charge property should be described by a tensor, *i.e.*, the Born effective charge tensor. Born effective charge tensor $Z^T_{\alpha,ij}$ describes the linear relation between the polarization per unit cell along the direction i and the displacement along the direction j at site α under the condition of a zero electric field, which is equivalent to the coefficient of the linear relation between the force on an atom and the macroscopic electric field. These two coefficients are both related to the mixed second-order derivative of the energy over a macroscopic electric field and atomic displacements [103].

If we take a careful look at the form of SPI, it can be found that it has the similar form as the Hamiltonian containing a Lorentz force, therefore, to generalize it to couple with the Born effective charge, we should start from the magnetic energy. The energy of a magnetic moment is

$$V_m = -\boldsymbol{m} \cdot \boldsymbol{B}, \tag{5.13}$$

where usually $\boldsymbol{m} = \frac{e}{2}\boldsymbol{r} \times \boldsymbol{v}$, e is the charge of the particle. Since the Born effective charge is a tensor, we should insert it into the equation carefully. A reasonable argument is from the way Born effective charge acting on the electric field, which is $\boldsymbol{Z}^T\boldsymbol{E}$. Here we take the transpose of $\boldsymbol{Z}$ because the first index of it is associated with the electric field [103]. If we change the reference system so that the charge appears to move with a velocity $\boldsymbol{v}$, it will also feel a magnetic field $\boldsymbol{E} \to \boldsymbol{E} + \boldsymbol{v} \times \boldsymbol{B}$.

Therefore, $\boldsymbol{Z}^T$ should act on $\boldsymbol{v} \times \boldsymbol{B}$, not on $\boldsymbol{B}$ directly. Moreover, in electronic system, the rate of change of the polarization is $\frac{d\boldsymbol{P}}{dt} = e\boldsymbol{Z}\boldsymbol{v}$. Analogous to this, we propose that in magnetic case, $\boldsymbol{Z}$ acts on $\boldsymbol{v}$. However, this replacement breaks the antisymmetry over $\boldsymbol{r}$ and $\boldsymbol{v}$. To restore it, we add a term with $\boldsymbol{Z}$ act also on $\boldsymbol{r}$ so that the energy becomes

$$\begin{aligned} V_m &= -\frac{e}{4}[\boldsymbol{r} \times (\boldsymbol{Z}\boldsymbol{v}) + (\boldsymbol{Z}\boldsymbol{r}) \times \boldsymbol{v}] \cdot \boldsymbol{B} \\ &= -\frac{e}{4}[\Big((\boldsymbol{v}\boldsymbol{Z}^T) \times \boldsymbol{B}\Big) \cdot \boldsymbol{r} + (\boldsymbol{v} \times \boldsymbol{B}) \cdot (\boldsymbol{Z}\boldsymbol{r})] \\ &= -\frac{e}{4}[v_i Z_{ki} B_l \epsilon^{klj} r_j + \epsilon^{ikl} v_i B_k Z_{lj} r_j] \\ &\equiv -\frac{e}{4}[\boldsymbol{v} \cdot (\boldsymbol{Z}^T \times \boldsymbol{B} + \boldsymbol{B} \times \boldsymbol{Z}) \cdot \boldsymbol{r}]. \end{aligned} \tag{5.14}$$

Then compare it with the form of the SPI, $H_I = u^T A p = -p^T A u$, we can conclude that

$$A = \frac{e}{4M_\alpha}(\boldsymbol{Z}_\alpha^T \times \boldsymbol{B} + \boldsymbol{B} \times \boldsymbol{Z}_\alpha). \tag{5.15}$$

5.2.2 Analytic and Non-analytic Part of the Dynamic matrix

In standard solid state physics, the dynamic matrix is given by

$$D_{nn'}(jj';\boldsymbol{q}) = \frac{1}{\sqrt{M_j M_{j'}}} \sum_{l'} \Phi_{nn'}(lj;lj') e^{i\boldsymbol{q}\cdot(\boldsymbol{R}_{l'} - \boldsymbol{R}_l)}, \tag{5.16}$$

where n represents the total degrees of freedom within the unit cell, M_j is the atomic mass of atom j, Φ is the force constant matrix, $\boldsymbol{R}_l$ locates the unit cell, and $\boldsymbol{q}$ is the wave vector. By Diagonalizing this matrix, one can obtain the eigenvalues. However, this analytic dynamic matrix alone cannot correctly describe the phonon dispersion of ionic solids sometimes. There will be a so-called LO-TO splitting at Γ point in ionic materials because the Fourier transform of the long range Coulomb interaction

is not well-defined at Γ point [104]. To capture this splitting, we need to add a non-analytic part of the dynamic matrix [103],

$$D^{\mathrm{NA}}_{nn'}(jj';\boldsymbol{q}) = \frac{1}{\sqrt{M_j M_{j'}}}\frac{4\pi}{V}\frac{(Z^*_j\boldsymbol{q})_n(Z^*_{j'}\boldsymbol{q})_{n'}}{\boldsymbol{q}\cdot\epsilon^{\infty}\boldsymbol{q}}, \tag{5.17}$$

where V is the volume of the primitive cell, Z_j is the Born effective charge tensor of atom j, ϵ^{∞} is the dielectric constant tensor. ALAMODE provides two ways to add this non-analytic part. One is the Parlinski's way [105],

$$D_{\mathrm{total}} = D(\boldsymbol{q}) + D^{\mathrm{NA}}(\boldsymbol{q})e^{-q^2/\sigma^2}, \tag{5.18}$$

where σ is a damping factor. The other one is the mixed-space approach [106],

$$D_{\mathrm{total}} = D(\boldsymbol{q}) + D^{\mathrm{NA}}(\boldsymbol{q})\frac{1}{N}\sum_{l'} e^{i\boldsymbol{q}\cdot(\boldsymbol{R}_{l'}-\boldsymbol{R}_l)}. \tag{5.19}$$

We choose the mixed-space approach since it does not need an extra parameter. Both the analytic and non-analytic part of the dynamic matrix are explicit, therefore, it is easy to calculate their partial derivatives over $\boldsymbol{q}$ which are required in the PHE framework.

5.3 Numerical Details, Results and Discussions

Dynamic matrix, vector potential, and Berry curvatures are the ingredients to calculate the phonon Hall conductivity. We determine the structures of the materials based on first-principles calculations using Quantum-Espresso (QE) [107], then calculate their interatomic force constants (IFC) up to the fourth-order with the help of the AIMD package in QE, and finally using the ALAMODE to extract the

corresponding dynamic matrix including both analytic and non-analytic (with LO-TO splitting) part. We assume the vector potential is just from the SPI introduced in the last section with the block diagonal A matrix. The Born effective charge dyadic is calculated by ph.x module in QE. As for the Berry curvatures, the equation (5.8) is too abstract to be used in a real calculation, but fortunately, convert it to a more explicit form using the eigen equation is already a common skill in topological physics. Taking the z-component of the Berry curvature as an example:

$$\Omega^{z}_{j,q_xq_y} = -\mathrm{Im}\Big[\sum_{j\neq j'} \frac{\bar{\psi}_j \frac{\partial \tilde{H}}{\partial q_x}\psi_{j'}\bar{\psi}_{j'}\frac{\partial \tilde{H}}{\partial q_y}\psi_j}{(\omega_j-\omega_{j'}+i\eta)^2} - (q_x \leftrightarrow q_y)\Big], \tag{5.20}$$

where ω_j is the eigenfrequency in the Eq. (5.7), η is related to the inverse of the phonon lifetime to avoid infinity when there are degenerate points. Since both the analytic and non-analytic part of the dynamic matrix have explicit formulas, and the SPI is independent of $\boldsymbol{q}$, the Berry curvatures can be explicitly worked out. Thereafter, the phonon Hall conductivity can be obtained by the summation of the weighted Berry curvatures in the first Brillouin zone.

5.3.1 Numerical Results for NaCl

In 2011, Agarwalla *et al.* have calculated the PHE in NaCl using "General Utility Lattice Program" (GULP) with a Coulomb potential and a non-Coulomb Buckingham potential [29]. However, at that time, they used a not quite correct theory and their approach was still model-based. Therefore, we recalculate the PHE in NaCl in first-principles as a new benchmark. In our first-principles calculations, we apply structure optimization with the PAW-PBE pseudo-potential for Na and Cl to determine the lattice constant which turns out to be 5.65 Å with the energy

cutoff being 500 eV, and we use a $2 \times 2 \times 2$ supercell to calculate the IFCs. After several convergence tests, a $50 \times 50 \times 50$ grid and an $8 \times 8 \times 8$ grid, are employed in calculating the dynamic matrix according to Eq. (5.6) for $\boldsymbol{q}$ and $\boldsymbol{q'}$ respectively. The small η is chosen to be 0.1 cm^{-1}.

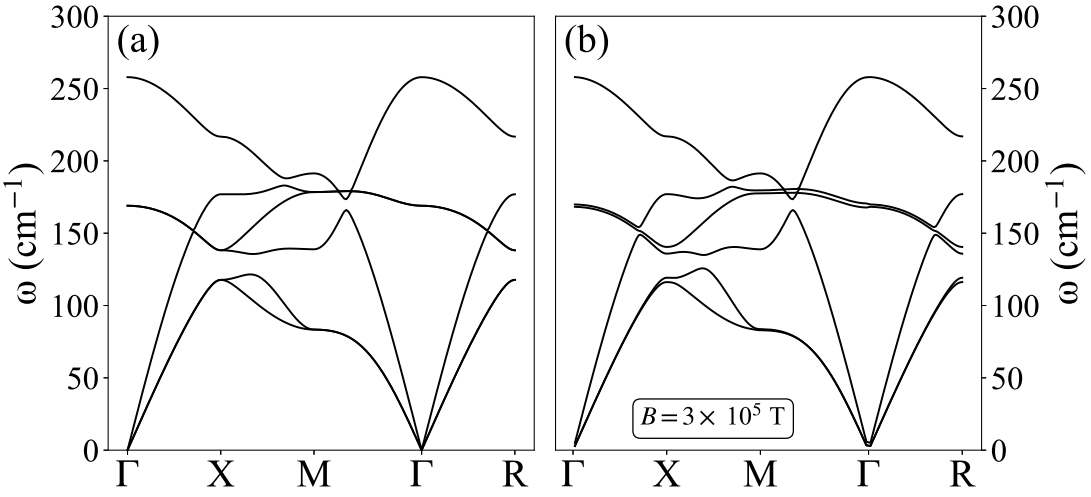

Figure 5.1: (a) Phonon dispersion of NaCl at $T = 300$ K without magnetic field. (b) Phonon dispersion of NaCl at $T = 300$ K with an external magnetic field being 3×10^5 T.

Figure 5.1(a) shows the phonon dispersion of NaCl at $T = 300$ K without an external magnetic field with LO-TO splitting included by the mixed-space approach [106]. It can be seen that in Fig. 5.1(a) there are many degenerate points. If we apply a magnetic field (along z-direction throughout the paper) of 3×10^5 T, those degenerate points will be lifted especially for the two TO modes as Figure 5.1(b) illustrates. Therefore, the role magnetic field plays is to open gaps in the phonon dispersion. Since NaCl has a simple structure, the branches in phonon dispersion can be well separated from each other by the applied magnetic field. As a result, we can

draw the corresponding Berry curvatures of each branch, which are shown in Fig. 5.2. Certain symmetries are observed in Fig. 5.2. The first and second acoustic branches are almost opposite to each other, so are the first and second optical branches, while the third acoustic branch and the third optical branch have their own patterns. This behaviour is consistent with the phonon dispersion of NaCl.

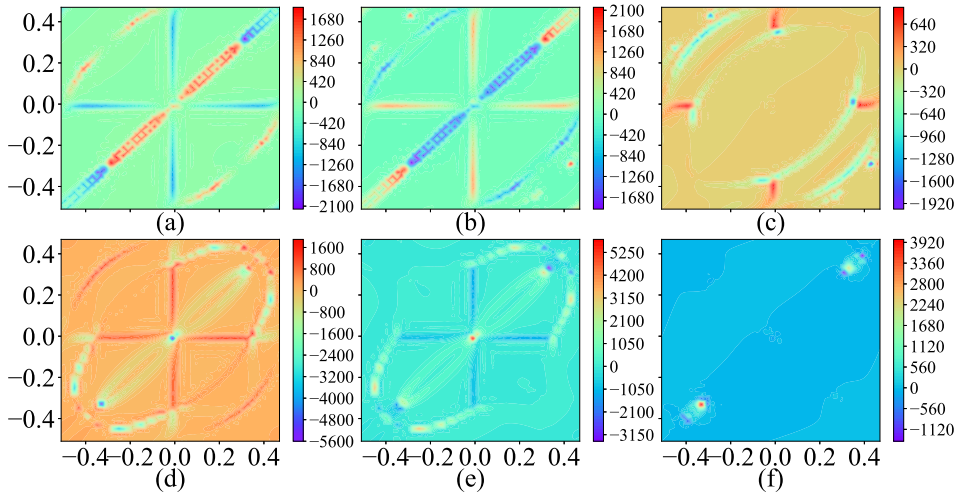

Figure 5.2: The Berry curvatures of six positive branches in $\boldsymbol{b}_1 - \boldsymbol{b}_2$ reciprocal plane of NaCl under the magnetic field $B = 3 \times 10^5$ T at temperature $T = 300$ K, where $\boldsymbol{b}_1 = \frac{2\pi}{a}(-\hat{q}_x + \hat{q}_y + \hat{q}_z)$, $\boldsymbol{b}_2 = \frac{2\pi}{a}(\hat{q}_x - \hat{q}_y + \hat{q}_z)$ are the two of three basis vectors with a being the lattice constant. The horizontal and vertical axes represent the fraction of $\boldsymbol{b}_1$ and $\boldsymbol{b}_2$ in the range of $(-0.5, 0.5)$. The unit of the Berry curvatures is a_0^2, where a_0 is the Bohr radius. From (a) to (f), the associated eigenvalues are in ascending order.

Figure 5.3 illustrates the dependence of the phonon Hall conductivity on magnetic field and temperature. It can be seen that as the temperature goes to 0, conductivity also decreases to 0. This is a favorable correction compared with the blowup of the conductivity near 0 K in Agarwalla *et al.*'s plots. For a small magnetic field, the magnitude of the conductivity is roughly linearly growing up, and when the

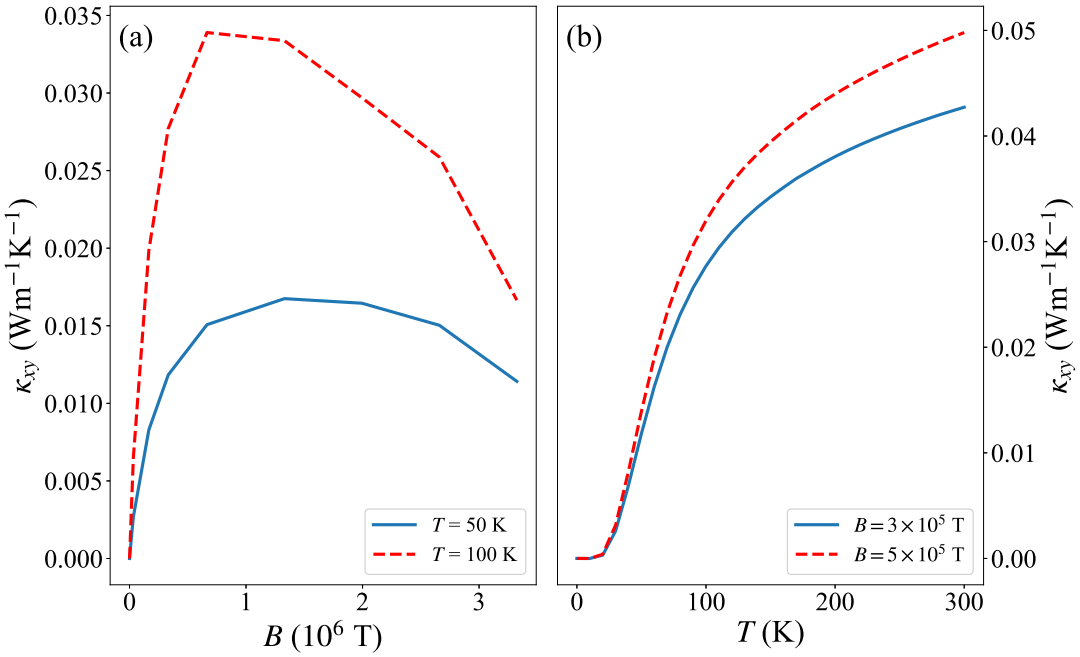

Figure 5.3: (a) Phonon Hall conductivity versus the applied magnetic field at $T = 50$ K and $T = 100$ K respectively. (b) Phonon Hall conductivity versus temperature at $B = 3 \times 10^5$ T and $B = 5 \times 10^5$ T respectively.

magnetic field increases further, the magnitude starts to decrease, the same behavior as that in Agarwalla *et al.*'s results. However, the conductivity does not change sign in the same range of the magnetic field. Moreover, the magnitudes of our results are about one order larger than Agarwalla *et al.*'s, which is another progress of the *ab initio* approach for stronger PHE can more easily be measured in experiments.

Although we obtain observable values of the phonon Hall conductivity, it requires a rather large magnetic field, about 10^5 T at least. In experiments, a magnetic field with an order of magnitude 1 is enough to induce observable and even large phonon Hall conductivity in complex materials [19, 21]. Therefore, it deserves to implement our approach in some much more complicated materials such as materials in the

family of perovskites.

5.3.2 Numerical Results for BTO

BTO has a large dielectric constant, and it was argued that it is due to its soft optical phonons [46] at Γ point. Previous study implies that a large dielectric constant could result in large phonon Hall conductivity [30], therefore, we calculate the PHE in BTO to verify this point. At different temperature ranges, BTO has different structures, while this structural diversity is difficult to be precisely caught by first-principles calculations [108]. Therefore, for simplicity, we still choose the simple cubic BTO to implement the calculation. PAW-PBE pseudo-potentials for Ba, Ti, and O are employed with a $2 \times 2 \times 2$ supercell to calculate the dynamic matrix. The lattice constant is optimized to be 4.024 Å, and the energy cutoff is set to be 800 eV. $\boldsymbol{q}$ and $\boldsymbol{q'}$ grids are $50 \times 50 \times 50$ and $8 \times 8 \times 8$ respectively. The small η is still chosen to be 0.1 cm^{-1}.

The phonon dispersion of BTO at $T = 60$ K is illustrated in Fig. 5.4 where the two soft TO modes can be clearly seen near Γ point whose frequencies are close to 0. Applying magnetic field results in a similar behavior as in NaCl which is trying to open gaps in dispersion. Since our goal for NaCl is to provide a benchmark while for BTO is to compare with experimental values, we use a reasonably large magnetic field with an order of magnitude 1 in this case. Within this range, the phonon dispersion almost remains the same under the magnetic field, therefore, it is not necessary to demonstrate it here.

Similar to Fig. 5.3, Figure 5.5 shows the behaviors of the phonon Hall conductivity

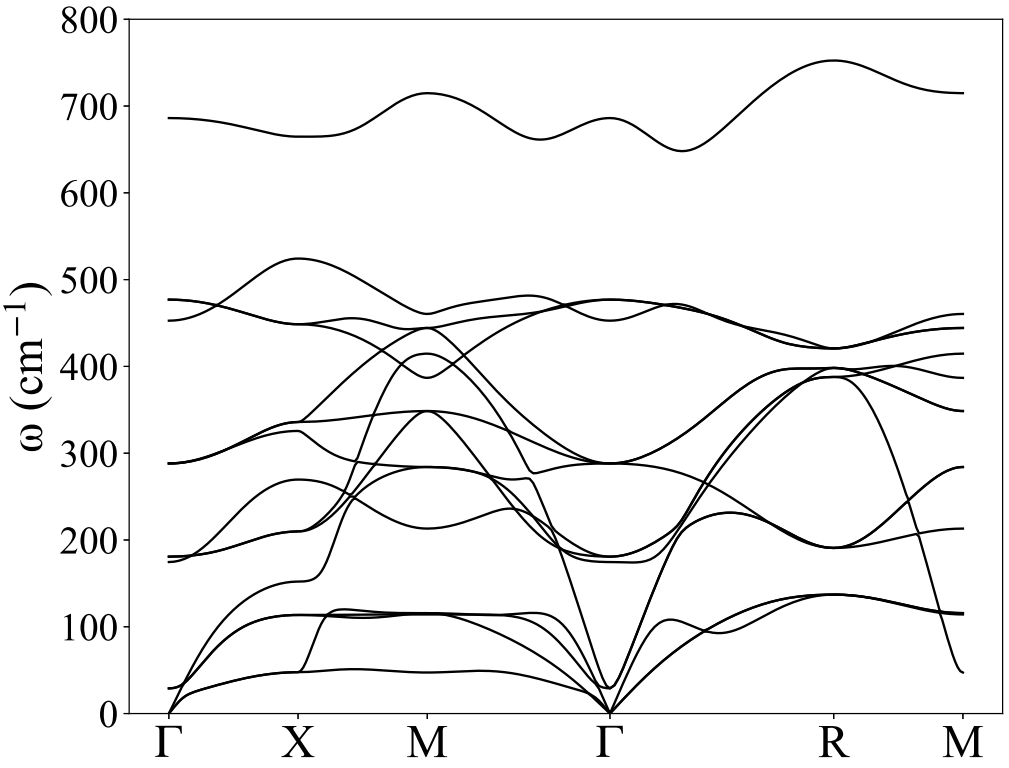

Figure 5.4: Phonon dispersion of BTO at $T = 60$ K without magnetic field.

against the magnetic field and temperature. Figure 5.5(a) is drawn at 60 K for this is roughly the lowest temperature range that first-principles calculations can correctly address the soft optical phonons in BTO [46]. Again, for a small magnetic field, the Hall conductivity demonstrates a linear relationship with the magnetic field. For large fields, the phonon Hall conductivity also becomes large and even has a sign change. Figure 5.5(b) is under a magnetic field of 16 T, the absolute value of Hall conductivity increases at first and reaches a peak near 150 K, then starts to decrease. However, the order of magnitude is two orders smaller than the order of the experimental values in STO. Although STO and BTO are different materials,

they have very similar crystal structures and both have soft optical modes at low temperature [45]. Therefore, we think the comparison is reasonable.

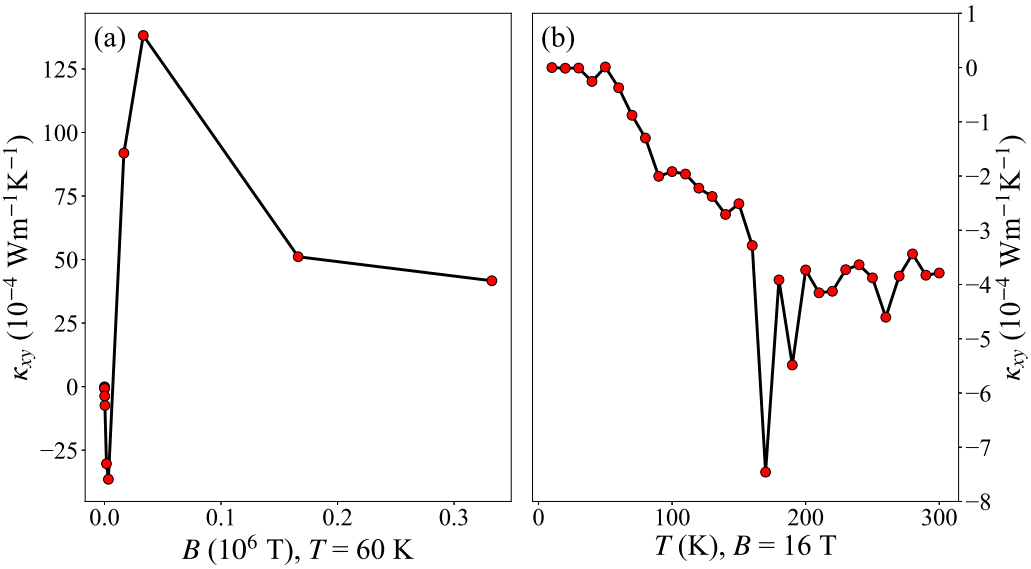

Figure 5.5: (a) Phonon Hall conductivity versus the applied magnetic field at $T = 60$ K. (b) Phonon Hall conductivity versus temperature at $B = 16$ T.

We note that when we increase the magnetic field, the phonon Hall conductivity in the BTO encounters a sign change. Since the conductivity is just the sum of the weighted Berry curvatures in the first Brillouin zone, we should observe clues for the sign change from the Berry curvatures and phonon dispersion of the BTO. Usually, the great change of Berry curvatures comes from band-openings or band-crossings. However, monitoring the evolution of each branch in the BTO is not a good idea. In the phonon dispersion of the BTO, many branches are deeply entangled so that we cannot always distinguish each branch correctly traveling around the whole Brillouin zone, neither the Berry curvatures of each branch. Moreover, the phonon Hall conductivity is an overall effect summing over all the weighted Berry curvatures so

we cannot only analyze the individual Berry curvatures along the high symmetry path. Therefore, we decide to simply split the branches into two groups, three acoustic branches and twelve optical branches, and draw a plot of contributions to the phonon Hall conductivity of the two groups, which is the Fig. 5.6. Comparing with the Fig. 5.5(a), we can conclude that the acoustic contributions are larger than optical for small magnetic fields so that the total conductivity is negative initially, and when the magnetic field surpasses some value, the situation gets reversed. Once a small magnetic field is applied to the system, the degenerate branches will be slightly lifted (points near the Γ point are dominant) so that the Berry curvatures rapidly increase as shown in Fig. 5.6. Initial tiny gaps nearly produce symmetric Berry curvatures (dominated by the same η in the Eq. (5.20)) among all the branches. However, due to the Θ function, the acoustic branches with much smaller eigenvalues will contribute more resulting in a negative conductivity (with a transformation, it is valid to just consider the positive branches [2]). When the magnitude of the magnetic field keeps increasing, by zooming in the phonon dispersion, we find that the gaps in the acoustic branches grow faster than those in the optical branches against the magnetic field. As a result, the magnitude of the Berry curvatures of the acoustic branches decrease faster than those in the optical branches. The slopes of the two groups in Fig. 5.6 verify this statement. Finally, at some value of the magnetic field, the optical branches contribute more to the phonon Hall conductivity so that a sign change shows up.

Why are the results so small? Our intuition is that the spin-phonon interaction, in this case, is too weak for it cannot even remove the degeneracy of the soft optical

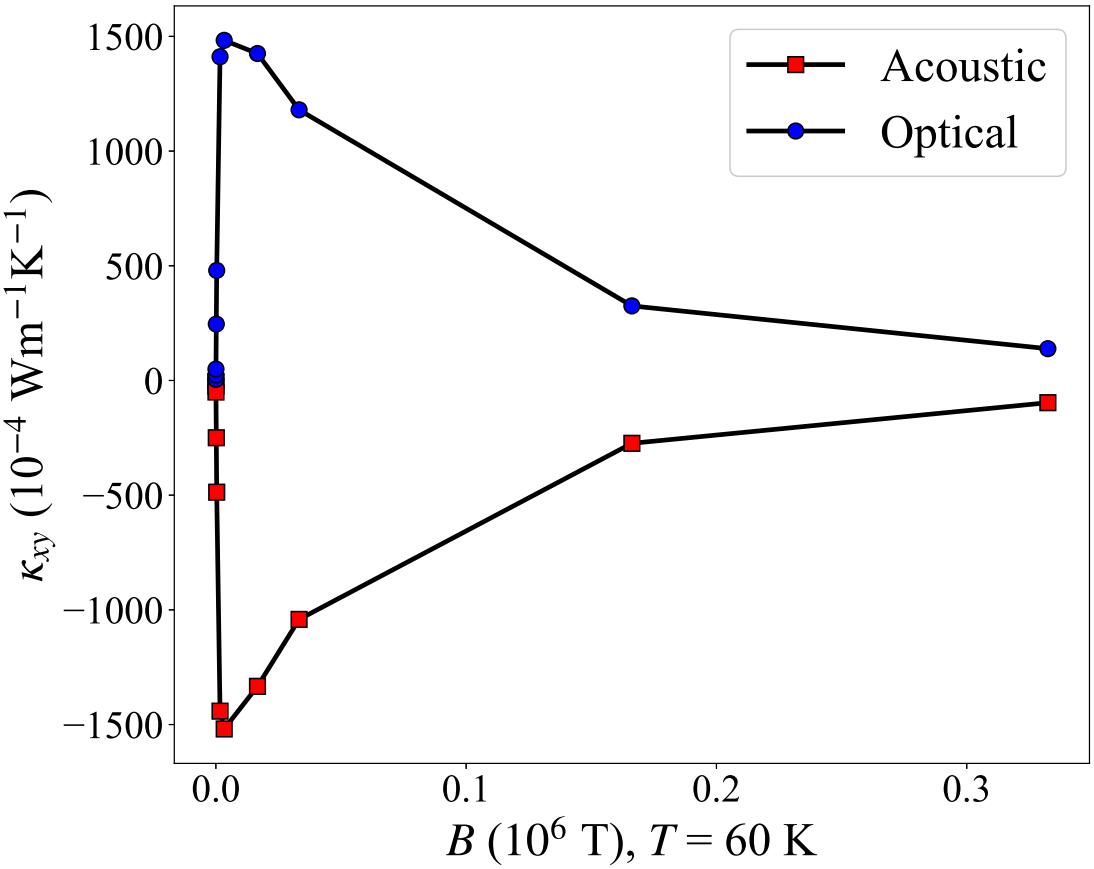

Figure 5.6: Mode-dependent contributions to the phonon Hall effect for varying magnetic field at $T = 60$ K. The red squares stand for the acoustic contributions and the blue dots for the optical contributions.

phonons. With this degeneracy, although we have soft optical phonons, their effects just get canceled. This canceling can be easily checked by looking at the mode contribution to the phonon Hall conductivity. However, currently we have no idea what are the suitable ingredients to open a gap between soft optical phonons from first-principles calculations, and we would like to leave it as an open question that deserves our further exploration. Therefore, we perform a numerical test to open a gap by hand.

There are two ways to manually open a small gap at and near the Γ point, one

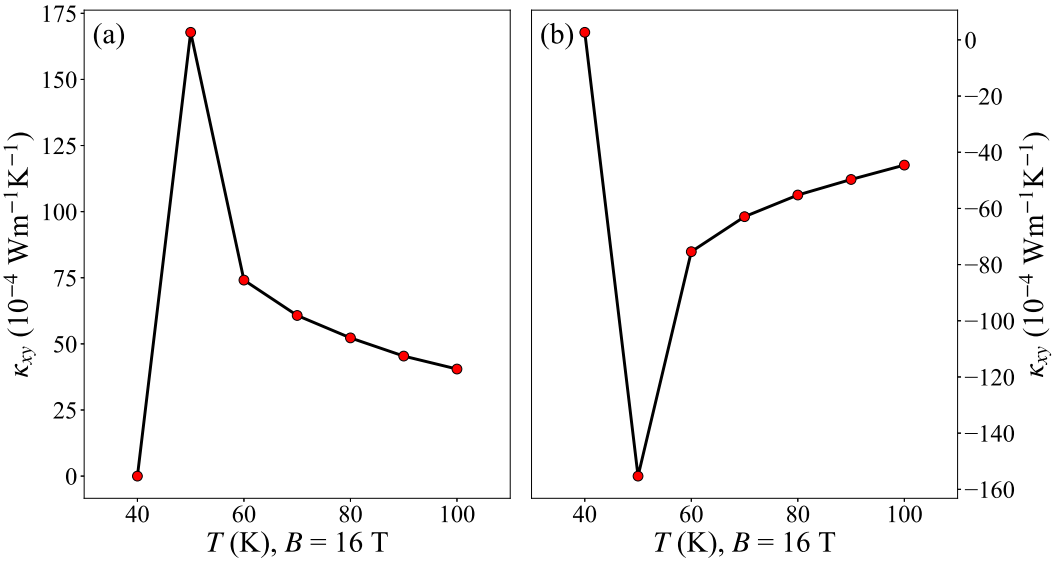

Figure 5.7: (a) Open a small gap by manually lifting 1% of the value of the higher soft optical phonon branch at and near Γ point (the chosen range is where the frequencies are lower than 100 cm^{-1}). (b) Open a small gap with the same value and range as (a), but by manually lifting 1% of the value of the lower soft optical phonon branch which will introduce band-crossing points near Γ point. These two operations can be imagined considering a partially degenerate two-level system.

is to lift the higher soft optical phonon branch and the other is to lift the lower soft optical phonon branch. The latter one will induce band-crossing points near the Γ point. Figure 5.7 shows the Hall conductivity after these two operations. It can be seen that their magnitudes are indeed enlarged to be close to the experimental values. These two operations result in opposite signs, and usually the phonon Hall conductivity experiments measured has a negative sign.

5.3.3 Discussions for STO

Last year, an experimental group found a large phonon Hall conductivity in STO under the magnetic field around 15 T. Therefore, we also explored the PHE in STO by first-principles calculations. Since BTO and STO have a similar structure,

the numerical details are almost the same as BTO except for the pseudo-potential files. Our optimized lattice constant for STO is 3.852 Å based on the PBEsol exchange-correlation functional for Sr, Ti, and O [109], which performs better than other functionals and is consistent with the previous experimental value [110] and theoretical calculation [43]. However, we cannot obtain large phonon Hall conductivity even after manually open a gap, and the order of magnitude is still two orders smaller than the experiments in STO. The failure could result from many reasons. Firstly, we choose a cubic structure while at low temperature, STO has different phases of structure. Secondly, we expect there should be soft phonon modes with frequencies being close to 0 near Γ point so that the dielectric constant of the STO will be as large as 10^4 at low temperature, while our current approach utilizing ALAMODE cannot produce that soft optical modes, and the dielectric constant we obtained is about three orders smaller than expected. Thirdly, perhaps we cannot produce large PHE with the SPI.

Right after the experiment, a theoretical paper by Chen *et al.* discussed this experiment in detail [30]. The authors pointed out that with Qin's theory, the phonon Hall conductivity can only be about four orders smaller than the experimental value. Although our results are two orders smaller, it is not enough. Moreover, according to our observation, the SPI we used is too weak to open a gap between two soft phonon modes at Γ point. Therefore the degeneration may cause canceling during the calculation. We obtain large values as those in the experiment if we open a gap by hand in BTO (not in STO for we cannot produce soft phonon modes in STO). In Chen *et al.*'s paper, they also provide another direction to explain the

experiment, which is using the Boltzmann transport theory. With their approach, they made a successful prediction of the ratio between the longitudinal conductivity and the phonon Hall conductivity. However, there is another new experiment in STO challenging their theory. Just by replacing the ^{16}O in STO with the isotope ^{18}O, researchers found that the phonon Hall conductivity will be reduced by two orders [31]. It is difficult to explain this behavior using Boltzmann transport theory for the replacement only changes the mass. Moreover, it is unnatural that we can only explain the PHE with macroscopic methods.

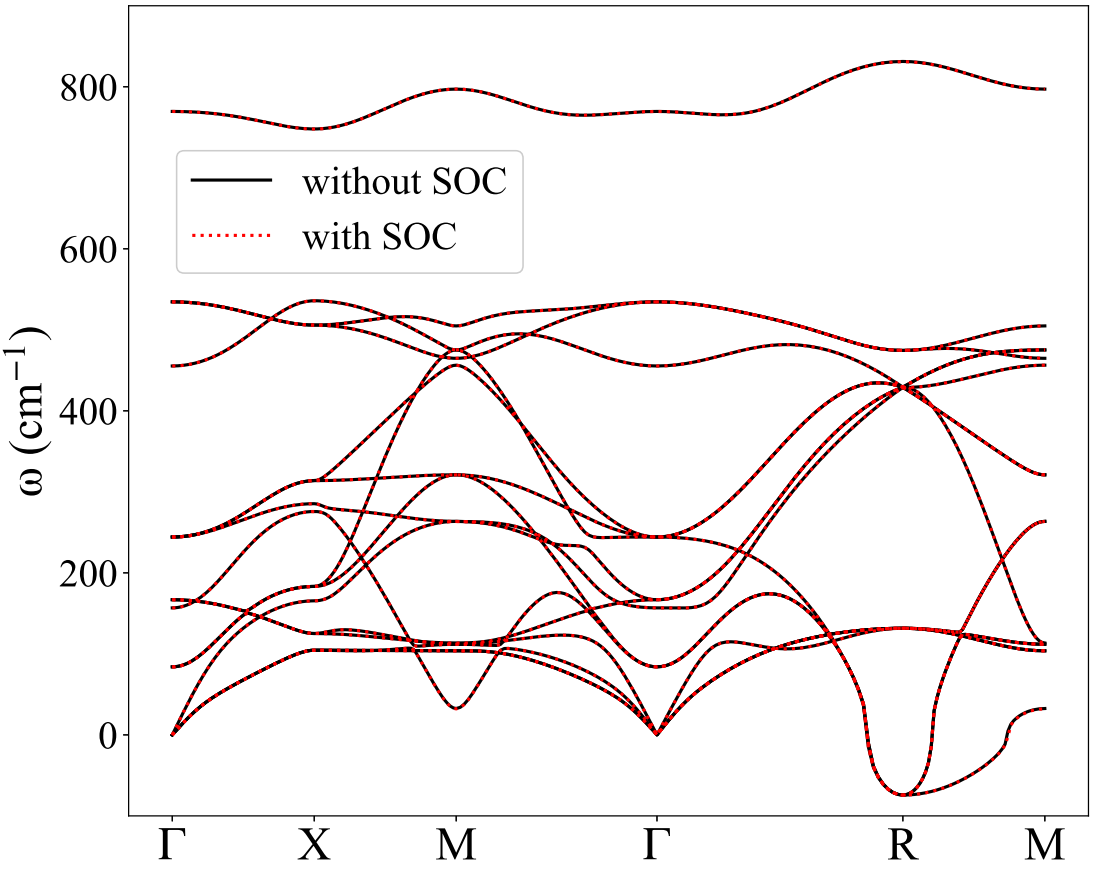

Figure 5.8: The phonon dispersion of the STO with and without the SOC at 0 K. The black solid line stands for the case without the SOC, and the red dotted line for the case with the SOC.

When there is an external magnetic field, the ion will experience two effective vector potentials: one is from the real magnetic field (the SPI in our case), and the other is from the "Berry phase" due to the phase of electron ground state, which was first pointed out by Mead and Truhlar [86]. The latter one has already been considered in Qin's theory, and Saito *et al.* have discussed in detail how to include it in a square lattice model [27]. However, it seems that nobody knows how to calculate this electron-related vector potential in first-principles calculations. Another electron-related physical process is the spin-orbit coupling (SOC) of electrons. In our consideration, the SOC may affect the PHE in two ways. First, the SOC may relate to the electronic "Berry phase", but we cannot deal with it yet. Second, the SOC may modify the phonon dispersion directly [111, 112]. As a quick exploration, we calculate the phonon dispersion of the STO turning on the SOC at zero temperature, which is illustrated in Fig. 5.8. It can be seen that the effect of the SOC is so weak that the phonon dispersion almost remains the same. Although previous research reported the SOC in the STO-based heterostructures [113] and gating system [114], there are no studies on the SOC in bulk STO or BTO before. Therefore, the high temperature effect of the SOC in the STO or BTO deserves future exploration. Besides, in our calculations, we do not take care of the cubic potential term which is related to the phonon lifetime. Qin's theory starts from the harmonic assumption, therefore we cannot deal with cubic term with this theory. Currently, we simply add a small constant value η in the Eq. (5.20) to represent the inverse of the phonon lifetime. Although we can tune the η to modify the phonon Hall conductivity, a systematical theory for PHE considering the cubic term should be developed in future

work. Therefore, we think the experiments still lack a microscopic explanation, and our intuition is that it may be relevant to the inner electronic topological structure of the STO or the cubic potential term in the STO, which is a future project to explore.

5.4 Summary

In summary, we introduce an approach to calculate the phonon Hall conductivity in real materials using first-principles calculations, and apply it to NaCl, BTO, and STO. Although the approach is very direct, it highly relies on whether first-principles calculations can predict materials properly and how to introduce the effective vector potential in materials. We have provided a benchmark of the PHE in NaCl to be examined in the future, and based on our calculation, there is still a gap to address soft phonons in STO using first-principles calculations. We conclude that SPI is not a good candidate to explain the PHE in real materials, and propose that the inner electronic structure or cubic potential term in STO may be possible directions to explore in future work. Finally, we think the relationship between the soft mode and κ_{xy} is far from clear quantitatively and needs further exploration. This study provides an effective route to capture the PHE from the accurate first-principles calculations in any real materials and has implications in promoting related experimental investigations.

Chapter 6

Conclusions and Future Work

6.1 Conclusions

This dissertation explored the electron and phonon dynamics within the electron-phonon interaction. Multiple methods such as the nonequilibrium Green's function, Boltzmann transport equation, Green-Kubo formula, and density functional theory were employed to investigate the dynamics.

To inspect the electron dynamics coupled to phonons, a general nonlinear Schrödinger equation was derived to describe the evolution of electrons. However, this nonlinear equation is too complex to be solved numerically. Therefore, we split it into two equations, one for electrons and the other for phonons, and then we solved the coupled equations by molecular dynamics method. As an application, we applied our method to the 1-D SSH model with single electron. The results indicated the charge transport in this case with examined parameters is bandlike meaning that the diffusion constant decreases as the temperature increases. This behavior contradicted with the prediction derived by the BTE method both qualitatively and quantitatively. Therefore, the BTE method is inapplicable to this 1-D model. The reason we attributed to is that the BTE method incorrectly counts more

scattering events than what really occurs in 1-D case. Subsequently, we explored single electron's transport in a quasi 1-D polymer, the poly(Ni-C_2S_4), with data provided by our collaborator from first-principles calculations. In this polymer, the phonons lie in three dimensions while the electron still moves in one-dimensional space. Therefore, our simulation only differed quantitatively from the BTE method, both of which indicated high conductivity in this polymer except higher values implied by our results. Unfortunately, we could not explore further with larger size and longer simulation time due to the complexity of the polymer.

For the phonon dynamics, we focused on the phonon Hall effect, which has been a rather intriguing area in recent years. Summarizing previous research, we provided a general description of the PHE and a thorough derivation of the phonon Hall conductivity. Currently, all the experiments and theoretical mechanisms require a significant magnetic field, while generally, a magnetic filed is not necessary as long as there is a source of the effective vector potential. Therefore, we proposed a mechanism of the PHE induced by electric current with the help of the EPI. In this mechanism, only a very weak magnetic field was needed to perturb the phonon system in a graphene-like lattice model. The dependence of the phonon Hall conductivity on the drift velocity of the driving current and on the temperature were studied. It was found that the magnitude of the conductivity grows linearly against the increasing drift velocity in the perturbative region. With increasing temperature, the PHE becomes stronger, while the exact relation could not determined. The topology of this system was kind of trivial without jumping of the Chern numbers. We also discussed a way to observe this current-induced PHE to be examined by

experiments.

As a first attempt, we linked the general theory of the PHE with first-principles calculations trying to bridge the gap between experiments and theoretical research. We obtained dynamic matrix and effective vector potential (provided by the spin-phonon interaction in our calculation) with the help of the first-principles packages, and then substituted them into the framework of the PHE to calculate the phonon Hall conductivity. Our first goal was to provide a new benchmark of the PHE in NaCl which has been explored in previous work. A major revision that PHE disappears when temperature goes to zero and a minor revision about the magnitude of the phonon Hall conductivity were achieved. Another goal was to investigate the PHE in perovskite BTO/STO since large PHE has been observed in experiments. According to previous research, soft phonon modes should play a crucial role in determining the PHE. However, although we successfully produced soft phonons in BTO from first-principles calculations, the results are much smaller than experimental values. With further exploration, we found that the two soft modes are degenerate, thereby the dominant Berry curvatures they produce cancel each other, and if we manually open a small gap here, the Hall conductivity will be comparable with experiments. Therefore, we thought the SPI we used to generate the effective vector potential was too weak to break the degeneration between soft modes. However, PHE in STO is more challenging since first-principles calculations cannot predict its structure at low temperature correctly. The results we obtained in normal STO cannot explain experiment even if we manually open the gap between soft modes, but they are close to the measurements in $SrTi^{18}O_3$, which could be an inspiration for future research.

There is still a long way to go to fully understand the PHE in real materials. New theory and better tools are in demand.

6.2 Future Research Directions

For electron dynamics, our current implementation only considered 1-D or quasi 1-D models with phonon baths. Therefore, the model settings can be enriched such as adding electron baths, setting different temperature for baths, applying electric field, and so on. Since we found the BTE method does not give a consistent prediction in 1-D with our simulation, we may seek a way to improve the BTE method in future. Moreover, we have tried to detect a polaron in our model but failed, and currently, polaron physics still lacks investigation, which is another valuable future direction.

Although this thesis has dived into the field of the PHE deeply, we have not reached the end of the story. New ingredients are needed to explain experiments with current microscopic theory, and possible candidates may be the inner electronic structure or other anharmonic potential terms, for exampe, cubic potential of the materials. To capture the inner electronic structure, we need to find a way to compute the electron Berry connection $\boldsymbol{A}(\boldsymbol{R}) = i\hbar\langle\alpha(\boldsymbol{R})|\boldsymbol{\nabla}|\alpha(\boldsymbol{R})\rangle$ in Mead and Truhlar's theory by first-principles calculations directly. There is also a possibility that better theory for the PHE should be developed.

We believe the above (but not limited to) future research directions will advance the methodologies presented in this thesis and boost our understandings to associated fields.

Bibliography

[1] F. Giustino, "Electron-phonon interactions from first principles", *Rev. Mod. Phys.*, vol. 89, p. 015 003, 1 Feb. 2017. [Online]. Available: https://link.aps.org/doi/10.1103/RevModPhys.89.015003.

[2] T. Qin, J. Zhou, and J. Shi, "Berry curvature and the phonon hall effect", *Phys. Rev. B*, vol. 86, p. 104 305, 10 Sep. 2012. [Online]. Available: https://link.aps.org/doi/10.1103/PhysRevB.86.104305.

[3] C. K. Chiang, C. R. Fincher, Y. W. Park, A. J. Heeger, H. Shirakawa, E. J. Louis, S. C. Gau, and A. G. MacDiarmid, "Electrical conductivity in doped polyacetylene", *Phys. Rev. Lett.*, vol. 39, pp. 1098–1101, 17 Oct. 1977. [Online]. Available: https://link.aps.org/doi/10.1103/PhysRevLett.39.1098.

[4] W. P. Su, J. R. Schrieffer, and A. J. Heeger, "Solitons in polyacetylene", *Phys. Rev. Lett.*, vol. 42, pp. 1698–1701, 25 Jun. 1979. [Online]. Available: https://link.aps.org/doi/10.1103/PhysRevLett.42.1698.

[5] Y. Aharonov and D. Bohm, "Significance of electromagnetic potentials in the quantum theory", *Physical Review*, vol. 115, no. 3, p. 485, 1959.

[6] M. V. Berry, "Quantal phase factors accompanying adiabatic changes", *Proceedings of the Royal Society of London. A. Mathematical and Physical Sciences*, vol. 392, no. 1802, pp. 45–57, 1984.

[7] D. Xiao, M.-C. Chang, and Q. Niu, "Berry phase effects on electronic properties", *Reviews of modern physics*, vol. 82, no. 3, p. 1959, 2010.

[8] B. Simon, "Holonomy, the quantum adiabatic theorem, and berry's phase", *Physical Review Letters*, vol. 51, no. 24, p. 2167, 1983.

[9] D. J. Thouless, M. Kohmoto, M. P. Nightingale, and M. den Nijs, "Quantized hall conductance in a two-dimensional periodic potential", *Physical review letters*, vol. 49, no. 6, p. 405, 1982.

[10] M. Kohmoto, "Topological invariant and the quantization of the hall conductance", *Annals of Physics*, vol. 160, no. 2, pp. 343–354, 1985.

[11] N. Nagaosa, J. Sinova, S. Onoda, A. H. MacDonald, and N. P. Ong, "Anomalous hall effect", *Reviews of modern physics*, vol. 82, no. 2, p. 1539, 2010.

[12] Z. Fang, N. Nagaosa, K. S. Takahashi, A. Asamitsu, R. Mathieu, T. Ogasawara, H. Yamada, M. Kawasaki, Y. Tokura, and K. Terakura, "The anomalous hall effect and magnetic monopoles in momentum space", *Science*, vol. 302, no. 5642, pp. 92–95, 2003.

[13] D. Xiao, Y. Yao, Z. Fang, and Q. Niu, "Berry-phase effect in anomalous thermoelectric transport", *Physical review letters*, vol. 97, no. 2, p. 026 603, 2006.

[14] D. Sheng, Z. Weng, L. Sheng, and F. Haldane, "Quantum spin-hall effect and topologically invariant chern numbers", *Physical review letters*, vol. 97, no. 3, p. 036 808, 2006.

[15] M. König, H. Buhmann, L. W. Molenkamp, T. Hughes, C.-X. Liu, X.-L. Qi, and S.-C. Zhang, "The quantum spin hall effect: Theory and experiment", *Journal of the Physical Society of Japan*, vol. 77, no. 3, p. 031 007, 2008.

[16] D. Vanderbilt, "Berry Phases in Electronic Structure Theory: Electric Polarization, Orbital Magnetization and Topological Insulators", Cambridge University Press, 2018.

[17] J. Ren, P. Hänggi, B. Li, *et al.*, "Berry-phase-induced heat pumping and its impact on the fluctuation theorem", *Physical review letters*, vol. 104, no. 17, p. 170 601, 2010.

[18] J.-T. Lü, M. Brandbyge, and P. Hedegård, "Blowing the fuse: Berry's phase and runaway vibrations in molecular conductors", *Nano Letters*, vol. 10, no. 5, pp. 1657–1663, 2010. eprint: https://doi.org/10.1021/nl904233u. [Online]. Available: https://doi.org/10.1021/nl904233u.

[19] C. Strohm, G. Rikken, and P. Wyder, "Phenomenological evidence for the phonon hall effect", *Physical review letters*, vol. 95, no. 15, p. 155 901, 2005.

[20] A. V. Inyushkin and A. Taldenkov, "On the phonon hall effect in a paramagnetic dielectric", *JETP Letters*, vol. 86, no. 6, pp. 379–382, 2007.

[21] X. Li, B. Fauqué, Z. Zhu, and K. Behnia, "Phonon thermal hall effect in strontium titanate", *Phys. Rev. Lett.*, vol. 124, p. 105 901, 10 Mar. 2020. [Online]. Available: https://link.aps.org/doi/10.1103/PhysRevLett.124.105901.

[22] J.-S. Wang and L. Zhang, "Phonon hall thermal conductivity from the green-kubo formula", *Phys. Rev. B*, vol. 80, p. 012 301, 1 Jul. 2009. [Online]. Available: https://link.aps.org/doi/10.1103/PhysRevB.80.012301.

[23] L. Sheng, D. Sheng, and C. Ting, "Theory of the phonon hall effect in paramagnetic dielectrics", *Physical review letters*, vol. 96, no. 15, p. 155 901, 2006.

[24] Y. Kagan and L. Maksimov, "Anomalous hall effect for the phonon heat conductivity in paramagnetic dielectrics", *Physical review letters*, vol. 100, no. 14, p. 145 902, 2008.

[25] L. Zhang, J. Ren, J.-S. Wang, and B. Li, "Topological nature of the phonon hall effect", *Phys. Rev. Lett.*, vol. 105, p. 225 901, 22 Nov. 2010. [Online]. Available: https://link.aps.org/doi/10.1103/PhysRevLett.105.225901.

[26] T. Qin, Q. Niu, and J. Shi, "Energy magnetization and the thermal hall effect", *Physical review letters*, vol. 107, no. 23, p. 236 601, 2011.

[27] T. Saito, K. Misaki, H. Ishizuka, and N. Nagaosa, "Berry phase of phonons and thermal hall effect in nonmagnetic insulators", *Physical Review Letters*, vol. 123, no. 25, p. 255 901, 2019.

[28] X. Zhang, Y. Zhang, S. Okamoto, and D. Xiao, "Thermal hall effect induced by magnon-phonon interactions", *Phys. Rev. Lett.*, vol. 123, p. 167 202, 16 Oct. 2019. [Online]. Available: https://link.aps.org/doi/10.1103/PhysRevLett.123.167202.

[29] B. K. Agarwalla, L. Zhang, J.-S. Wang, and B. Li, "Phonon hall effect in ionic crystals in the presence of static magnetic field", *The European Physical Journal B*, vol. 81, no. 2, pp. 197–202, 2011.

[30] J.-Y. Chen, S. A. Kivelson, and X.-Q. Sun, "Enhanced thermal hall effect in nearly ferroelectric insulators", *Physical Review Letters*, vol. 124, no. 16, p. 167 601, 2020.

[31] S. Sim, H. Yang, H.-L. Kim, M. J. Coak, M. Itoh, Y. Noda, and J.-G. Park, "Sizable suppression of thermal hall effect upon isotopic substitution in srtio 3", *Physical Review Letters*, vol. 126, no. 1, p. 015 901,

[32] R. d. L. Kronig, "On the mechanism of paramagnetic relaxation", *Physica*, vol. 6, no. 1, pp. 33–43, 1939.

[33] J. Van Vleck, "Paramagnetic relaxation times for titanium and chrome alum", *Physical Review*, vol. 57, no. 5, p. 426, 1940.

[34] H. Capellmann and K. Neumann, "Intermediate valency i: Couplings, hamiltonian, and electrical resistivity", *Zeitschrift für Physik B Condensed Matter*, vol. 67, no. 1, pp. 53–61, 1987.

[35] H. Capellmann, S. Lipinski, and K. Neumann, "A microscopic model for the coupling of spin fluctuations and charge fluctuation in intermediate valency", *Zeitschrift für Physik B Condensed Matter*, vol. 75, no. 3, pp. 323–329, 1989.

[36] H. Capellmann and S. Lipinski, "Spin-phonon coupling in intermediate valency: Exactly solvable models", *Zeitschrift für Physik B Condensed Matter*, vol. 83, no. 2, pp. 199–205, 1991.

[37] A. Ioselevich and H. Capellmann, "Strongly correlated spin-phonon systems: A scenario for heavy fermions", *Physical Review B*, vol. 51, no. 17, p. 11 446, 1995.

[38] A. Bhalla, R. Guo, and R. Roy, "The perovskite structure—a review of its role in ceramic science and technology", *Materials research innovations*, vol. 4, no. 1, pp. 3–26, 2000.

[39] W. Zhang, G. E. Eperon, and H. J. Snaith, "Metal halide perovskites for energy applications", *Nature Energy*, vol. 1, no. 6, pp. 1–8, 2016.

[40] K. A. Müller and H. Burkard, "Srti o 3: An intrinsic quantum paraelectric below 4 k", *Physical Review B*, vol. 19, no. 7, p. 3593, 1979.

[41] D. Fu and M. Itoh, "Role of ca off-centering in tuning ferroelectric phase transitions in ba (zr, ti) o3 system", *Ferroelectric Materials—Synthesis and Characterization*, 2015.

[42] H. Bilz, G. Benedek, and A. Bussmann-Holder, "Theory of ferroelectricity: The polarizability model", *Physical Review B*, vol. 35, no. 10, p. 4840, 1987.

[43] T. Tadano and S. Tsuneyuki, "Self-consistent phonon calculations of lattice dynamical properties in cubic $SrTiO_3$ with first-principles anharmonic force constants", *Phys. Rev. B*, vol. 92, p. 054 301, 5 Aug. 2015. [Online]. Available: https://link.aps.org/doi/10.1103/PhysRevB.92.054301.

[44] J.-J. Zhou, O. Hellman, and M. Bernardi, "Electron-phonon scattering in the presence of soft modes and electron mobility in srtio 3 perovskite from first principles", *Physical review letters*, vol. 121, no. 22, p. 226 603, 2018.

[45] X. He, D. Bansal, B. Winn, S. Chi, L. Boatner, and O. Delaire, "Anharmonic eigenvectors and acoustic phonon disappearance in quantum paraelectric srtio 3", *Physical review letters*, vol. 124, no. 14, p. 145 901, 2020.

[46] J.-S. Wang, "Phonon soft modes and para-to ferro-electric phase transitions", *Physica A: Statistical Mechanics and its Applications*, p. 125 641, 2020.

[47] J.-S. Wang, J. Wang, and J. Lü, "Quantum thermal transport in nanostructures", *The European Physical Journal B*, vol. 62, no. 4, pp. 381–404, 2008.

[48] J.-S. Wang, "Quantum thermal transport from classical molecular dynamics", *Physical review letters*, vol. 99, no. 16, p. 160 601, 2007.

[49] J. Schwinger, "On the green's functions of quantized fields. i", *Proceedings of the National Academy of Sciences*, vol. 37, no. 7, pp. 452–455, 1951.

[50] J. Schwinger, "On the green's functions of quantized fields. ii", *Proceedings of the National Academy of Sciences*, vol. 37, no. 7, pp. 455–459, 1951.

[51] J. Schwinger, "Brownian motion of a quantum oscillator", *Journal of Mathematical Physics*, vol. 2, no. 3, pp. 407–432, 1961.

[52] L. P. Kadanoff, "Quantum statistical mechanics", CRC Press, 2018.

[53] L. V. Keldysh *et al.*, "Diagram technique for nonequilibrium processes", *Sov. Phys. JETP*, vol. 20, no. 4, pp. 1018–1026, 1965.

[54] Y. Meir and N. S. Wingreen, "Landauer formula for the current through an interacting electron region", *Physical review letters*, vol. 68, no. 16, p. 2512, 1992.

[55] A.-P. Jauho, N. S. Wingreen, and Y. Meir, "Time-dependent transport in interacting and noninteracting resonant-tunneling systems", *Physical Review B*, vol. 50, no. 8, p. 5528, 1994.

[56] A. Ozpineci and S. Ciraci, "Quantum effects of thermal conductance through atomic chains", *Physical Review B*, vol. 63, no. 12, p. 125 415, 2001.

[57] J.-S. Wang, J. Wang, and N. Zeng, "Nonequilibrium green's function approach to mesoscopic thermal transport", *Physical Review B*, vol. 74, no. 3, p. 033 408, 2006.

[58] J.-S. Wang, N. Zeng, J. Wang, and C. K. Gan, "Nonequilibrium green's function method for thermal transport in junctions", *Physical Review E*, vol. 75, no. 6, p. 061 128, 2007.

[59] N. Mingo, "Anharmonic phonon flow through molecular-sized junctions", *Physical Review B*, vol. 74, no. 12, p. 125 402, 2006.

[60] J.-S. Wang, B. K. Agarwalla, H. Li, and J. Thingna, "Nonequilibrium green's function method for quantum thermal transport", *Frontiers of Physics*, vol. 9, no. 6, pp. 673–697, 2014.

[61] D. C. Langreth, "Linear and nonlinear response theory with applications", in *Linear and Nonlinear Electron Transport in Solids*, J. T. Devreese and V. E. van Doren, Eds. Boston, MA: Springer US, 1976, pp. 3–32, ISBN: 978-

1-4757-0875-2. [Online]. Available: https://doi.org/10.1007/978-1-4757-0875-2_1.

[62] J. M. Ziman, "Electrons and phonons: the theory of transport phenomena in solids", Oxford university press, 2001.

[63] T. Fukui, Y. Hatsugai, and H. Suzuki, "Chern numbers in discretized brillouin zone: Efficient method of computing (spin) hall conductances", *Journal of the Physical Society of Japan*, vol. 74, no. 6, pp. 1674–1677, 2005.

[64] M. S. Green, "Markoff random processes and the statistical mechanics of time-dependent phenomena. ii. irreversible processes in fluids", *The Journal of Chemical Physics*, vol. 22, no. 3, pp. 398–413, 1954.

[65] R. Kubo, "Statistical-mechanical theory of irreversible processes. i. general theory and simple applications to magnetic and conduction problems", *Journal of the Physical Society of Japan*, vol. 12, no. 6, pp. 570–586, 1957. eprint: https://doi.org/10.1143/JPSJ.12.570. [Online]. Available: https://doi.org/10.1143/JPSJ.12.570.

[66] D. R. Hartree, "The wave mechanics of an atom with a non-coulomb central field. part i. theory and methods", Сборник статей к мультимедийному электронному учебно-методическому комплексу по дисциплине «физика атома и атомных явлений»/отв. ред. Шундалов МБ; БГУ, Физический факультет, 1928.

[67] V. Fock, "Näherungsmethode zur lösung des quantenmechanischen mehrkörperproblems", *Zeitschrift für Physik*, vol. 61, no. 1-2, pp. 126–148, 1930.

[68] P. Hohenberg and W. Kohn, "Inhomogeneous electron gas", *Physical review*, vol. 136, no. 3B, B864, 1964.

[69] W. Kohn and L. J. Sham, "Self-consistent equations including exchange and correlation effects", *Physical review*, vol. 140, no. 4A, A1133, 1965.

[70] J. P. Perdew, K. Burke, and M. Ernzerhof, "Generalized gradient approximation made simple", *Physical review letters*, vol. 77, no. 18, p. 3865, 1996.

[71] W. Shi, G. Wu, X. Yong, T. Deng, J.-S. Wang, J.-C. Zheng, J. Xu, M. B. Sullivan, and S.-W. Yang, "Orbital-engineering-based screening of π-conjugated d8 transition-metal coordination polymers for high-performance n-type thermoelectric applications", *ACS Applied Materials & Interfaces*, vol. 10, no. 41, pp. 35 306–35 315, 2018. eprint: https://doi.org/10.1021/acsami.8b13877. [Online]. Available: https://doi.org/10.1021/acsami.8b13877.

[72] J. T. Lü and J.-S. Wang, "Coupled electron–phonon transport from molecular dynamics with quantum baths", *Journal of Physics: Condensed Matter*, vol. 21, no. 2, p. 025 503, Dec. 2008. [Online]. Available: https://doi.org/10.1088%2F0953-8984%2F21%2F2%2F025503.

[73] M. P. L. Sancho, J. M. L. Sancho, J. M. L. Sancho, and J. Rubio, "Highly convergent schemes for the calculation of bulk and surface green functions", *Journal of Physics F: Metal Physics*, vol. 15, no. 4, pp. 851–858, Apr. 1985. [Online]. Available: https://doi.org/10.1088%2F0305-4608%2F15%2F4%2F009.

[74] J.-S. Wang, N. Zeng, J. Wang, and C. K. Gan, "Nonequilibrium green's function method for thermal transport in junctions", *Phys. Rev. E*, vol. 75, p. 061 128, 6 Jun. 2007. [Online]. Available: https://link.aps.org/doi/10.1103/PhysRevE.75.061128.

[75] A. Troisi and G. Orlandi, "Charge-transport regime of crystalline organic semiconductors: Diffusion limited by thermal off-diagonal electronic disorder", *Phys. Rev. Lett.*, vol. 96, p. 086 601, 8 Mar. 2006. [Online]. Available: https://link.aps.org/doi/10.1103/PhysRevLett.96.086601.

[76] D. Wang, W. Shi, J. Chen, J. Xi, and Z. Shuai, "Modeling thermoelectric transport in organic materials", *Physical Chemistry Chemical Physics*, vol. 14, no. 48, pp. 16 505–16 520, 2012.

[77] J. Bardeen and W. Shockley, "Deformation potentials and mobilities in non-polar crystals", *Phys. Rev.*, vol. 80, pp. 72–80, 1 Oct. 1950. [Online]. Available: https://link.aps.org/doi/10.1103/PhysRev.80.72.

[78] Z. Shuai, L. Wang, and C. Song, "Theory of charge transport in carbon electronic materials", Springer Science & Business Media, 2012.

[79] S. Jeyadev and E. M. Conwell, "Polaron mobility in trans-polyacetylene", *Phys. Rev. B*, vol. 35, pp. 6253–6259, 12 Apr. 1987. [Online]. Available: https://link.aps.org/doi/10.1103/PhysRevB.35.6253.

[80] C. Lee, W. Yang, and R. G. Parr, "Development of the colle-salvetti correlation-energy formula into a functional of the electron density", *Physical review B*, vol. 37, no. 2, p. 785, 1988.

[81] M. J. Frisch, G. W. Trucks, H. B. Schlegel, G. E. Scuseria, M. A. Robb, J. R. Cheeseman, G. Scalmani, V. Barone, B. Mennucci, G. A. Petersson, H. Nakatsuji, M. Caricato, X. Li, H. P. Hratchian, A. F. Izmaylov, J. Bloino, G. Zheng, J. L. Sonnenberg, M. Hada, M. Ehara, K. Toyota, R. Fukuda, J. Hasegawa, M. Ishida, T. Nakajima, Y. Honda, O. Kitao, H. Nakai, T. Vreven, J. A. Montgomery Jr., J. E. Peralta, F. Ogliaro, M. Bearpark, J. J. Heyd, E. Brothers, K. N. Kudin, V. N. Staroverov, R. Kobayashi, J. Normand, K. Raghavachari, A. Rendell, J. C. Burant, S. S. Iyengar, J. Tomasi, M. Cossi, N. Rega, J. M. Millam, M. Klene, J. E. Knox, J. B. Cross, V. Bakken, C. Adamo, J. Jaramillo, R. Gomperts, R. E. Stratmann, O. Yazyev, A. J. Austin, R. Cammi, C. Pomelli, J. W. Ochterski, R. L. Martin, K. Morokuma, V. G. Zakrzewski, G. A. Voth, P. Salvador, J. J. Dannenberg, S. Dapprich, A. D. Daniels, Ö. Farkas, J. B. Foresman, J. V. Ortiz, J. Cioslowski, and D. J. Fox, Gaussian, Inc.: Wallingford, CT, USA, 2009.

[82] P. J. Hay and W. R. Wadt, "Ab initio effective core potentials for molecular calculations. potentials for the transition metal atoms sc to hg", *The Journal of chemical physics*, vol. 82, no. 1, pp. 270–283, 1985.

[83] R. Ditchfield, W. J. Hehre, and J. A. Pople, "Self-consistent molecular-orbital methods. ix. an extended gaussian-type basis for molecular-orbital studies of organic molecules", *The Journal of Chemical Physics*, vol. 54, no. 2, pp. 724–728, 1971.

[84] G. Fishman, "Monte Carlo: concepts, algorithms, and applications", Springer Science & Business Media, 2013.

[85] P. W. Anderson, "Absence of diffusion in certain random lattices", *Physical review*, vol. 109, no. 5, p. 1492, 1958.

[86] C. A. Mead and D. G. Truhlar, "On the determination of born–oppenheimer nuclear motion wave functions including complications due to conical intersections and identical nuclei", *The Journal of Chemical Physics*, vol. 70, no. 5, pp. 2284–2296, 1979. eprint: https://doi.org/10.1063/1.437734. [Online]. Available: https://doi.org/10.1063/1.437734.

[87] G. D. Mahan, "Many-particle physics", Springer Science & Business Media, 2013.

[88] J. Luttinger, "Theory of thermal transport coefficients", *Physical Review*, vol. 135, no. 6A, A1505, 1964.

[89] R. J. Hardy, "Energy-flux operator for a lattice", *Physical Review*, vol. 132, no. 1, p. 168, 1963.

[90] J.-T. Lü, H. Zhou, J.-W. Jiang, and J.-S. Wang, "Effects of electron-phonon interaction on thermal and electrical transport through molecular nanoconductors", *AIP Advances*, vol. 5, no. 5, p. 053 204, 2015. eprint: https://doi.org/10.1063/1.4917017. [Online]. Available: https://doi.org/10.1063/1.4917017.

[91] J.-W. Jiang and J.-S. Wang, "Joule heating and thermoelectric properties in short single-walled carbon nanotubes: Electron-phonon interaction effect",

Journal of Applied Physics, vol. 110, no. 12, p. 124 319, 2011. eprint: https://doi.org/10.1063/1.3671069. [Online]. Available: https://doi.org/10.1063/1.3671069.

[92] J. Peng and J.-S. Wang, "Current-induced heat transfer in double-layer graphene", *arXiv preprint arXiv:1805.09493*, 2018.

[93] Y. Liu, Y. Xu, S.-C. Zhang, and W. Duan, "Model for topological phononics and phonon diode", *Physical Review B*, vol. 96, no. 6, p. 064 106, 2017.

[94] P. Souvatzis, O. Eriksson, M. Katsnelson, and S. Rudin, "Entropy driven stabilization of energetically unstable crystal structures explained from first principles theory", *Physical review letters*, vol. 100, no. 9, p. 095 901, 2008.

[95] O. Hellman, P. Steneteg, I. A. Abrikosov, and S. I. Simak, "Temperature dependent effective potential method for accurate free energy calculations of solids", *Physical Review B*, vol. 87, no. 10, p. 104 111, 2013.

[96] S. Baroni, S. De Gironcoli, A. Dal Corso, and P. Giannozzi, "Phonons and related crystal properties from density-functional perturbation theory", *Reviews of Modern Physics*, vol. 73, no. 2, p. 515, 2001.

[97] K. Esfarjani and H. T. Stokes, "Method to extract anharmonic force constants from first principles calculations", *Physical Review B*, vol. 77, no. 14, p. 144 112, 2008.

[98] T. Sun, D.-B. Zhang, and R. M. Wentzcovitch, "Dynamic stabilization of cubic ca si o 3 perovskite at high temperatures and pressures from ab initio molecular dynamics", *Physical Review B*, vol. 89, no. 9, p. 094 109, 2014.

[99] N. Werthamer, "Self-consistent phonon formulation of anharmonic lattice dynamics", *Physical Review B*, vol. 1, no. 2, p. 572, 1970.

[100] I. Errea, M. Calandra, and F. Mauri, "Anharmonic free energies and phonon dispersions from the stochastic self-consistent harmonic approximation: Application to platinum and palladium hydrides", *Physical Review B*, vol. 89, no. 6, p. 064 302, 2014.

[101] R. Car and M. Parrinello, "Unified approach for molecular dynamics and density-functional theory", *Phys. Rev. Lett.*, vol. 55, pp. 2471–2474, 22 Nov. 1985. [Online]. Available: `https://link.aps.org/doi/10.1103/PhysRevLett.55.2471`.

[102] Y. Xu, J.-S. Wang, W. Duan, B.-L. Gu, and B. Li, "Nonequilibrium green's function method for phonon-phonon interactions and ballistic-diffusive thermal transport", *Physical Review B*, vol. 78, no. 22, p. 224 303, 2008.

[103] X. Gonze and C. Lee, "Dynamical matrices, born effective charges, dielectric permittivity tensors, and interatomic force constants from density-functional perturbation theory", *Physical Review B*, vol. 55, no. 16, p. 10 355, 1997.

[104] M. Born and K. Huang, "Dynamical theory of crystal lattices", Clarendon press, 1954.

[105] K. Parlinski, Z. Li, and Y. Kawazoe, "Parlinski, li, and kawazoe reply", *Physical Review Letters*, vol. 81, no. 15, p. 3298, 1998.

[106] Y. Wang, J. Wang, W. Wang, Z. Mei, S. Shang, L. Chen, and Z. Liu, "A mixed-space approach to first-principles calculations of phonon frequencies

for polar materials", *Journal of Physics: Condensed Matter*, vol. 22, no. 20, p. 202 201, 2010.

[107] P. Giannozzi, S. Baroni, N. Bonini, M. Calandra, R. Car, C. Cavazzoni, D. Ceresoli, G. L. Chiarotti, M. Cococcioni, I. Dabo, A. Dal Corso, S. de Gironcoli, S. Fabris, G. Fratesi, R. Gebauer, U. Gerstmann, C. Gougoussis, A. Kokalj, M. Lazzeri, L. Martin-Samos, N. Marzari, F. Mauri, R. Mazzarello, S. Paolini, A. Pasquarello, L. Paulatto, C. Sbraccia, S. Scandolo, G. Sclauzero, A. P. Seitsonen, A. Smogunov, P. Umari, and R. M. Wentzcovitch, "Quantum espresso: A modular and open-source software project for quantum simulations of materials", *Journal of Physics: Condensed Matter*, vol. 21, no. 39, 395502 (19pp), 2009. [Online]. Available: `http://www.quantum-espresso.org`.

[108] R. A. Evarestov and A. V. Bandura, "First-principles calculations on the four phases of batio3", *Journal of computational chemistry*, vol. 33, no. 11, pp. 1123–1130, 2012.

[109] J. P. Perdew, A. Ruzsinszky, G. I. Csonka, O. A. Vydrov, G. E. Scuseria, L. A. Constantin, X. Zhou, and K. Burke, "Restoring the density-gradient expansion for exchange in solids and surfaces", *Phys. Rev. Lett.*, vol. 100, p. 136 406, 13 Apr. 2008. [Online]. Available: `https://link.aps.org/doi/10.1103/PhysRevLett.100.136406`.

[110] A. Okazaki and M. Kawaminami, "Lattice constant of strontium titanate at low temperatures", *Materials Research Bulletin*, vol. 8, no. 5, pp. 545–550, 1973.

[111] M. J. Verstraete, M. Torrent, F. ç. Jollet, G. Zérah, and X. Gonze, "Density functional perturbation theory with spin-orbit coupling: Phonon band structure of lead", *Phys. Rev. B*, vol. 78, p. 045 119, 4 Jul. 2008. [Online]. Available: https://link.aps.org/doi/10.1103/PhysRevB.78.045119.

[112] L. E. Díaz-Sánchez, A. H. Romero, and X. Gonze, "Phonon band structure and interatomic force constants for bismuth: Crucial role of spin-orbit interaction", *Phys. Rev. B*, vol. 76, p. 104 302, 10 Sep. 2007. [Online]. Available: https://link.aps.org/doi/10.1103/PhysRevB.76.104302.

[113] Y. Kim, R. M. Lutchyn, and C. Nayak, "Origin and transport signatures of spin-orbit interactions in one-and two-dimensional srtio 3-based heterostructures", *Physical Review B*, vol. 87, no. 24, p. 245 121, 2013.

[114] H. Nakamura, T. Koga, and T. Kimura, "Experimental evidence of cubic rashba effect in an inversion-symmetric oxide", *Physical Review Letters*, vol. 108, no. 20, p. 206 601, 2012.